The Spitzer c2d Survey of Large, Nearby, Interstellar Clouds. XI. Lupus Observed With IRAC and MIPS

Bruno Merín[1,2], Jes Jørgensen[3], Loredana Spezzi[4], Juan M. Alcalá[4], Neal J. Evans II[5], Paul M. Harvey[5], Nicholas Chapman[6], Tracy Huard[7], Ewine F. van Dishoeck[2], Fernando Comerón[8]

ABSTRACT

We present c2d Spitzer/IRAC observations of the Lupus I, III and IV dark clouds and discuss them in combination with optical and near-infrared and c2d MIPS data. With the Spitzer data, the new sample contains 159 stars, 4 times larger than the previous one. It is dominated by low- and very-low mass stars and it is complete down to M $\approx 0.1 M_{\odot}$. We find 30-40% binaries with separations between 100 to 2000 AU with no apparent effect in the disk properties of the members. A large majority of the objects are Class II or Class III objects, with only 20 (12%) of Class I or Flat spectrum sources. The disk sample is complete down to "debris"-like systems in stars as small as M ≈ 0.2 $M_{\odot}$ and includes sub-stellar objects with larger IR excesses. The disk fraction in Lupus is 70 – 80%, consistent with an age of 1 – 2 Myr. However, the young population contains 20% optically thick accretion disks and 40% relatively less flared disks. A growing variety of inner disk structures is found for larger inner disk clearings for

[1]Research and Scientific Support Department, European Space Agency (ESTEC), PO Box 299, 2200 AG Noordwijk, The Netherlands

[2]Leiden Observatory, Leiden University, PO Box 9513, 2300 RA Leiden, The Netherlands

[3]Argelander-Institut für Astronomie, University of Bonn, Auf dem Hügel 71, 53121 Bon, Germany

[4]INAF - Osservatorio Astronomico di Capodimonte, via Moiariello 16, I-80131, Naples, Italy

[5]Department of Astronomy, University of Texas at Austin, 1 University Station C1400 Austin, TX 78712-0259, USA

[6]Astronomy Department, University of Maryland, College Park, MD 20742, USA

[7]Smithsonian Astrophysical Observatory, 60 Garden Street, MS42, Cambridge, MA 02138, USA

[7]European Southern Observatory, Karl-Schwarzschild-Strasse 2, 85748 Garching bei München, Germany

equal disk masses. Lupus III is the most centrally populated and rich, followed by Lupus I with a filamentary structure and by Lupus IV, where a very high density core with little star-formation activity has been found. We estimate star formation rates in Lupus of 2 – 10 $M_\odot$ Myr^{-1} and star formation efficiencies of a few percent, apparently correlated with the associated cloud masses.

Subject headings: stars: formation – stars: pre-main sequence – stars: low-mass star-forming-regions:individual (Lupus I, Lupus III, Lupus IV)

1. Introduction

The Lupus dark cloud complex is one of the main low-mass star forming regions within 200 pc of the sun. Located in the Scorpius-Centaurus OB association, it consists of a loosely connected group of dark clouds and low-mass pre-main sequence stars located between galactic coordinates $334^o < l < 352^o$ and latitudes $+5^o < b < +25^o$ (RA $\sim 16^h20^m$ – $15^h30'$ and DEC $\sim$ -43°00′ – -33°00′) (Krautter 1991). The low ecliptic latitudes ($\sim$ -33 – -41) of the clouds guarantee a low abundance of asteroids. Given its large size ($\sim 20^o$) and proximity, it has been subject of many studies. Large-scale ^{12}CO ($J = 1 \rightarrow 0$) millimeter maps of the whole complex give total molecular gas masses of several times $10^4 M_\odot$ (Murphy et al. 1986; Tachihara et al. 2001) and a relatively small spread of cloud velocities among the different sub-clouds ($\leq$ 3 km s^{-1} Vilas-Boas et al. 2000). It hosts four active star-forming regions, including the rich T Tauri association in Lupus 3, plus five other looser dark clouds with signs of moderate star-formation activity (Hara et al. 1999). Objects in all evolutionary phases, from embedded Class I objects to evolved Class III stars, are found in the Lupus clouds. A comprehensive review about the Lupus clouds by Comerón (2008) provides more details on previous observations and is used throughout this work to assess the new results from the Spitzer data. The Lupus dark cloud is one of the five large nearby star-forming regions observed as part of the Spitzer Legacy Project "From Molecular Cores to Planet-forming Disks" (c2d) Evans et al. (2003). From the several Lupus subclouds (Thé 1962; Murphy et al. 1986), only Lupus I, III and IV were observed by c2d and are discussed in this paper.

Optical and near-infrared (near-IR) ground-based observations of Lupus identified three regions, denominated as Lupus I, II and III, with large numbers of classical T Tauri stars (Henize 1954; Thé 1962). Schwartz (1977) made a catalog of Hα emitting young stars which contained the vast majority of the objects in the clouds known until today. His observations also showed that Lupus 3 (roughly consistent with Cambrésy's Lupus III) is one of the most active star-forming regions in the southern sky, followed by Lupus I, II and IV and that a

large number of the stars in these clouds are low-mass stars. In addition to these classical T Tauri stars, Krautter et al. (1997) reported a much larger number of weak-line T Tauri stars with X-ray emission, which are believed to be older stars not physically bound to the dark clouds but rather belonging to a more nearby structure (Wichmann et al. 1999, see also Cieza et al. 2007 for a confirmation of this conclusion from c2d observations). Finally, there is evidence for different distances to the different subclouds: *Hipparcos* parallaxes and extinction source counts yield reasonable distance estimates of 150 ± 20 pc for Lupus I and IV and 200 ± 20 pc for Lupus III (Comerón 2008 in prep. and references therein), which we assume for this work.

Following previous c2d standards, observational results from the Spitzer Space Telescope (Werner et al. 2004) Infrared Array Camera (IRAC, Fazio et al. 2004) and from the Multiband Imaging Photometer for Spitzer (MIPS, Rieke et al. 2004) are reported separately for each cloud, followed by a "synthesis" paper which combines all the c2d Spitzer and complementary observations made of the region (see e.g. Harvey et al. 2006, 2007b,a for Serpens or Young et al. 2005; Porras et al. 2007, and Alcalá et al. 2008 for Chamaeleon II). For Lupus, the observational results obtained with MIPS have been reported by Chapman et al. (2007) (Paper I) and this paper describes the IRAC observations and analyzes the complete data set for the region. In that sense, this paper merges the contents of the IRAC and "synthesis" papers of the c2d observations in Lupus: it presents the 3.6 to 8.0 μm IRAC observations of the clouds for the first time and combines it with all previously available information from the optical to the millimeter.

All the observations analysed in this study are presented in § 2, with a discussion of the complementary observations and stellar multiplicity in the optical in § 2.1 and a detailed description of the Spitzer IRAC observations in § 2.2 and 2.3. These data are used to construct a high-reliability catalog of young stars in the clouds in § 3. This catalog is composed of Young Stellar Objects (YSO) identified with the Spitzer data (selected in § 3.1) and previously known Pre-Main Sequence stars (PMS, discussed in § 3.2). The rest of the paper is organized in two main sections, which deal with the individual sources (§ 4) and with the global cloud properties (§ 5), respectively. In the first one, the disk populations are studied with color-color diagrams (§ 4.1), multi-wavelength Spectral Energy Distributions (SEDs, § 4.2), stellar and disk luminosity functions (§ 4.3 and 4.4), and finally with a new '2D' classification system of the SEDs (§ 4.5). The Spitzer observations of outflows and Herbig-Haro objects in the region are also described in § 4.6. The second section describes the structures of the clouds with the help of Spitzer-derived extinction maps (§ 5.1), the spatial distribution of the YSOs in the clouds and a nearest-neighbor analysis of their clustering properties (§ 5.2). Finally, the Star Formation Rates and Star Formation Efficiencies are computed and discussed in § 5.3 and 5.4, respectively. A complete summary of this work is

given in § 6.

2. Observations and data analysis

The observations discussed in this paper come from the Spitzer Space Telescope's Infrared Array Camera (IRAC hereafter) and Multiband Imaging Photometer for Spitzer (MIPS) observations of Lupus I, III and IV made by the c2d Spitzer Legacy Program (Evans et al. 2003), together with an optical coordinated survey of the three clouds (F. Comerón et al., in preparation) and data from the literature. Detailed information about the MIPS observations can be found in Chapman et al. (2007).

2.1. Complementary data and multiple visual systems

An optical survey of the three clouds was performed with the Wide-Field Imager (WFI) attached to the ESO 2.2m telescope, at La Silla Observatory in Chile. The areas observed in the R_C (0.652 μm), I_C (0.784 μm), and z_{WFI} (0.957 μm) optical bands in Lupus I, III and IV were defined to overlap completely with the areas observed with Spitzer shown in Figures 1 to 3. The observational strategy, data reduction and source extraction are described in detail elsewhere (F. Comerón et al., in preparation). These observations were complemented with photometry from the *NOMAD* optical and near-IR catalog (Zacharias et al. 2005), which contains B, V and R_C magnitudes and from the J, H and K_S 2MASS near-IR all-sky catalog (Cutri et al. 2003). This paper also includes the c2d MIPS observations of the Lupus clouds. Figures 19 to 22 also show the areas mapped with MIPS at 24, 70 and 160 μm as part of the c2d project. They were defined to provide the maximum overlap and minimum observing time and cover completely the areas mapped with IRAC. The MIPS data acquisition, reduction and source extraction is presented and discussed in detail in Chapman et al. (2007).

The optical images were inspected to search for visual binaries in the sample. Table 10 reports all apparent companions detected in the images. The WFI images in Rc, Ic and z_{WFI} bands were inspected for all sources. Those observations were performed in service mode over several nights in two different observing seasons and have a range of seeing values, but an average seeing of $1.5''$ limits the smallest separation detectable to $\sim 0.7''$ in our case. The range of separations for which we report the presence of possible companions is 0.7 to $10''$ (140 to 2000 AU in Lupus III and 105 to 1500 AU at the distance of Lupus I and IV).

There are several pairs of stars with disks which are binaries. Inspection of the optical

images indicates that the probability of projection effects might be small given the relatively low number of optical sources at distances smaller than $10''$ in most of the examined stars. We recover all binaries listed by Ghez et al. (1997) which fell in our field except HR 5999, which was too bright to allow a shape analysis. We also recover the two objects in common with a yet unpublished AO/ADONIS survey of multiplicity in Lupus which probe at angular distances as close as $0.2''$ (A. Knockx et al., in prep.). The total binary fractions of 41±12% (7/17), 29±9% (39/124) and 44±13% (8/18) in the three clouds, respectively, compare well with the numbers given for Taurus and Ophiuchus in a similar range of angular distances (e.g. Padgett et al. 1997).

In any case, given the difficulty in apportioning the excess among the companions with separations smaller than $2.0''$, in which the IRAC fluxes could have been merged, and those with separations smaller than $4.0''$, which could have merged fluxes in MIPS, we set those fluxes as upper limits in the SEDs for the disk evolution studies. More discussion on the effects of binarity in the disks is presented in § 4.4.

2.2. Spitzer IRAC data

Lupus I, Lupus III and Lupus IV were observed with all IRAC bands (3.6, 4.5, 5.8 and 8.0 μm) on the 3rd and 4th of September of 2004 as part of the c2d Spitzer Legacy Program (P.I.: N. Evans, program ID: 174) and as part of GTO observations (P.I.: G. Fazio, program ID: 6). The total observed areas were defined to cover all the regions with extinctions $A_V \geq 2$ for Lupus III and IV and $A_V \geq 3$ for Lupus I (see Fig. 2 of Evans et al. 2003) as measured in the extinction maps by Cambrésy (1999). The combined mosaics of the three regions overlap in all IRAC bands with areas of 1.39, 1.34 and 0.37 deg^2 in Lupus I, Lupus III and Lupus IV, respectively. Furthermore 4 off-cloud regions, each of ~ 0.08 deg^2 were observed in low-extinction regions with a range of galactic latitudes for statistical comparison with the on-cloud fields. Each of them contains a 0.05 deg^2 overlap between all IRAC bands. All c2d maps were observed in two epochs at least 6 hours apart to guarantee the production of highly reliable catalogs of sources clean of asteroids and transient artifacts. The GTO observation of Lupus III was only observed once. For more information about the c2d mapping strategies, methods and results, consult the delivery documentation (Evans et al. 2007).

Table 1 shows the details of the individual pointings for all three clouds and the off cloud regions. Figures 19 to 22 show the different coverages of the c2d IRAC, MIPS and optical mosaic areas overlaid on the optical extinction map of Lupus from Cambrésy (1999).

Table 1: c2d Spitzer IRAC Observations summary in Lupus

Field	Position $(\alpha,\delta)_{J2000}$	Date (2004)	AOR epoch 1	AOR epoch 2
Lupus I c2d Observations				
LupI_1	(15:45:09.0, -34:23:11.0)	Sept 3	0005717248	0005719808
LupI_2	(15:43:26.0, -34:06:27.0)	Sept 3	0005717504	0005720064
LupI_2a	(15:42:23.0, -34:00:55.0)	Sept 3	0005717760	0005720320
LupI_3	(15:41:16.0, -33:43:33.0)	Sept 3	0005718272	0005720832
LupI_4	(15:40:08.0, -33:35:16.0)	Sept 3	0005718528	0005721088
LupI_5	(15:38:34.0, -33:20:18.0)	Sept 3	0005718784	0005721344
LupI_6	(15:39:09.0, -34:23:11.0)	Sept 3	0005717248	0005721600
LupI_7	(15:40:34.0, -34:36:34.0)	Sept 3,4	0005719296	0005721856
LupI_8	(15:38:08.0, -34:39:27.0)	Sept 3	0005719552	0005722112
LupI_9	(15:42:18.0, -34:33:50.0)	Sept 3	0005737472	0005737728
LupI_10	(15:40:55.0, -34:06:31.0)	Sept 3,4	0005739008	0005739264
Lupus III c2d Observations				
LupIII_1	(16:12:28.0, -38:05:43.0)	Sept 4	0005724416	0005725696
LupIII_2	(16:10:35.0, -37:50:04.0)	Sept 4	0005724672	0005725952
LupIII_3	(16:11:59.0, -38:58:30.0)	Sept 4	0005724928	0005726208
LupIII_4	(16:10:32.0, -39:07:18.0)	Sept 4	0005725184	0005726464
LupIII_6	(16:07:24.0, -39:07:03.0)	Sept 4	0005725440	0005726976
LupIII_7	(16:12:45.0, -38:31:31.0)	Sept 4	0005737984	0005738240
LupIII_8	(16:10:38.0, -38:35:24.0)	Sept 4	0005738496	0005738752
Lupus III GTO & c2d Observations				
LupIII_5	(16:08:55.8, -39:08:33.2)	Sept 4	0003652608	0005726720
Lupus IV c2d Observations				
LupIV_1	(16:02:46.0, -41:59:49.0)	Sept 4	0005728768	0005729536
LupIV_2	(16:01:27.0, -41:41:00.0)	Sept 4	0005729024	0005729792
LupIV_3	(16:00:43.0, -42:02:37.0)	Sept 4	0005729280	0005730048
Off-Cloud c2d Observations				
LupOC_2	(16:13:00.0, -34:00:00.0)	Sept 4	0005731072	0005735680
LupOC_6	(16:40:00.0, -40:30:00.0)	Sept 4	0005732096	0005736704
LupOC_7	(15:50:00.0, -41:00:00.0)	Sept 3	0005732352	0005736960
LupOC_8	(16:07:00.0, -43:00:00.0)	Sept 4	0005732608	0005737216

The IRAC images were processed by the Spitzer Science Center (SSC) using the standard pipeline version S13 to produce the Basic Calibrated Data (BCDs). These images were then processed and combined into mosaics and source catalogs by the c2d pipeline version 2007/January. Harvey et al. (2006) and Jørgensen et al. (2006) describe in detail the processing of the IRAC images for Serpens and Perseus, respectively. The observations presented here were processed in exactly the same way so we refer the reader to those articles and to the Delivery Documentation for details about the data reduction. Here we will just describe briefly the basic steps carried out to produce the presented images and catalogs.

In total 63384, 138270 and 42737 sources were detected with at least IRAC in Lupus I, III and IV, respectively. Table 2 summarizes the number of sources detected in the three surveyed areas with S/N of at least 5. This corresponds to selecting all sources with detections of quality 'A' or 'B' in any of the IRAC bands from the delivered c2d catalogs. Most of the sources in this catalog can be well fitted with reddened stellar atmospheres from field stars. IRAC bands 1 and 2 are the most sensitive in all three catalogs and produce an average of 7 times more high quality detections than those in IRAC bands 3 and 4. About 300, 400, and 350 sources in Lupus I, III and IV respectively of the four band detections are found to be extended in one or more bands (classified with the "image type" 2 in the c2d catalogs). Our final catalogs contain 2776, 7539 and 2403 four-band IRAC sources in the three Lupus clouds, respectively (see Table 2).

Table 2: Total numbers of IRAC sources detected with S/N $\geq 5\sigma$ in Lupus

	Lupus I	Lupus III	Lupus IV
Detection in at least one IRAC band	63384	138270	42737
Detection in all four IRAC bands	2834	7638	2418
Detection in three IRAC bands	3012	6559	2001
Detection in two IRAC bands	29301	67039	21125
Detection in one IRAC band	28237	57034	17193
Detection in 2MASS only[a]	0	7	1
Detection in IRAC only	56219	122166	37904
Detection in 4 IRAC bands and not 2MASS[a]	136	268	80
Excluding extended sources			
Four band detections	2776	7536	2403
Four band detections with 2MASS association[a]	2637	7244	2262
Detected in IRAC1+2 and 2MASS[a]	6913	15702	4581

[a] A source is counted as detected in 2MASS if it has a S/N of at least 10 in both H and K_s.

Figures 1 to 3 show RGB color-composite images of Lupus I, III and IV respectively,

with IRAC2 band at 4.5 μm in blue, IRAC4 band at 8 μm in green and MIPS1 band at 24 μm in red. The images show the overlapping areas between the mosaics done with both instruments and include the GTO-imaged area in the core of Lupus III at RA $\sim 16^h09^m$ and DEC $\sim$ -39°10′ (Allen et al. 2007). The images show a large and dense concentration of cold dust in the North-West of Lupus I and South of Lupus III. The cloud emissions in Lupus are consistent with the Cambrésy's extinction maps, but now shown in much more detail. A general 8 μm emission gradient coming from the nearby Galactic plane was compensated in the color scales to bring up the cloud structure. The bright green emission to the North-East of the core in Lupus III is likely produced by interstellar PAH molecules, which emit strongly at 8 μm, possibly illuminated by the two bright Herbig Ae/Be stars HR 5999 and HR 6000 in the core.

2.3. Differential source counts

Given the proximity to the Galactic plane and center (see Table 3), the Lupus clouds are expected to show a relatively high number of background stars compared to the other clouds surveyed by c2d. Figures 4 to 6 show the differential source counts for the Lupus regions. Since Lupus I, at +17°, is further from the Galactic plane than Lupus III and IV (at 8–9°) and likewise the two off-cloud fields with both IRAC and MIPS observations are at +4° and +12° closer to the Galactic plane than the on-cloud fields on average, we expect larger differences between the counts of individual regions compared to the other c2d clouds. Figures 5 and 6 therefore separate the Lupus I cloud from the III and IV clouds. The observed differential source counts are compared to the predictions of the Galactic source counts by Wainscoat et al. (1992). In all plots a steady increase is seen in number of sources per magnitude bin up to a break at about 16–16.5 magnitudes in IRAC bands 1 and 2 and 15–15.5 in bands 3 and 4 corresponding roughly to the sensitivity levels of the surveys.

Table 3: Ecliptic and galactic coordinates for the centers of the mapped IRAC regions and their areas.

	(α, δ) deg	(l, b) deg	area deg^2
Lupus I	235.4 ; −34.2	338.6 ; 16.7	1.391
Lupus III	242.7 ; −38.6	340.2 ; 9.4	1.336
Lupus IV	240.4 ; −41.8	336.7 ; 8.2	0.374
OC2	243.2 ; −34.1	343.7 ; 12.4	0.051
OC6	250.0 ; −40.6	342.7 ; 4.0	0.051

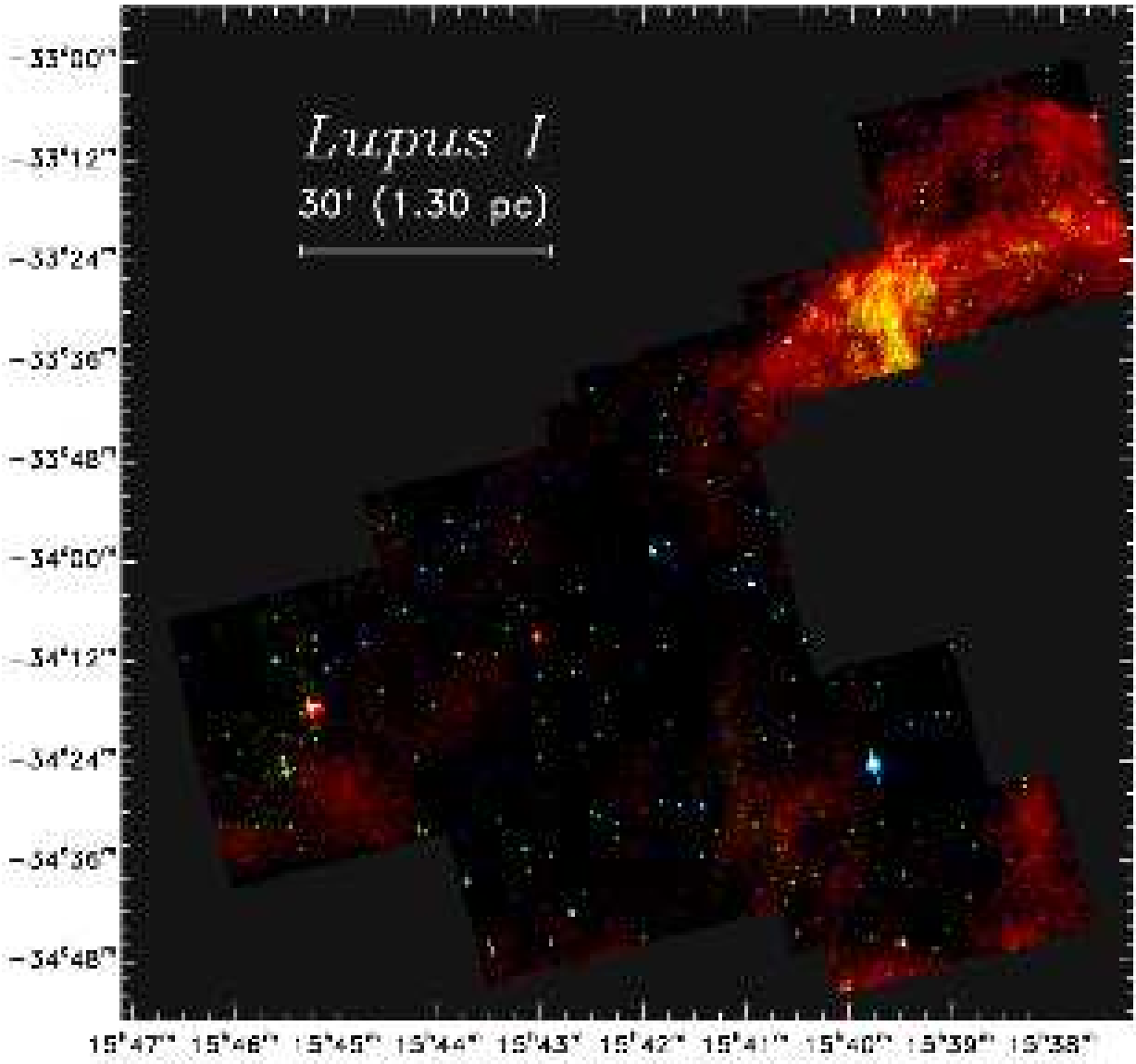

Fig. 1.— Color-composite image of the mapped area in Lupus I by c2d. The color mapping is blue for IRAC2 at 4.5 μm, green for IRAC4 at 8.0 μm and red for MIPS1 at 24 μm. The bright red emission in the North-West of the cloud is produced by cold dust.

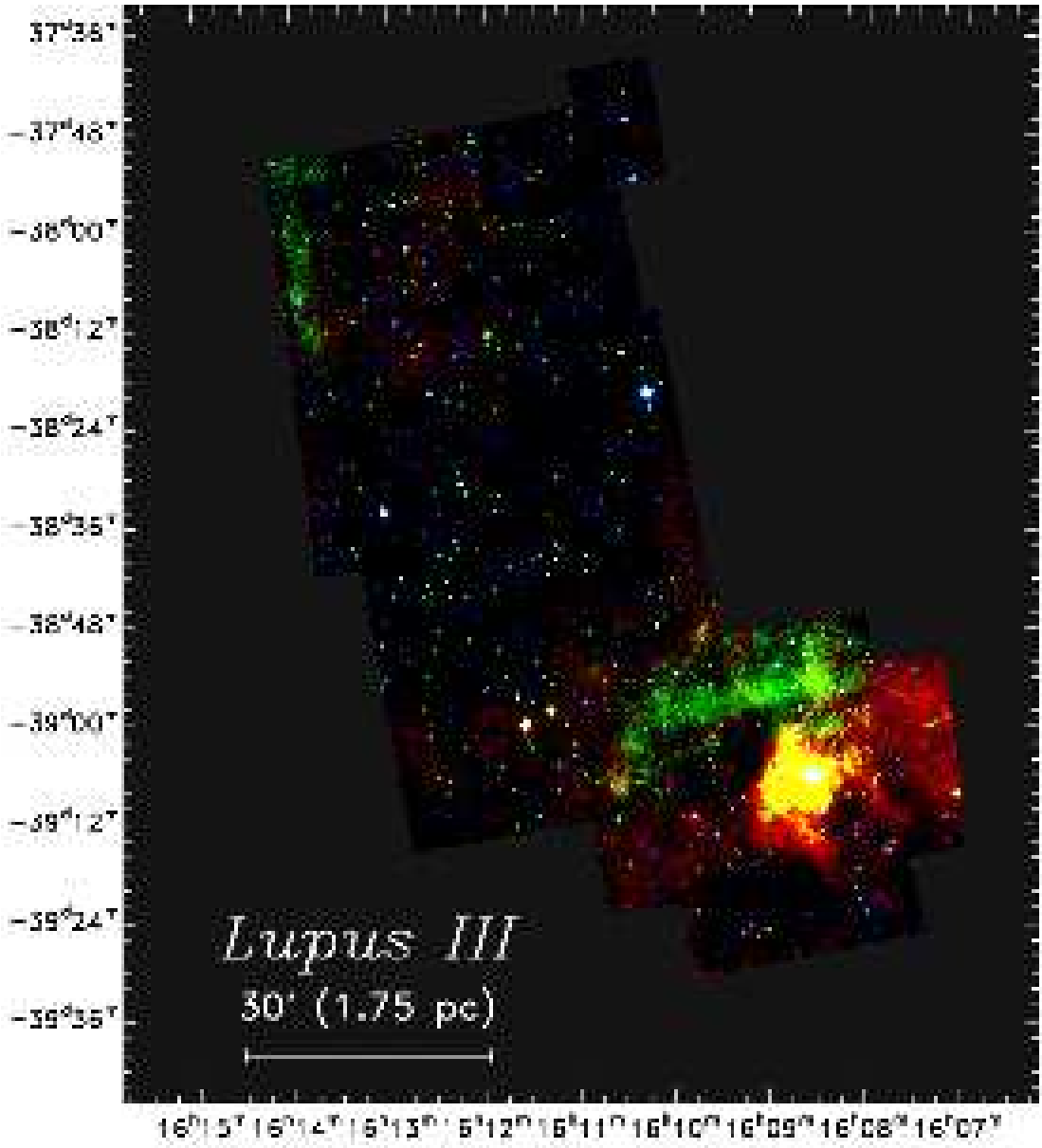

Fig. 2.— Color-composite image of the mapped area in Lupus III by c2d. The color mapping is the same as in Figure 1. The figure shows the very active star-forming core, which contains the two Herbig Ae/Be stars HR 5999 and HR 6000 at RA $\sim 16^h09^m$ and DEC $\sim$ -39°10′ and a stream of PAH emission to the North of the core (RA $\sim 16^h10^m$ – 16^h08^m and DEC $\sim$ -39°).

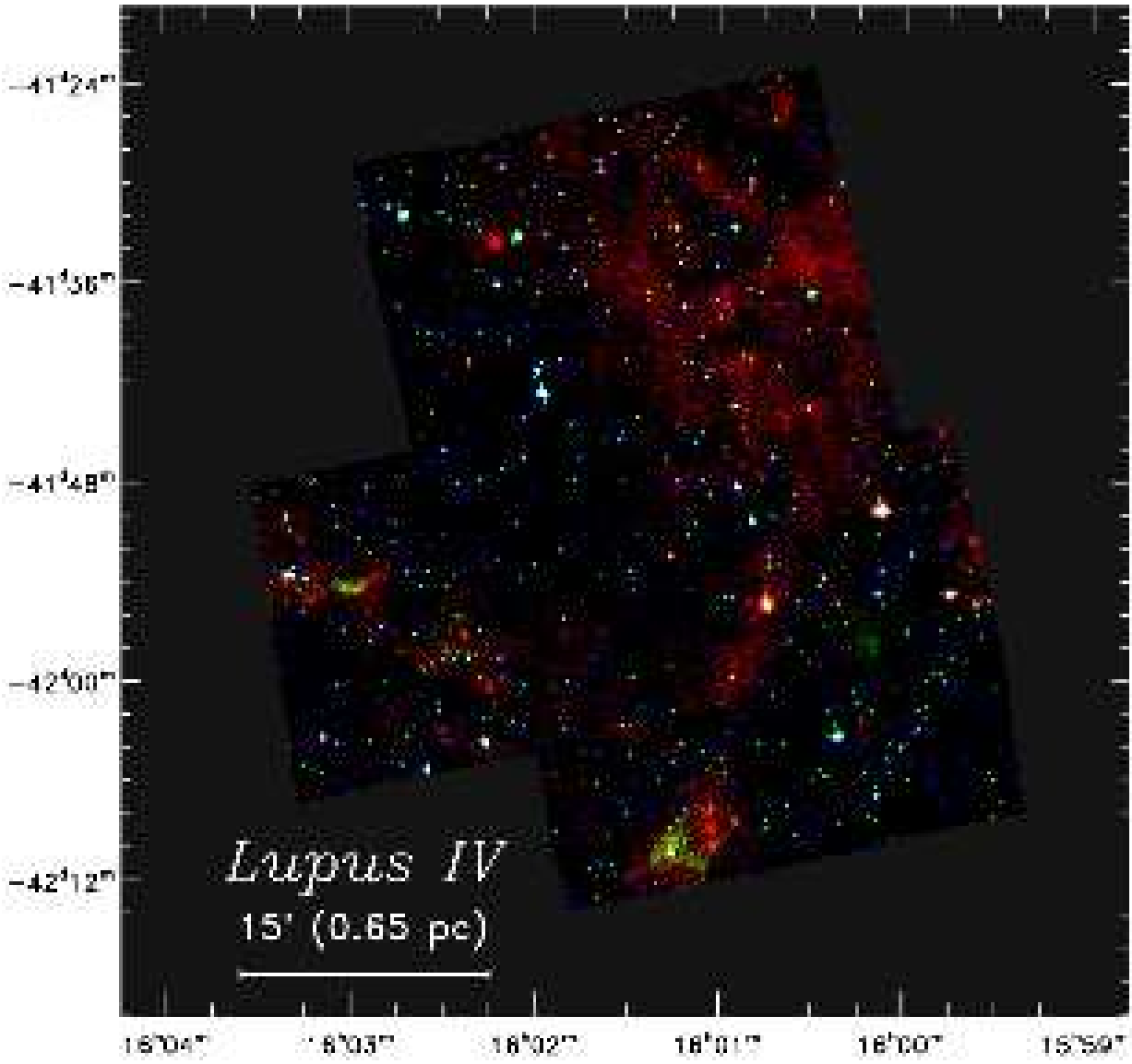

Fig. 3.— Color-composite image of the mapped area in Lupus IV by c2d. The color mapping is the same as in Figure 1. The figure shows the remnant cloud structure emitting at long wavelengths and many young stellar objects covering a large range of evolutionary types. The very red source in the South of the mosaic is the unrelated Planetary Nebula PN G336.3+08.0.

Some interesting differences are seen between the shorter wavelength IRAC bands 1 and 2 compared to the longer wavelength bands 3 and 4. In the shorter bands the match between the on- and off-cloud counts is poor with the off-cloud fields showing significantly more sources in given magnitude bins than do the on-cloud fields; consistent with their proximity to the Galactic plane. The on-cloud source counts are clearly higher in the Lupus III and IV regions than the Lupus I region. In each plot the observed on-cloud source counts at IRAC bands 1 and 2 are traced reasonably well by the Wainscoat model predictions. These effects all suggest that the source counts in the shorter IRAC bands are dominated by background stars as expected. In the longer IRAC bands the situation is slightly different: both the off-cloud and on-cloud source counts are here seen to exceed the predictions of the Wainscoat models at faint magnitudes. Also the difference between the different on-cloud regions internally or compared to the off-cloud regions are found to be smaller than in IRAC bands 1 and 2. This is likely due to the longer wavelength source counts starting to be dominated by the extra-galactic background, which naturally is independent of the Galactic location.

Compared to other c2d clouds, the differential source counts towards the Lupus clouds show a similar behaviour to that seen in Serpens, where the source counts exceed the galactic models in IRAC bands 3 and 4 and match better in IRAC bands 1 and 2 (Harvey et al. 2006). Both clouds are the closest to the direction of the galactic centre, with the Lupus off-cloud fields being the closest of the whole c2d data set (Table 3). The source counts in the Chamaleon II (Cha II hereafter) and Perseus clouds, well away from the Galactic plane, show good matches with the Wainscoat models at all bands (Porras et al. 2007 and Jørgensen et al. 2006, respectively). This illustrates the strong dependence of the source counts on galactic coordinates and suggests the presence of a larger number of mid-IR sources close to the Galacic center than those predicted by the Wainscoat models. Of course, the excess of mid-IR source counts towards the Lupus clouds could also be partially attributed to the presence of YSO's in these clouds in cases where the excesses are larger in the on-cloud than in the off-cloud regions. This would also imply a larger number of YSO's in Lupus III and IV than in Lupus I.

3. Young stellar objects and pre-main-sequence stars in Lupus

This section presents and discusses the complete list of Young Stellar Objects (YSOs hereafter) and Pre-Main Sequence (PMS) stars in the three Lupus clouds, obtained from the new Spitzer observations. The final list of objects is obtained by merging the IR-excess sources from Spitzer (YSOs) with the list of all other known young stars in the clouds from

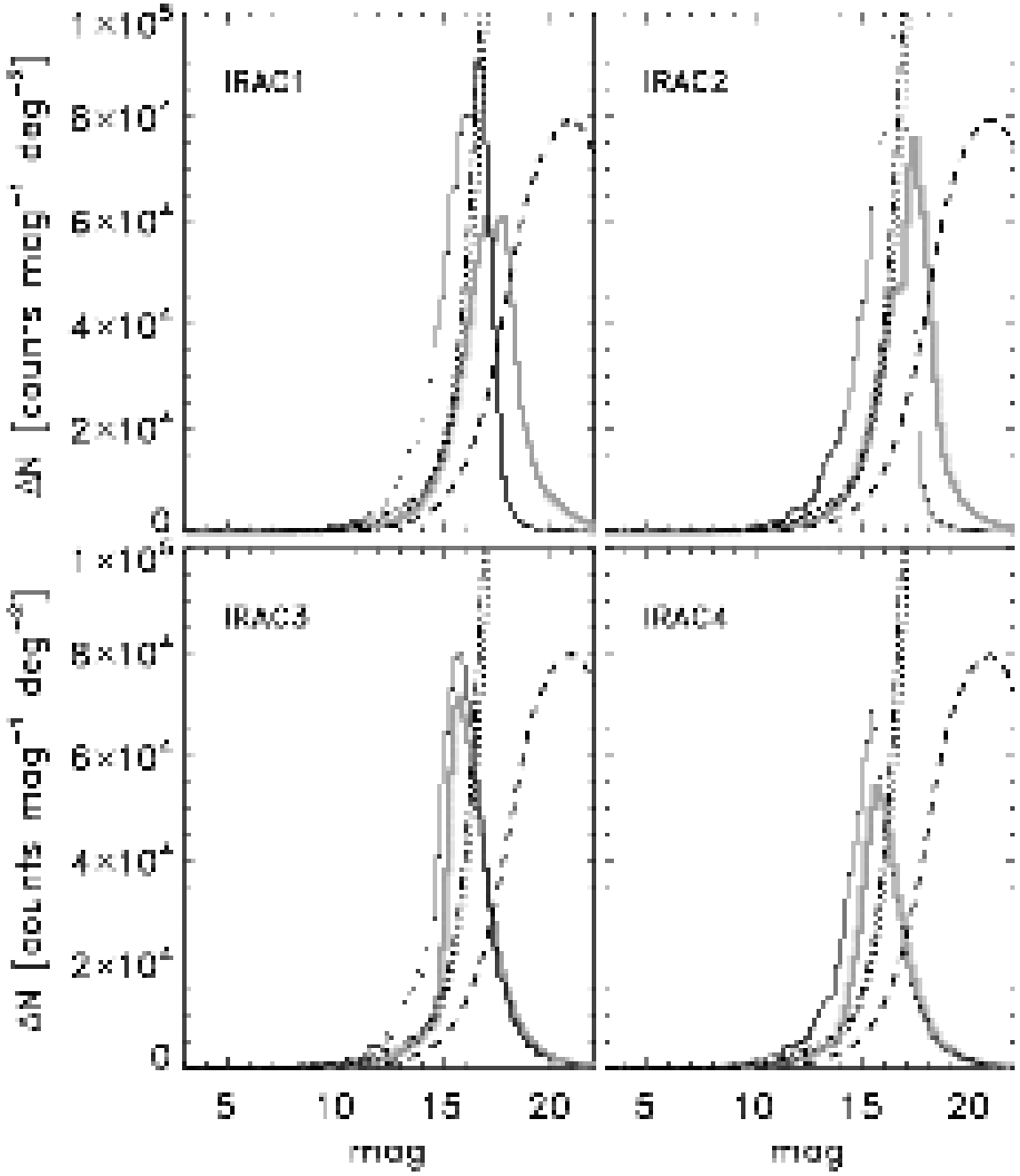

Fig. 4.— Differential source counts for the on- and off-cloud regions (grey and black, respectively). The predictions from the Wainscoat models are shown with the dashed lines for each of the three parts of the cloud (Lupus IV in dot-dashed line, Lupus III in dotted line and Lupus I with dashed line).

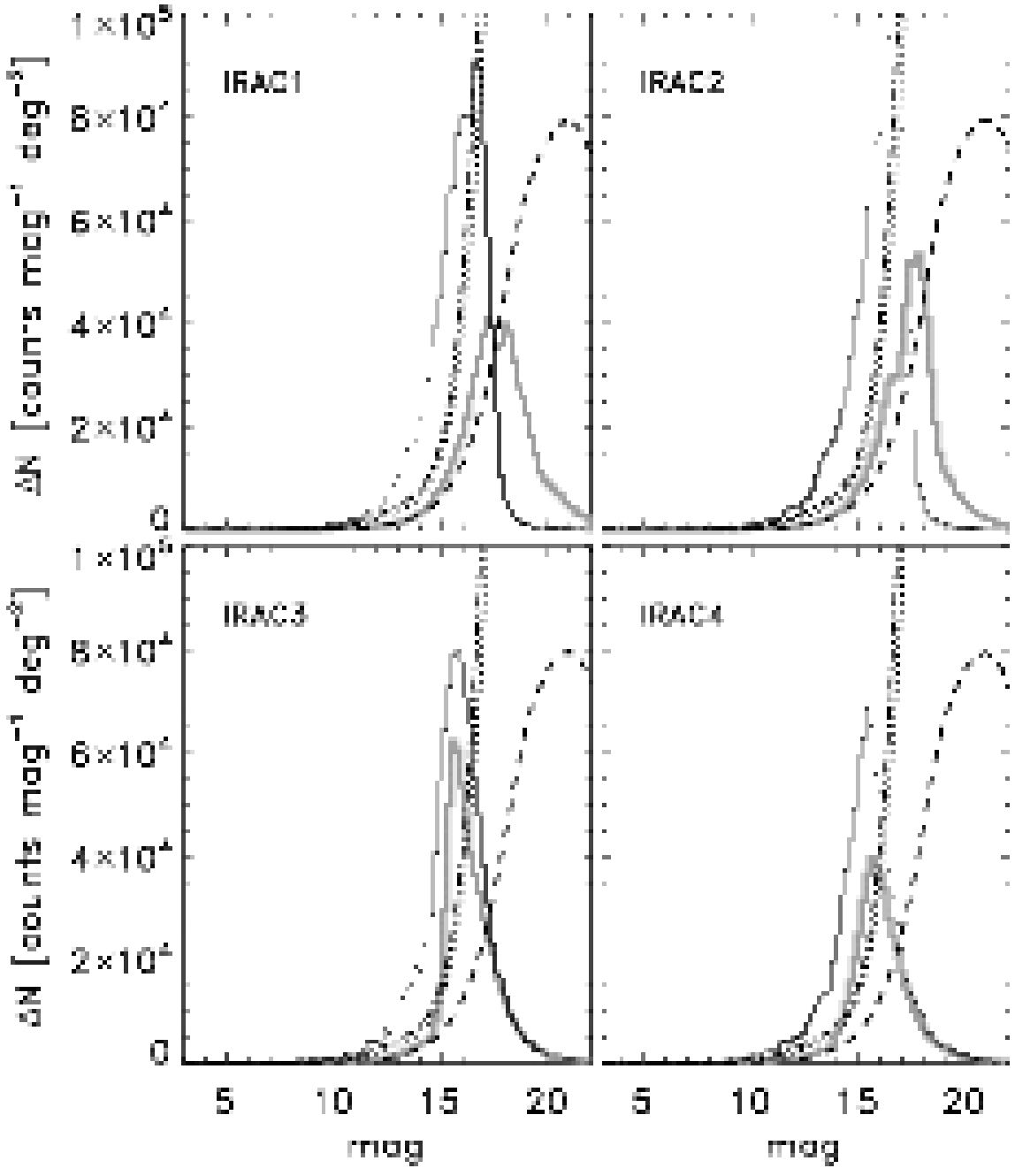

Fig. 5.— As in Fig. 4 but here only for the Lupus I cloud.

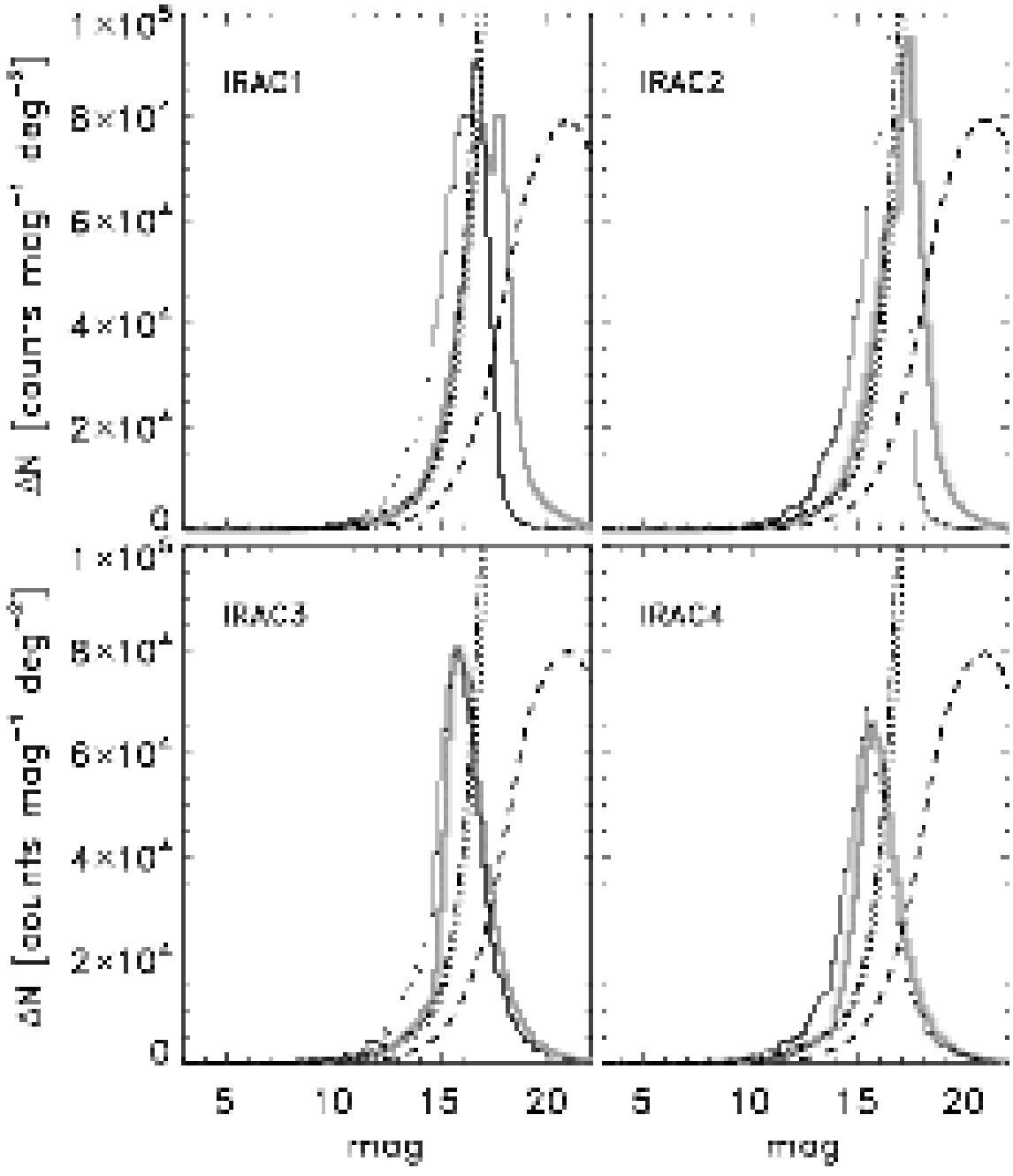

Fig. 6.— As in Fig. 4 but here only for the Lupus III and IV clouds.

previous optical and near-IR surveys inside the Spitzer covered area (PMS stars). These two c2d standards were introduced in Harvey et al. (2007b) and Alcalá et al. (2008). The full list of YSOs and PMS stars is given in Table 9.

3.1. Selection of YSOs with IRAC and MIPS data

We call an object a Young Stellar Object candidate (YSOc) if it appears in the catalog of such objects delivered in the c2d delivery (Evans et al. 2007). This sample of objects was also visually inspected to subtract suspect galaxies and to add obvious YSOs missed by the c2d criteria either because they were too faint at short wavelengths, but associated with millimeter emission, or because they were saturated in the Spitzer images. The objects in the resulting list are called simply YSOs; however some caution should still be exercised.

Complete details on the YSO selection method can be found in the c2d Delivery Documentation (Evans et al. 2007) and in Harvey et al. (2007b), but in short, it consists in the definition of an empirical probability function which depends on the relative position of any given source in several color-color and color-magnitude diagrams where diffuse boundaries have been determined to obtain an optimal separation between young stars and galaxies. For that comparison, the SWIRE catalog (Surace et al. 2004) was "extincted" and resampled to match as accurately as possible the c2d sensitivity limits for each star forming cloud and to provide the statistical color distributions expected for the background galaxies in our fields. The filter also includes a flux cut-off to exclude bright galactic post-AGB stars in the background which resemble Class III objects in the cloud. Figure 7 shows the Spitzer color-color and color-magnitude diagrams used to select the YSOs in Table 9.

The application of this method in the Lupus catalogs yields 18, 69 and 12 YSO candidates in Lupus I, III and IV respectively (shown in Figure 7 as red dots and crosses for point- and extended sources, respectively). Out of these, only 4 (22 %), 26 (38 %) and 2 (16 %) were already known from previous ground-based optical and near-IR observations. This shows that the space observatory, with its highly sensitive detectors, has multiplied by 5, 4, and 6 the number of known YSOs in the three clouds respectively, capturing very low-mass young objects which escaped detection due to low sensitivities and also getting the stars with moderate excess only in the mid-IR which were not identified as excess sources in near-IR surveys.

The optical, IRAC and MIPS images of all the objects in the sample were examined to confirm the point-source nature and to search for blended features or long-period visual binaries. In Lupus I we identified two galaxies, clearly resolved in the optical data, which

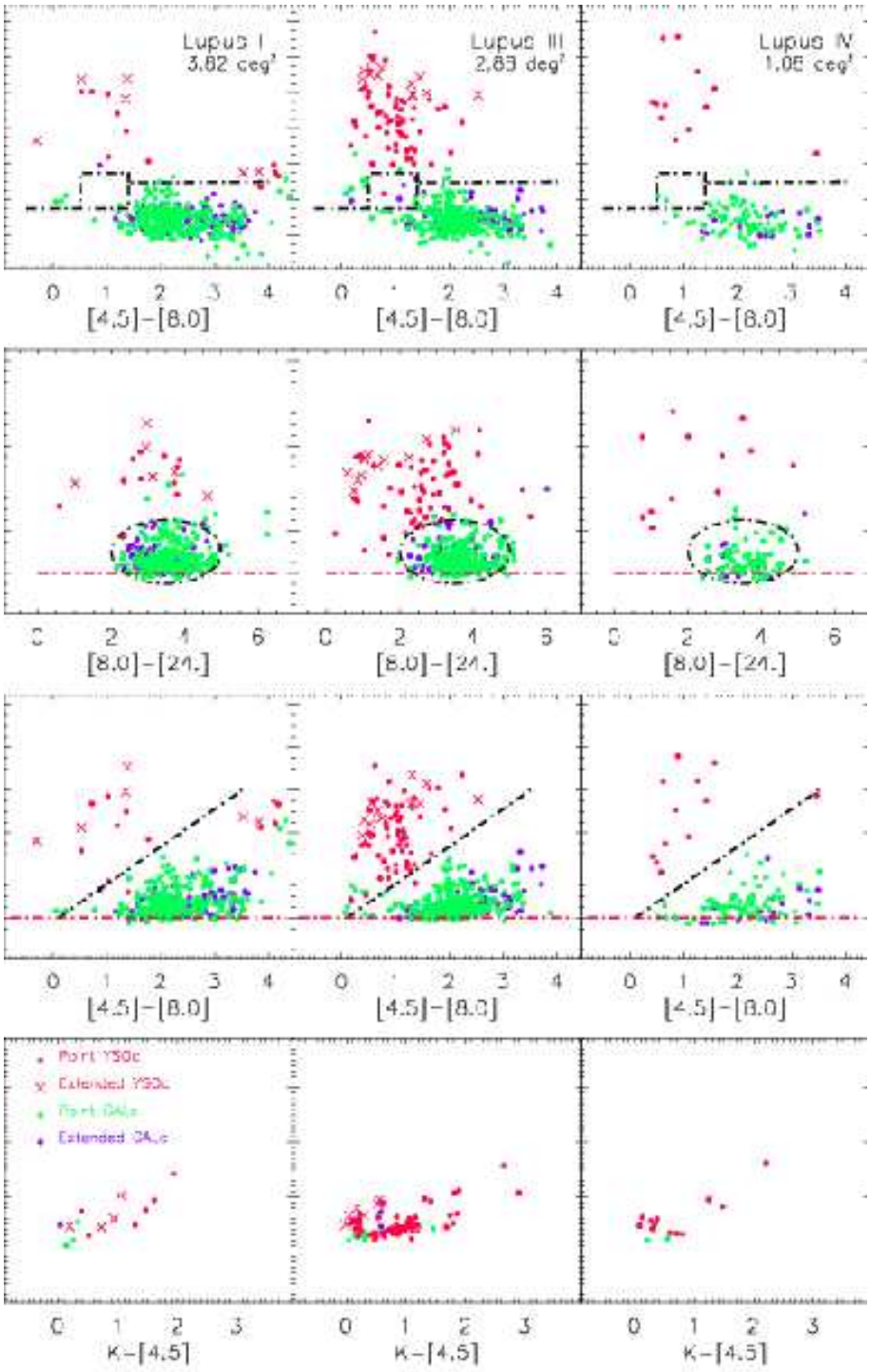

Fig. 7.— Color-magnitude and color-color diagrams for the Lupus I (left), III (center) and IV (right) clouds. The black dot-dashed lines show the "fuzzy" color-magnitude cuts that define the YSO candidate criterion (Harvey et al. 2007b) in the various color-magnitude spaces. The red dot-dashed lines show hard limits, fainter than which objects are excluded from the YSO category.

corresponded to two sources each in the Spitzer bands. Interestingly, all of them were classified as 'YSOc_PAH_em' in the Spitzer catalog of the region, due to their strong 8 μm emission due to PAHs (see the delivery document for a description of these classes). No other resolved galaxies were found in the optical images of all the other YSO candidates in Lupus III and IV. However, a fake source was found in the extended IRAC emission around the embedded object IRAS 15356-3430 (see also § 4.6). These sources were taken off our YSO list and reduced the list of YSOs in Lupus I from 18 to 13.

3.2. Sample of PMS and PMS candidate stars in Lupus

We will use the term Pre-Main Sequence (PMS) star for other objects added to the list whose youth had already been confirmed using other observational techniques, mostly optical spectroscopy. If an object has not been spectroscopically confirmed as young but it was selected by its optical and near-IR photometry as such it will be labeled as a PMS candidate.

We have added to our list the PMS candidates found by Chapman et al. (2007) in the MIPS-only covered area. Because the MIPS coverage was much more extensive than the IRAC coverage, there are sources that have clear excesses over photospheres based on 2MASS and MIPS data, but for which we have no IRAC data (Chapman et al. 2007). They would have been classified as YSOs, but since they cannot be tested against the galaxy filter, we do not include them as YSOs or even YSOc. They are listed as PMS candidates. The embedded class 0 source Lupus3MMS, detected by Tachihara et al. (2007) at 1.2 mm, was added to the YSO sample in Lupus III. This object was detected at all IRAC and MIPS bands, but with too poor S/N in the shorter wavelengths to be classified as a YSO automatically.

Also, we added all previously known members of Lupus cited in Comerón (2008, in prep.), which come mostly from the list of Hα-selected PMS stars in Lupus of Schwartz (1977) after the revisions of Krautter (1991) , Hughes et al. (1994) and Comerón et al. (2003). This only added to our YSO list the PMS stars without any detectable IR excess with good enough S/N. It must be noted that the multi-color criteria described in the previous section already recovered the 28 Classical T Tauri stars in the cloud listed in Comerón 2008 (in prep.) with clear IR excess in the Spitzer wavelength range and good detections in all IRAC and MIPS1 bands and did not select the other 13 from that list that did not show detectable IR excesses. Interestingly, the only two bona-fide CTTs with IR excess but not selected as YSOs by our criteria are in high background emission regions and therefore have bad quality detection in one or more Spitzer bands.

The candidate PMS stars from the previous optical and near- and mid-IR surveys of Nakajima et al. (2000), López Martí et al. (2005), Allers et al. (2006), and Allen et al. (2007) were also added to our list of objects. These sources are labeled as PMS candidates in the "PMS" column of Table 9 and their respective original references are given in column "Sel". The percentages of candidates from these studies that show IR excess in the Spitzer bands are 6/18 (33 %), 5/15 (33 %), 1/3 (33 %), and 16/16 (100 %), respectively. According to this, the Hα narrow-band imaging criteria by López Martí et al. (2005) have a success rate equal to that of the optical and near-IR deep photometric surveys of Nakajima et al. (2000) and Allers et al. (2006). Overall, the small abundance of mid-IR excess sources in these samples is surprising since the all three estimators used to select them are traditional proxies for disk mass accretion towards the central star and should be correlated with the presence of a disk (see § 4 for a discussion on the disks properties). Finally, all the candidates selected by Allen et al. (2007) in the Lupus III core show mid-IR excess since IRAC data from the GTO observations were used to select them but those not classified as YSOs by our criteria fall in the galaxy areas of the color magnitude diagrams and have SEDs difficult to explain with star plus disk models. This comparison with other samples of YSO candidates gives us confidence on the robustness of the c2d color criteria for selecting a reliable set of YSOs in the clouds. In the following sections, we will analyze separately the YSO sample and the total list objects.

Table 4: Total Number of Stars and YSOs in the Lupus Clouds Organized by SED Class.

Lada Class	YSOs			Total		
	Lupus I	Lupus III	Lupus IV	Lupus I	Lupus III	Lupus IV
I	2 (15 %)	2 (3 %)	1 (8 %)	2 (12 %)	5 (4 %)	1 (6 %)
Flat	3 (23 %)	6 (9 %)	1 (8 %)	3 (18 %)	8 (6 %)	1 (6 %)
II	6 (47 %)	41 (59 %)	5 (42 %)	8 (47 %)	56 (45 %)	11 (61 %)
III	2 (15 %)	20 (29 %)	5 (42 %)	4 (23 %)	55 (44 %)	5 (28 %)
Total	13	69	12	17	124	18

Note. — The percentages for each class in the table are calculated with respect to the total numbers at the bottom of each column. The 'Total' population consists of the YSOs plus the PMS stars and candidates (§ 3).

3.3. Class distribution of the sample

The complete sample contains 17, 124 and 18 objects in Lupus I, III and IV, respectively. Table 4 shows the number of objects per cloud and their respective SED classes, as defined by Lada & Wilking (1984) and extended by Greene et al. (1994) (i.e. Class I for objects with $\alpha_{(K-24\mu m)} > 0.3$, Class Flat for $0.3 > \alpha_{(K-24\mu m)} \geq -0.3$, Class II for $-0.3 > \alpha_{(K-24\mu m)} \geq -1.6$, and finally Class III for $\alpha_{(K-24\mu m)} < -1.6$). The table also shows the total number of YSOs, as defined above, for each cloud to facilitate comparison to other c2d clouds where the PMS sample will be obviously different. The number of sources shows that Lupus in general presents a moderate star formation activity compared with the other clouds surveyed by the Spitzer c2d program, only larger than that measured in Cha II (Alcalá et al. 2008). It also shows that amongst them, the most active regions are Lupus III, followed by Lupus I and IV, which present a lower amount of YSOs.

Figure 8 shows the distribution of $\alpha_{(K-24\mu m)}$ values in the three clouds. It illustrates that Lupus III shows a larger variety of objects, from Class I to Class III, while Lupus I has a much smaller number of YSOs relatively rich in Class I and Flat spectrum objects, and Lupus IV shows a clear lack of early class objects. The figure also shows that the addition of spectroscopic or photometric member candidates to the YSO samples mostly adds Class III objects in Lupus III, whose association with the cloud cannot be confirmed until optical spectroscopy reveals youth signatures. This is a selection effect, since Lupus III is the most studied region of the three and illustrates that the difference in percentages between the YSO and the total sample is only driven by different available data and not based on physical characteristics of the stars. For this reason, we will concentrate in the YSO sample on the following discussion, which has been selected as genuine IR-excess objects and therefore likely belong to the star-forming clouds. The analysis below is only valid as a rough indicator of the relative abundances of objects within Lupus. A more solid statistical analysis which combines all the YSO samples in all c2d clouds will be presented elsewhere (N. Evans et al., in preparation).

One interesting difference is that the percentage of Class I and Flat sources compared to the number of Class II and III sources is particularly high in Lupus I, compared to Lupus III and IV. Assuming that the classes correspond to a succession of evolutionary phases from the cores to the disks, this suggests that Lupus I, the least active cloud of the three in terms of YSO abundance, is in a less evolved phase of evolution, while Lupus III and Lupus IV are respectively more evolved than Lupus I.

It is also possible to study the later phases of disk evolution: the percentage of Class III vs Class II plus III (i.e. N(III)/(N(II) + N(III))) YSOs in the clouds (50±25% in Lupus IV, 32±16% in Lupus III and 25±12% in Lupus I) suggests that star formation started

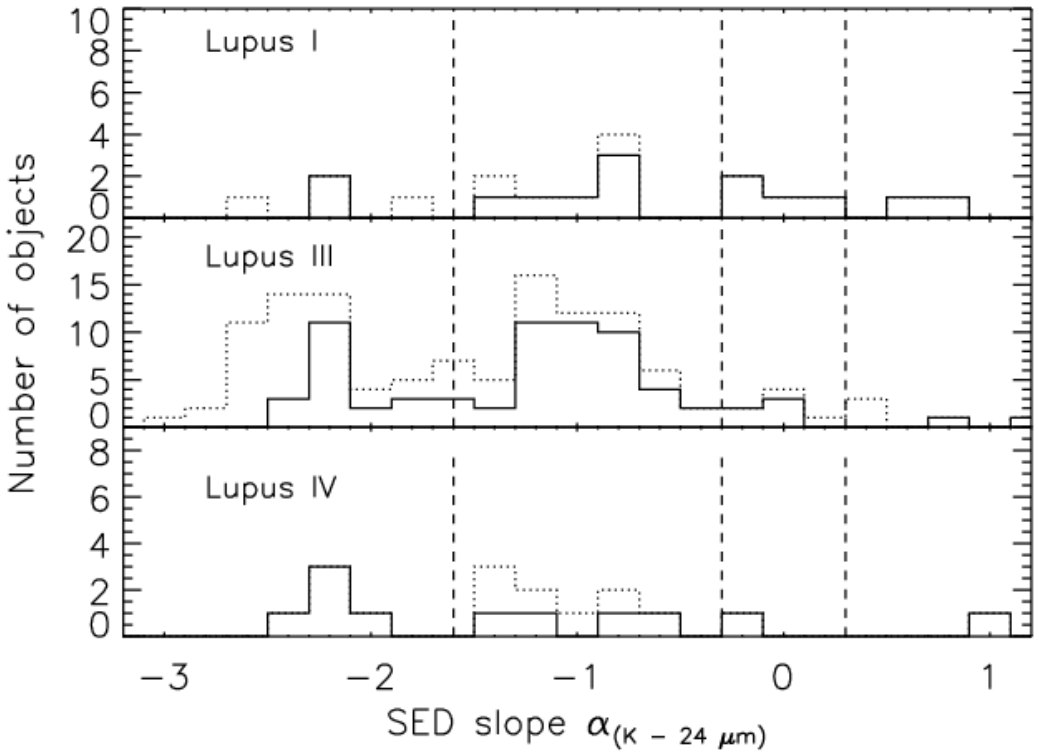

Fig. 8.— Distribution of objects in $\alpha_{(K-24\mu m)}$ for Lupus I, III and IV. Thin lines show the YSO population and dotted lines the total sample of stars. The intervals defining the Lada classes are marked with vertical dashed lines. The comparison illustrates that Lupus I is a region with a small number of YSOs, many of them being early classes, Lupus III contains all kinds of objects, with a great number of Class III sources while Lupus IV contains almost no early class sources and relatively more late classes.

longer ago in Lupus IV than in any of the other clouds. The errors are dominated by the actual number of Class III objects, or alternatively, the completeness of the sample for this kind of objects. Given our selection criteria based on presence of IR excess, the sample will be biased against the Class III objects with little excesses. However, we can estimate the Class III completeness level to be of the order of 50% from the number of spectroscopically confirmed young stars from the 'Sz' catalog which were observed to have detectable IR excess in the Spitzer bands (namely, 13 out of 28). This uncertainty dominates the total error budget of these ratios and let us only conclude significatively that Lupus IV has a larger percentage of Class III objects than any of the other two clouds. Actually, this is the largest number of Class III vs Class II+III sources in any of the c2d studied star-forming clouds (e.g. Harvey et al. 2007b; Alcalá et al. 2008). Comparing Lupus III and IV, which have a similar density of YSOs, these numbers also suggest that the major star-formation activity already took place (and is about to start again, see § 5.1) in Lupus IV, while it is currently taking place in Lupus III, mostly in its very dense star-forming core.

We can confirm our Class III completeness ratio of 50% given above with the list of XMM detections in the Lupus III core by Gondoin (2006), which is deeper than the ROSAT All Sky Survey by Krautter et al. (1997). That survey covers a circular area of 30′ in diameter around the Lupus III core and found 102 X-ray source detections, out of which 25 are associated with optical and IR counterparts. A cross-match of our total list of objects and the list of X-ray detections with a match range of 4 arcsec yielded 24 matches, 13 of which have SEDs indicating the presence of a disk and the remaining 11 showing no IR excess. All stars with associated X-ray emission were labeled in Table 9 with a reference to Gondoin (2006). Assuming that the presence of X-ray emission is a signature of youth, this yields an X-ray disk fraction in the core in Lupus III of 54% which is of the order of the Class III completeness we derived from the independent measurement with the Hα-selected 'Sz' catalog above.

The full list of PMS stars is given in Table 9: columns 2 to 5 give their c2d and previous names of the objects and their coordinates in the Spitzer catalog, column 6 gives the selection source as described above, a flag determining the status of membership spectroscopic confirmation (PMS status) of the object is given in column 7, the Spitzer-derived class based on the SED slope $\alpha_{(K-24\mu m)}$ is given in column 8 and the references to the objects are given in column 9.

4. Individual sources properties

The properties of the circumstellar material surrounding the young stars in Lupus can be studied with the optical to mid-infrared emission in several different ways. We are specifically interested in estimating the overall disk fraction, the amount of circumstellar dust, and the morphology of the circumstellar disks (flared versus flat) which is likely to represent some stage in the formation of planetary systems. The special interest that the new Spitzer data bring to the analysis comes from the fact that the IRAC and MIPS data, due to their wavelength coverage, probe the region in the disks around low-mass stars between ~ 0.1 and 5 AU, where planet formation may take place. Therefore, large samples of Spitzer SEDs of star-forming regions with ages in the critical time-frame between 1 and 10 Myr can be used to study statistically the initial conditions for planet formation.

4.1. Color-Color and Color-Magnitude diagrams

Infrared color-color (CC) and color-magnitude (CM) diagrams are good diagnostic tools for the investigation of circumstellar matter around YSOs in a statistical way (Hartmann et al. 2005; Lada et al. 2006, and references therein). In recent years, several authors have produced grids of YSO models and computed their colors in the Spitzer bands to allow direct comparison with the observations (Whitney et al. 2003; Allen et al. 2004; Robitaille et al. 2006). Both previous data sets and the models roughly agree in the spatial distributions of the objects of different Lada classes in the different CC and CM diagrams although the interplay between the presence or absence of envelopes and disks together with the whole possible range of system inclinations and total interstellar extinctions makes the problem highly degenerate. Therefore it is impossible to associate a position in those diagrams with a physical configuration for individual objects. Robitaille et al. (2006) computed a very large grid of YSOs with a broad range of physical parameters, and inclination angles that can be used to make statistical analyses. In discussing the evolutionary stages of our models, they adopt a "Stage" classification analogous to the Class scheme, but referring to the actual evolutionary stage of the object, based on its physical properties (e.g., disk mass or envelope accretion rate) rather than properties of its SED (e.g., slope). Stage 0 and I objects have significant infalling envelopes and possibly disks, Stage II objects have optically thick disks (and possible remains of a tenuous infalling envelope), and Stage III objects have optically thin disks. Figures 9 and 10 compare three CC and CM diagrams of the Lupus YSO sample with the synthetic colors of a model cluster from Robitaille et al. (2006). To make these comparisons, we have scaled the models to 150 pc in the first case to compare them with the YSOs in Lupus I and IV and to 200 pc to compare them with those in Lupus III.

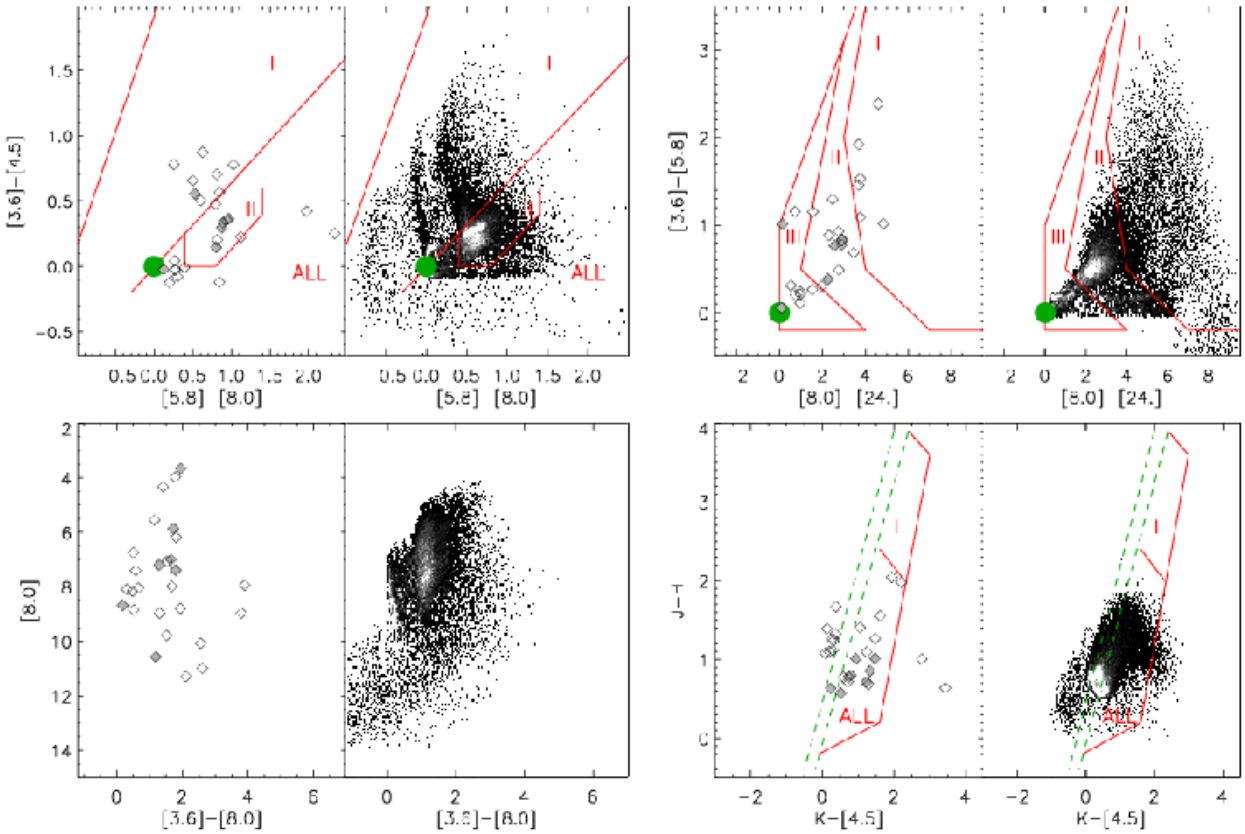

Fig. 9.— The Color-color and color-magnitude diagrams for the spectroscopically confirmed PMS objects (gray filled diamonds) and candidates (open diamonds) with Spitzer and 2MASS data reported in Table 9 in the Lupus I and IV clouds are plotted in the left panels of each diagram. The colors derived from the SED models by Robitaille et al. (2006) are plotted (in gray-scale intensity representing the density of points) in the right panels of each diagram. The areas corresponding to the Stages I, II, and III as defined by Robitaille et al. (2006) are also indicated in each diagram. The label 'ALL' mark the regions where models of all evolutionary stages can be present. The green circle represents normal reddening free photospheres. The PMS stars in Lupus I and IV fall in regions corresponding to Stage I to III sources.

The comparison between the position of the Lupus YSOs and those of the model grids in the [3.6]-[4.5] vs [5.8]-[8.0] CC diagram shows several early Class I and Flat source SEDs in Lupus I and IV (Figure 9), redder in [3.6]-[4.5] than the Stage II objects from Robitaille et al. and a large majority of Class II sources in Lupus III (Figure 10). The position of the maximum density of such kind of objects is also consistent with that predicted by Allen et al. (2004) with a grid of physical disk models of D'Alessio et al. (2005). The [8.0] vs [3.6]-[8.0]

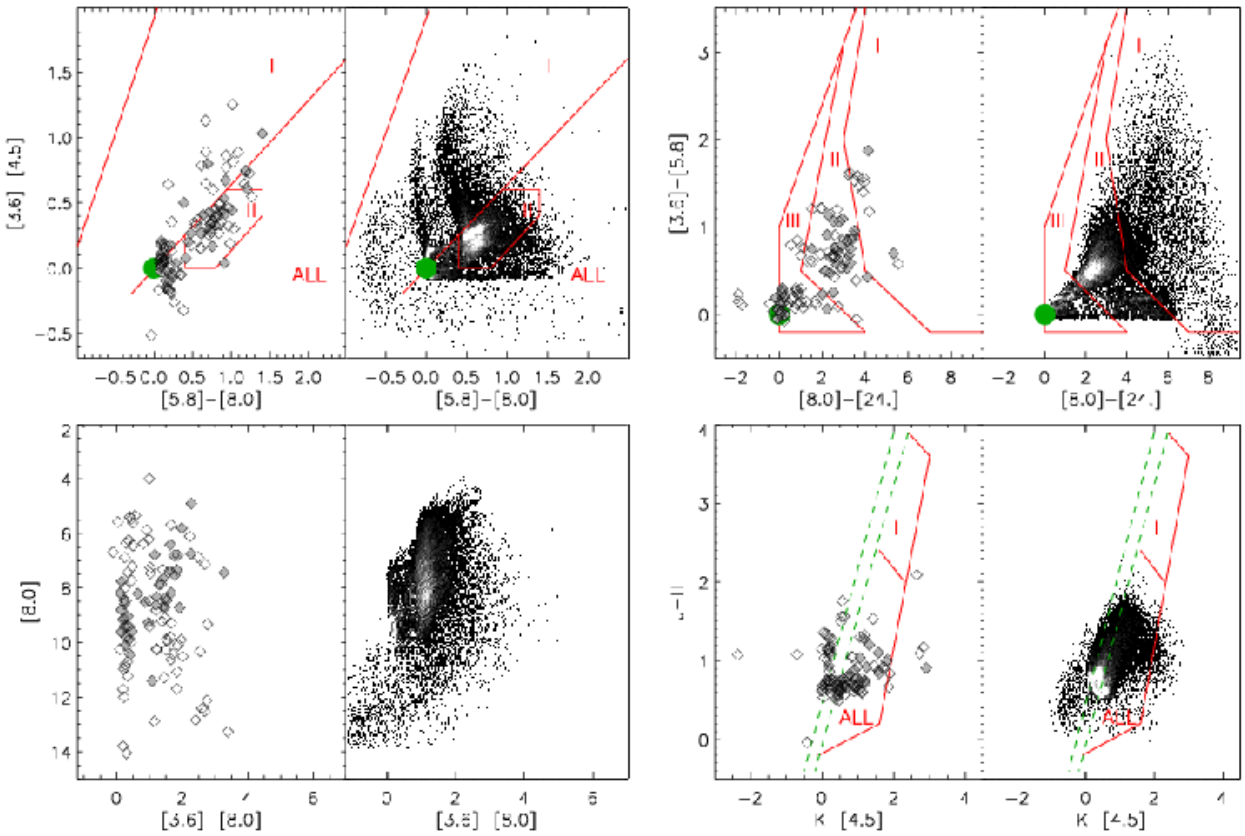

Fig. 10.— Same as figure 9 but with the YSOs in Lupus III.

CM diagram of Lupus III (Figure 10) shows a bimodal distribution with a large number of objects with photospheric [3.6]-[8.0] colors and a range of 8.0 μm magnitudes and another one with a similar range of luminosities and a range of color excesses in the IRAC bands compatible with the presence of moderate to large mid-IR excess. No special difference is found between the distributions of spectroscopically confirmed PMS objects (grey diamonds) and candidate YSOs in any of the diagrams, which suggests that both populations contain indeed the same kind of objects.

4.2. Spectral Energy Distributions

We have constructed SEDs for each source, similar to what has been done for other star-forming regions (e.g., Hartmann et al. 2005; Lada et al. 2006; Sicilia-Aguilar et al. 2006). These allow the full set of multiwavelegth data to be displayed for each source. Figure 11 shows the SEDs of all Class I and 'Flat' sources in the sample. For all objects, the c2d

catalog provides the 2MASS near-IR magnitudes and the IRAC1-4 and MIPS1-3 fluxes. We have added all the complementary data described in § 2.1 plus IRAS fluxes from the PSC and 1.3 mm fluxes from Nuernberger et al. (1997). The open dots are the observed fluxes and the Spitzer data have been highlighted in grey to compare with previous observations.

Figure 12 shows all the SEDs for the Class II and III objects in the Lupus sample for which there was sufficient data to make a good fit to a stellar SED and characterize the stars and disks separately. Two different procedures were applied for the SED fits: for the objects with known spectral types, marked as 'PMS' in Table 9, we obtained the best-fit visual extinction A_V by fitting all photometry between V and J to the stellar NEXTGEN models (Hauschildt et al. 1999). This method provides very good agreement with the traditional use of the $R_C - I_C$ color, as compared with the results by Alcalá et al. (2008). The χ^2 minimization is extended to try all spectral types between A0 and M9 and all visual extinctions A_V between 0 and 30 magnitudes for the new YSOs for which there is no spectral type available in the literature. This technique is similar to that used by Spezzi et al. (2007b, in preparation) with the c2d Cha II sample, and provides agreement within ± 200 K in the effective temperature when applied to objects with known spectral types and moderate extinctions. Once the spectral type and extinction are computed for the sample, the observed fluxes are dereddened with the extinction law by Weingartner & Draine (2001) with $R_V = 5.5$ and fitted to the appropriate NEXTGEN stellar atmosphere models. The sample of SEDs of stars from the Schwartz catalog (Sz) was also compared with the SED fits made by Hughes et al. (1994) and there is in general good agreement in the resulting dereddened stellar and disk energy distributions. The resulting spectral types and extinctions, together with their corresponding references are given in Table 11.

The SEDs show considerable variety. A useful classification system has to rely on disk models which are again degenerate in several parameters as e.g. the inclination angle of the disk or the degree of dust processing of the disk. Therefore, we will not attempt a full characterization of the SED types in this section but rather define four types of objects and give their frequencies in the sample. To help with the classification, we have plotted with a dashed line the median SED of the Classical T Tauri stars (CTTs) from Taurus (D'Alessio et al. 1999) normalized to the optical dereddened fluxes of all the low-mass stars. Based on this comparison benchmark, we can identify the systems whose colors from optical to the millimeter follow closely the decaying slope of a classical accreting optically thick disk around a low-mass star (e.g. Sz100 or SSTc2d J160901.4-392512). We will call these systems 'T'-type, for T Tauri. We then call 'L'-type (from 'low' IR excess) all those objects where the IR excess is clearly smaller than the median SED of a CTTs (e.g. ACK2006-19). These are what Lada et al. (2006) call the 'anemic' disks. We call 'H'-type objects, those systems with higher IR fluxes than those of the median CTTs SED (e.g. 2MASS J16081497-

3857145). Finally, we will call 'E'-type from *empty* the spectrally confirmed young stars in the clouds where no IR excess at all is detected in the Spitzer bands (e.g. Sz 67). These are systems with a very little amount of cold dust or "debris"-like disks (see also some in Sicilia-Aguilar et al. 2006 and Lada et al. 2006).

These classifications are given in Table 11 for each system. Considering the whole sample of YSOs and PMS stars and candidates in Lupus, 22±10% of them are 'T'-Type, 39±18% are 'L'-type, 6±2% are 'H'-type, and 19±8% are 'E'-type. The remaining 20% are the Class I and Flat SED sources. The large errors in this percentages come from the difficulty in classifying the borderline cases if we take into account the implicit uncertainties in the fitting process of the dereddened photometry to the stellar photospheres and from the completeness estimation for disk-less members presented in § 3.2. We can consider a negligible amount of 'H'-type objects, likely due to source variability at different wavelegths and problems with the stellar normalization. From the remaining sample, approximately 40% show 'L'-type SEDs, 20% show 'T'-type SEDs and another 20% show 'E'-type SEDs. The large pertentage of 'L'-type objects in Lupus is consistent with that found in Serpens (Harvey et al. 2007b) and suggests more evolved inner disks in these objects compared to the initial inner disk confguration in the T Tauri stars. This percentages contrasts interestingly with the 30% of 'T'-type and 20% of 'L'-type SEDs found in the older 3 Myr star-forming cluster IC 348 by Lada et al. (2006). These different disk populations in different clouds could be related to different environmental conditions (e.g. clustered vs extended star-formation), to a different stellar population (abundance of low-mass vs high-mass stars) or alternatively to a faster evolutionary time-scales for the less flared 'L'-type disks. More samples of disks will be needed to pursue this research, which is outside the scope of this paper.

One fifth of the sample are 'E'-type stars and this gives an overall disk fraction for the Lupus clouds of 68% to 81%, depending on whether the assume a 50% completeness ratio for diskless stars of or not. This range of values matches well with other disk fractions calculated for 1 to 2 Myr-old star forming regions with near and mid-IR data (Haisch et al. 2001; Sicilia-Aguilar et al. 2006), including Cha II (Alcalá et al. 2008). The 'E'-type objects in Lupus show photospheric IRAC and MIPS fluxes which indicate that the stars do not have any circumstellar dust out to a distance of at least 50 AU, depending on the stellar luminosity (see e.g. HR 6000, Sz 119 or Sz 124). Once spectroscopically confirmed as young members of the clouds and therefore with ages < 3 Myrs, they will provide very valuable constraints to the disk dissipation time-scales and mechanisms and will be the subject of a separate study.

Also interestingly, the Spitzer data of a subsample of the 'L'-type objects show a very peculiar SED, with almost photospheric IRAC and MIPS1 fluxes typical of Class III sources,

and a MIPS2 excess flux at 70 μm comparable to those of the CTTs. This subgroup has been labeled 'LU' in Table 11 and contains the objects SSTc2d J154240.3-341343, Sz 91, and Sz 111. It represents a 2±1% of the young population in Lupus. Similar objects have been found in Serpens (Harvey et al. 2007b) and Cha II (Alcalá et al. 2008) and seem to be extremely rare. These objects, called cold disks (Calvet et al. 2005; Brown et al. 2007), are interpreted as optically thick disks with large inner holes of several to tens of AUs, where potentially planets could be currently forming. However, both the objects in Lupus and the star ISO-ChaII 29 in Cha II (Alcalá et al. 2008) are different from previously known systems of this kind in that the long wavelength at which they show the sizable excess (70 μm) implies larger inner holes of up to 70 AU, while previously known objects show excess already at 24 μm, implying inner holes smaller than 50 AU.

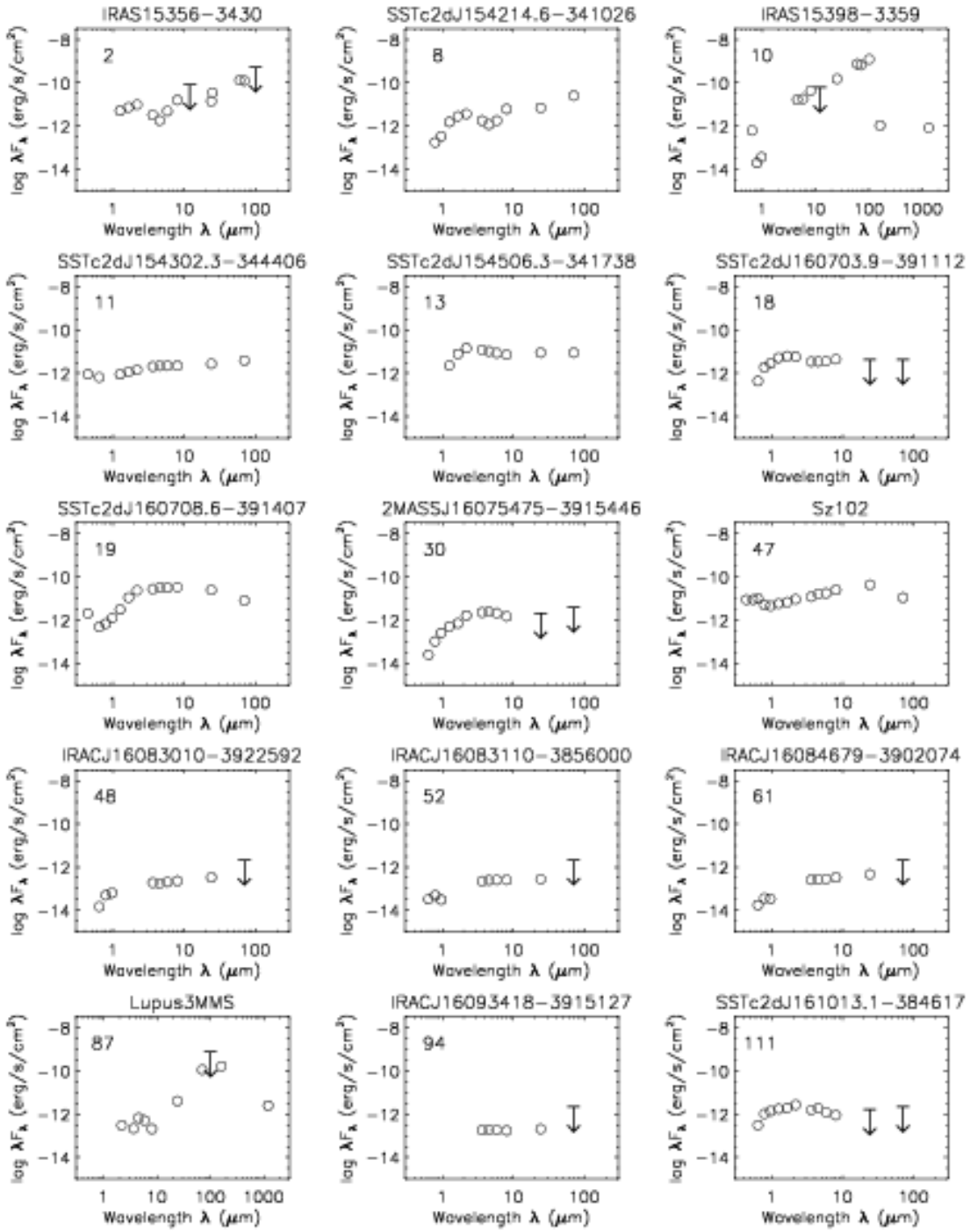

Fig. 11.— Spectral energy distributions of the Class I and Flat SED PMS objects and YSOs ordered by RA and labeled with their name and ID as in Table 9. Only the observed fluxes are plotted with open dots and upper limits with arrows. The new Spitzer data are shown in grey to distinguish them from previous data.

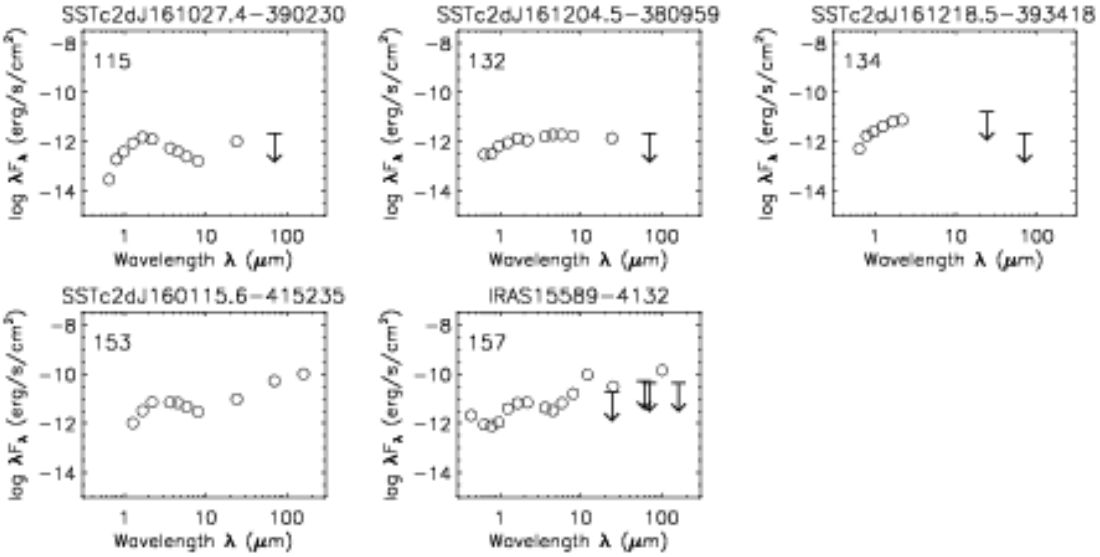

Fig. 11 - Continued

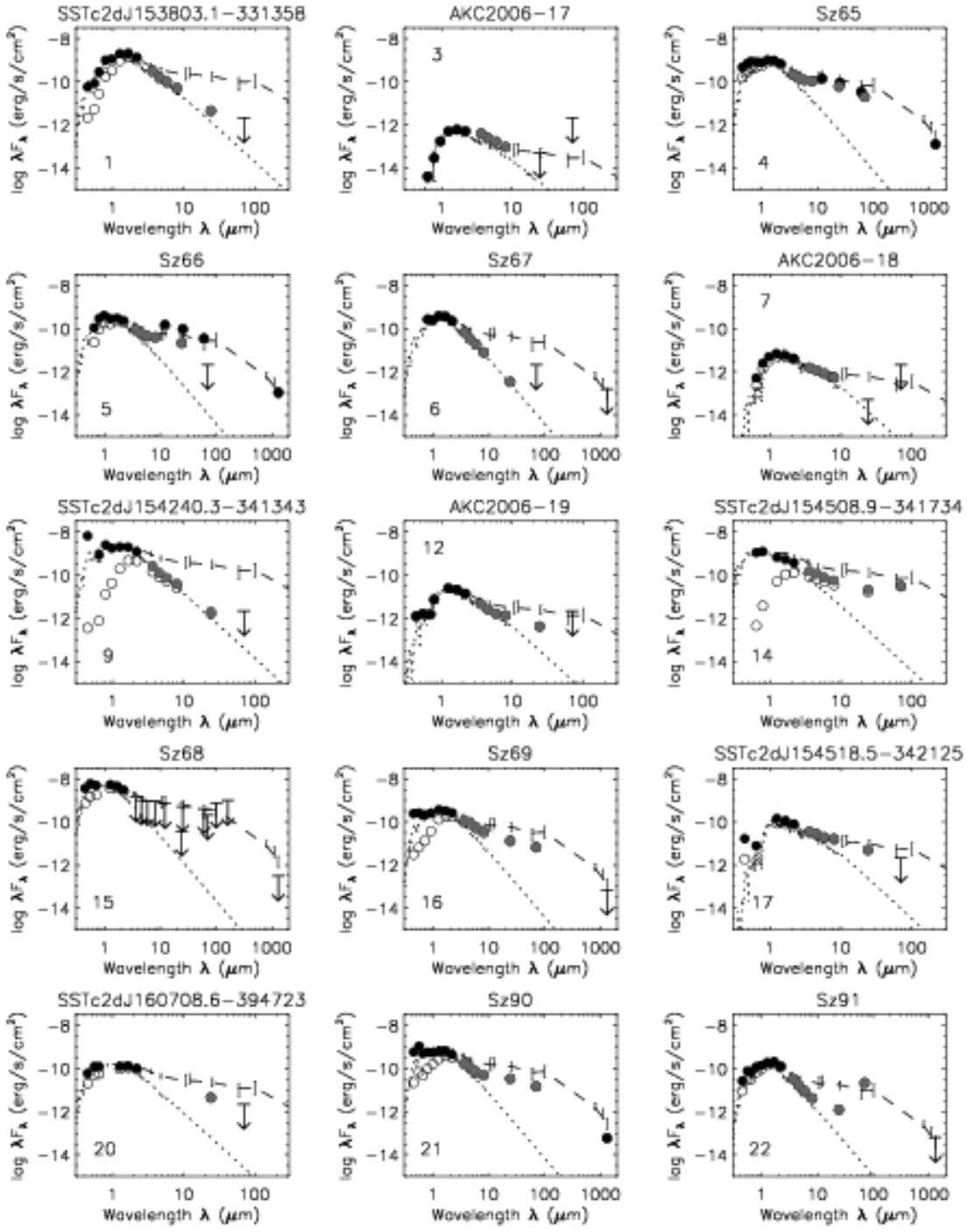

Fig. 12.— Spectral energy distributions of the Class II and Class III PMS objects and candidates ordered by RA and labeled with their names and ID as in Table 9. The observed, dereddened fluxes and upper limits are represented with open and solid dots and arrows, respectively. The plotted error bars are usually smaller than the symbols. NEXTGEN stellar models for the spectral type of each star are shown in dotted lines. For all low-mass objects, the median SED of the T Tauri stars in Taurus from D'Alessio et al. (1999) is shown normalized to the stellar photosphere in dashed line for comparison.

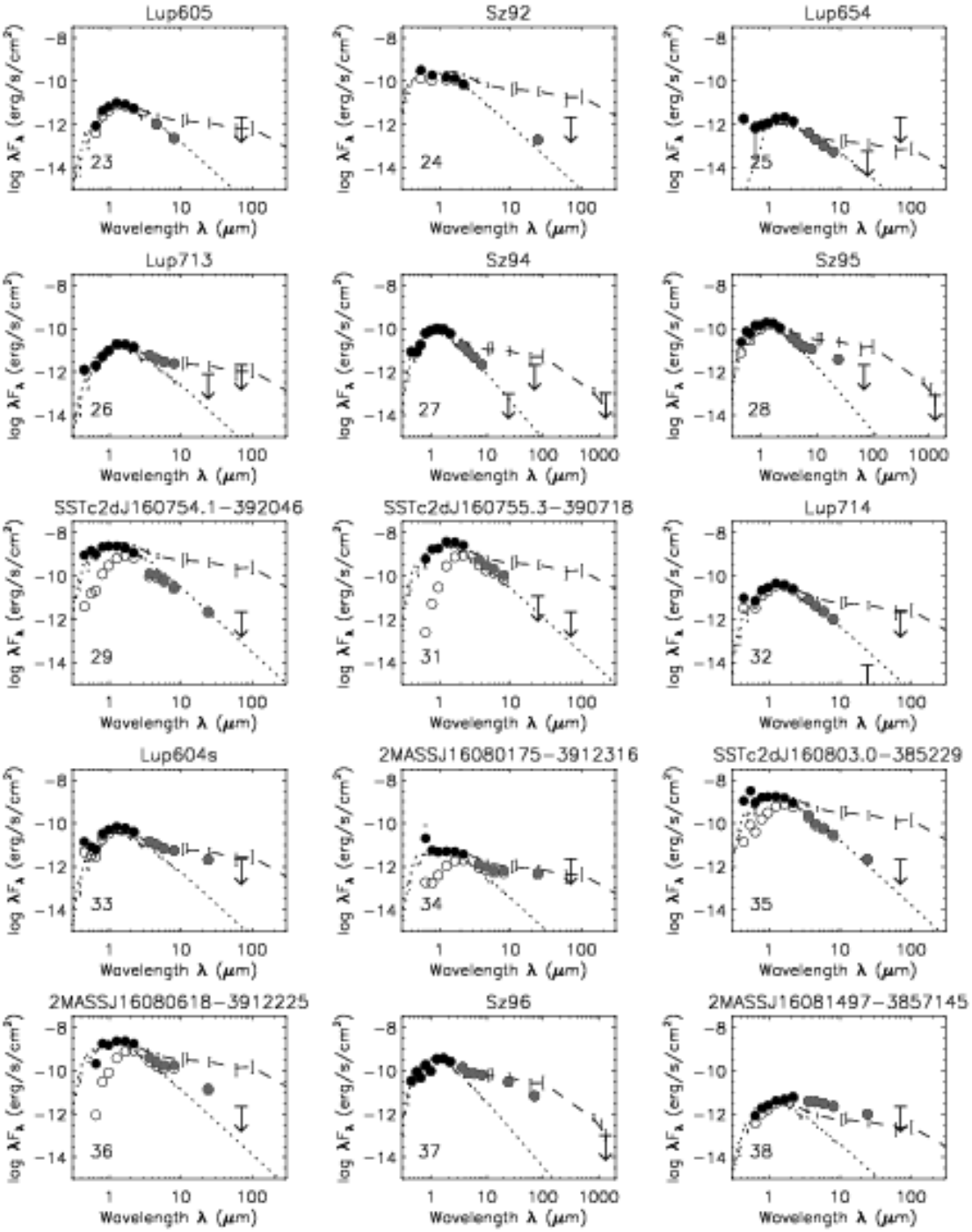

Fig. 12 - Continued.

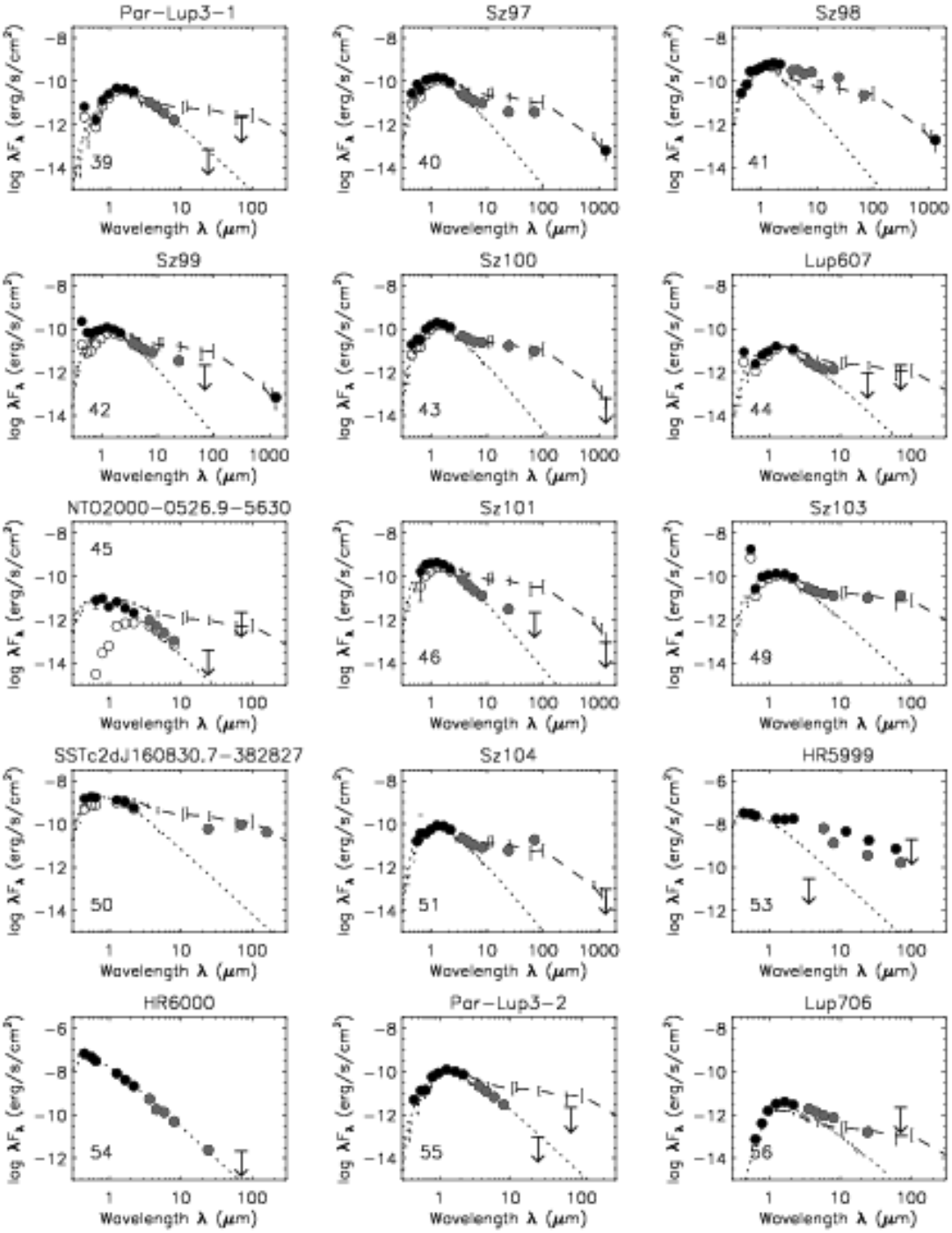

Fig. 12 - Continued.

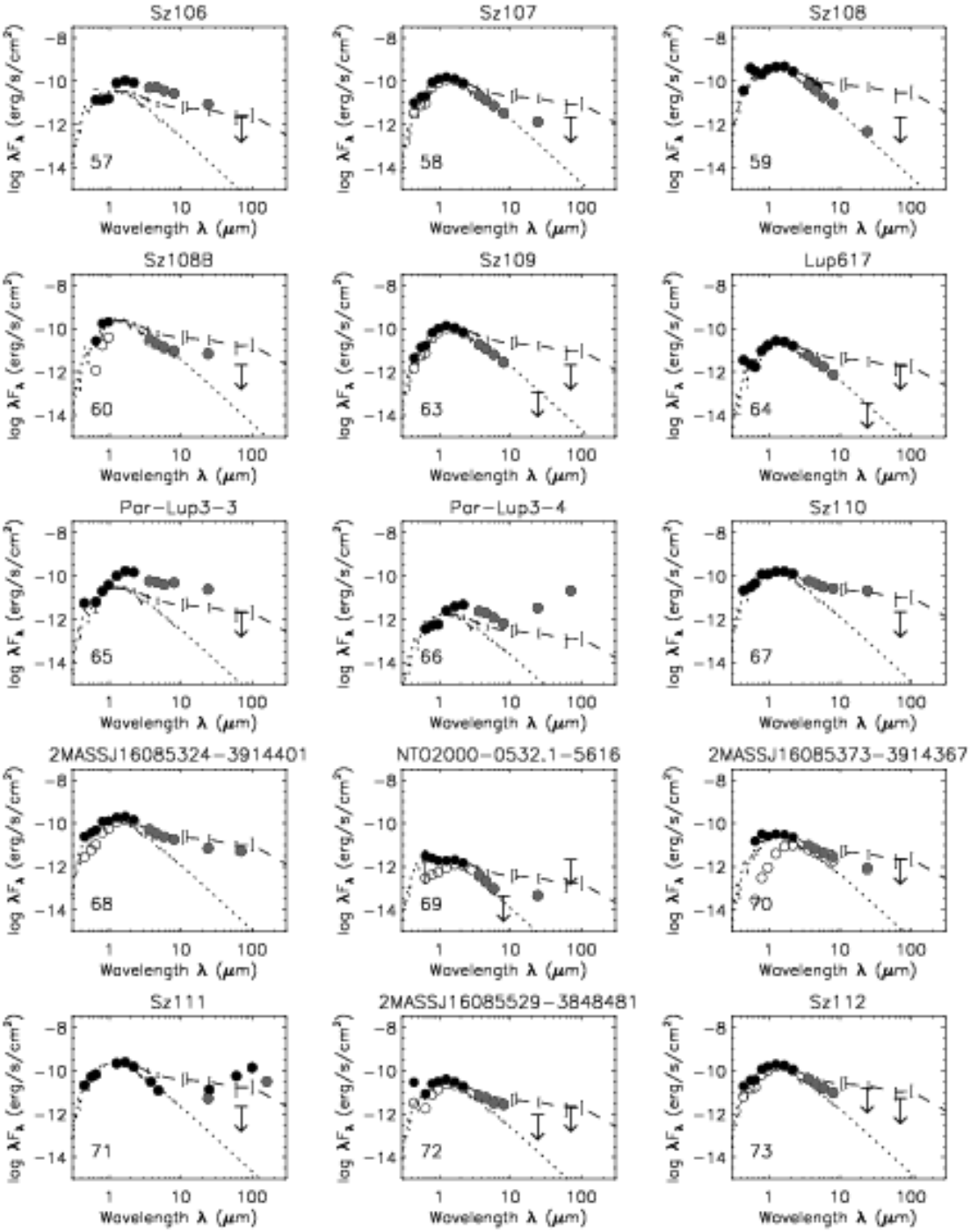

Fig. 12 - Continued.

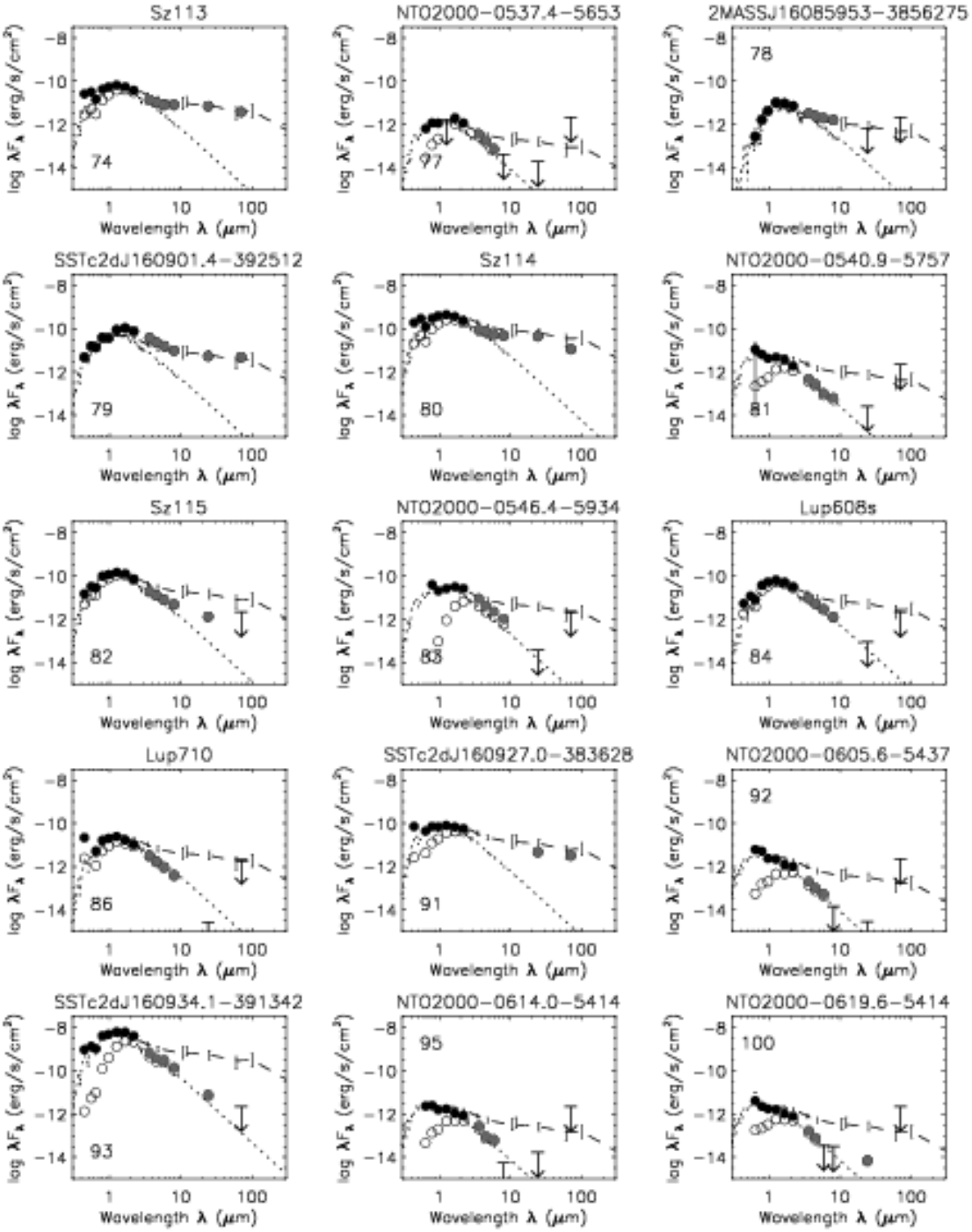

Fig. 12 - Continued.

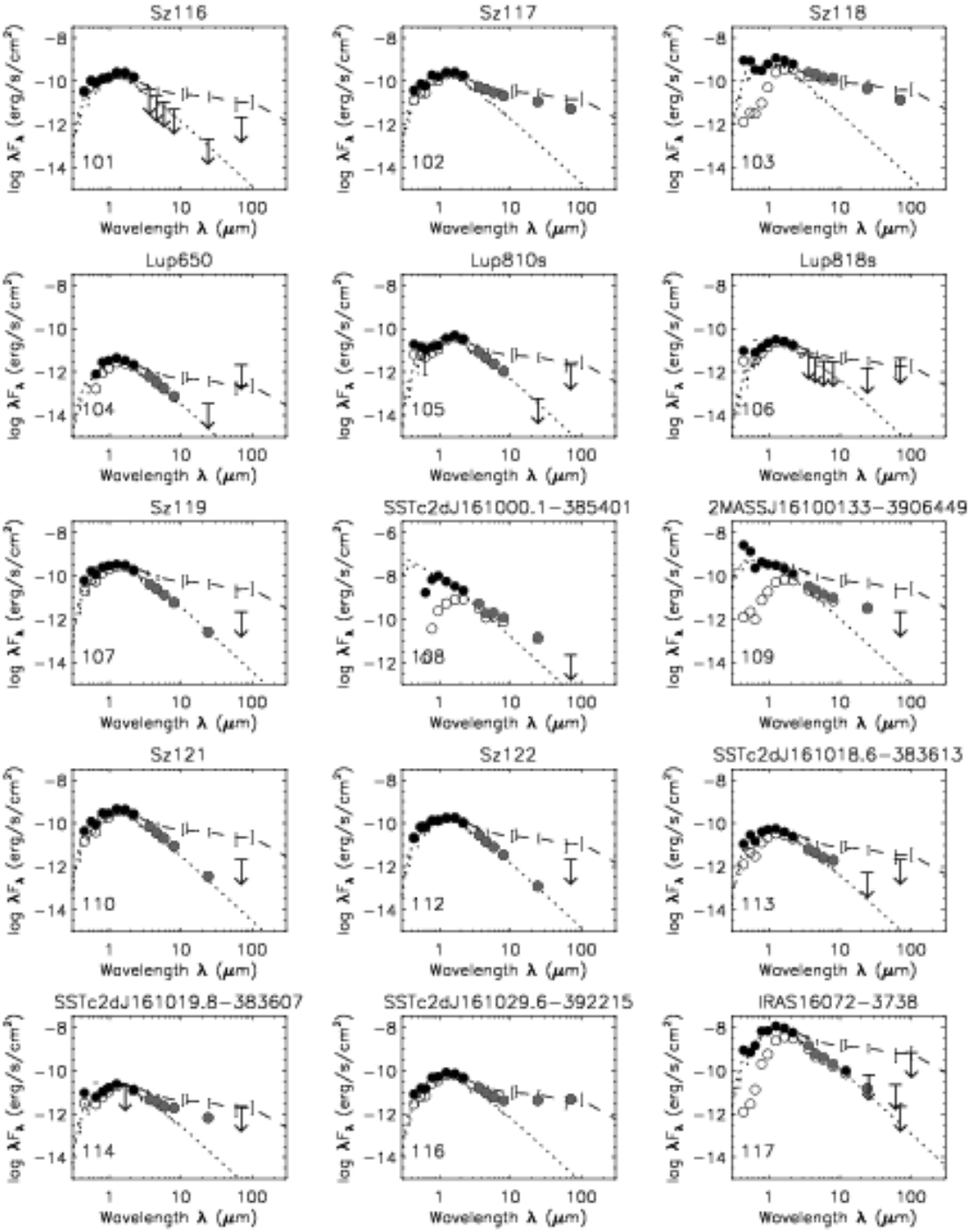

Fig. 12 - Continued.

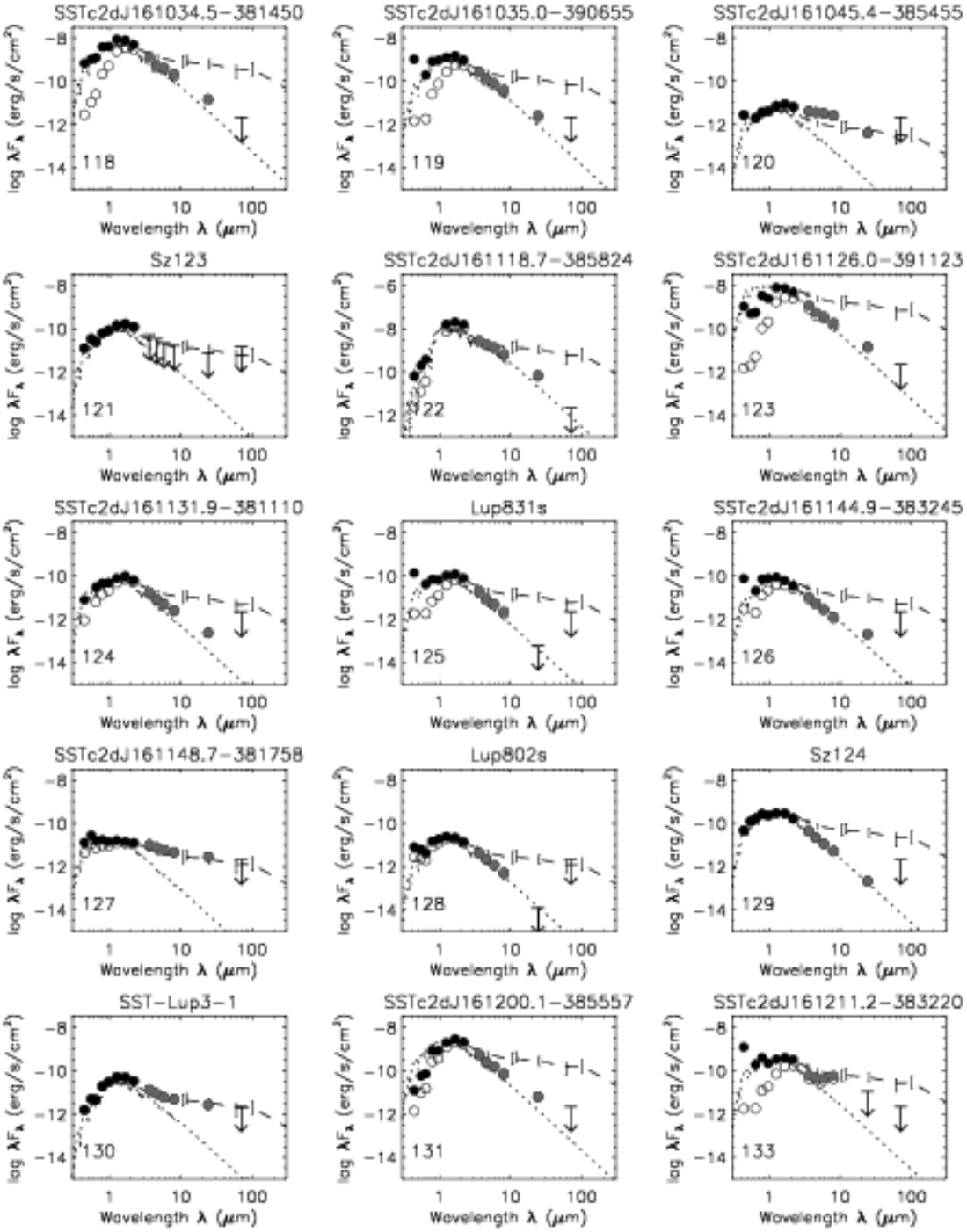

Fig. 12 - Continued.

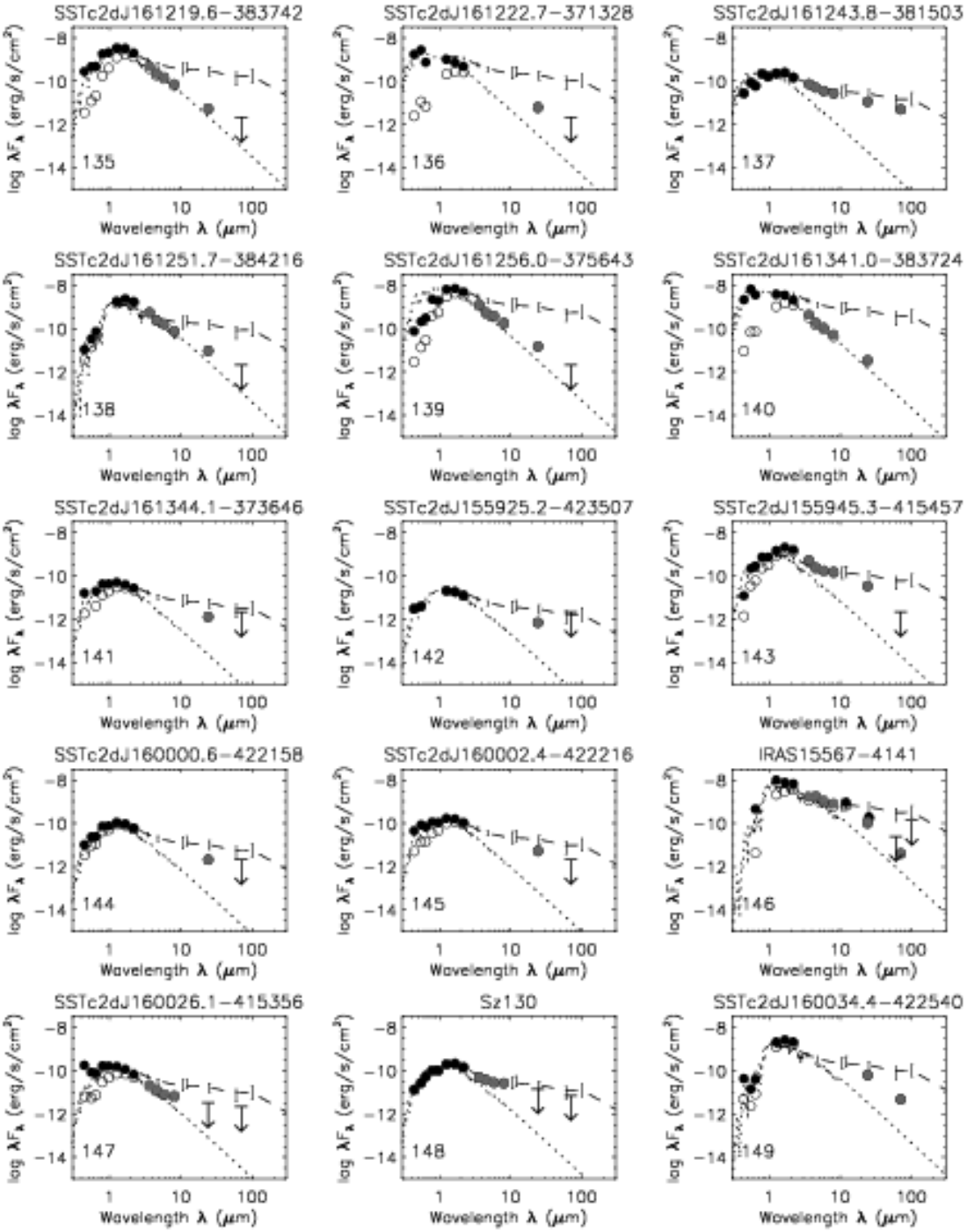

Fig. 12 - Continued.

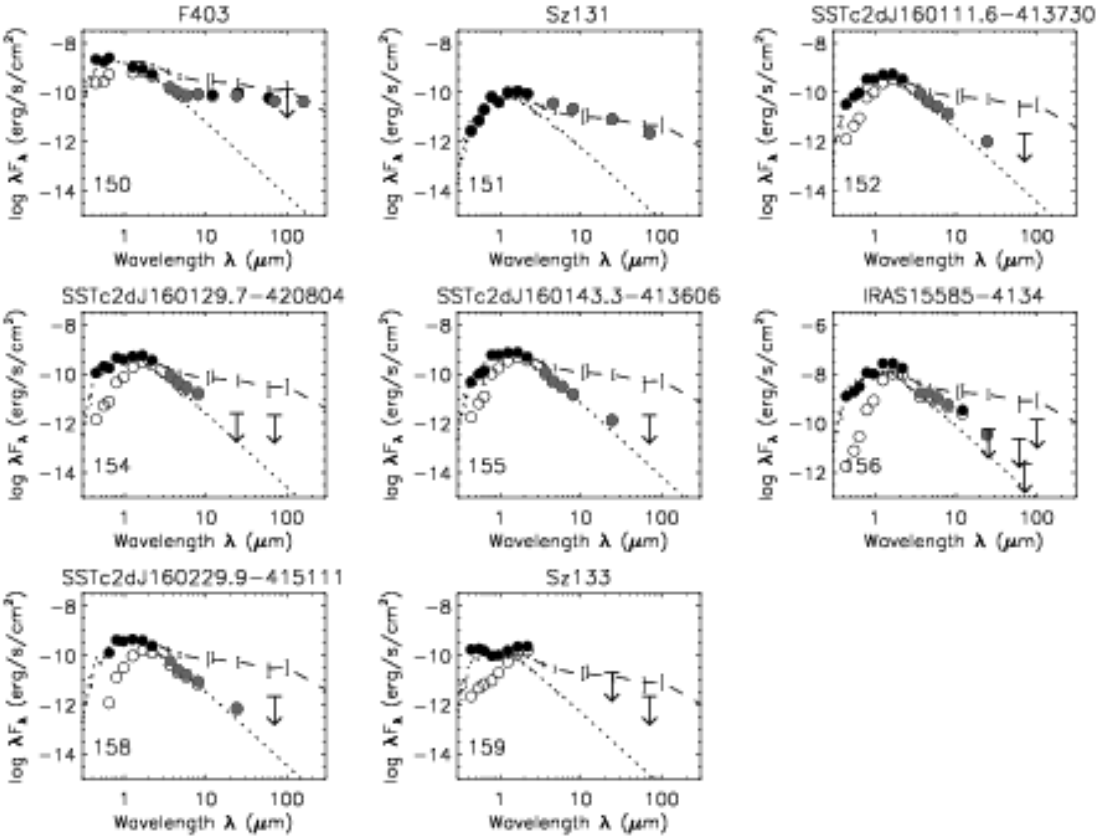

Fig. 12 - Continued.

4.3. The luminosity function in Lupus

A basic step in the characterization of the PMS population is the determination of its degree of completeness in the effective temperature and luminosity scales, which might be correlated in those objects that formed more or less simultaneously. Both parameters can be accurately determined from the spectral type and the SEDs shown in the previous section for Class II and III objects. In order to calculate the best possible stellar luminosities for the sample, we integrate the NEXTGEN stellar model normalized to the dereddened optical fluxes (dotted curves in Figure 12), and assume distances of 150 pc for Lupus I and IV and 200 pc for Lupus III. The computed stellar luminosities can be found in Table 11. The complete emission of the objects is obtained in the bolometric luminosity, where we integrate under all the observed fluxes of the SED, the corresponding bolometric flux is then converted to luminosities with the same distances quoted above for the different clouds.

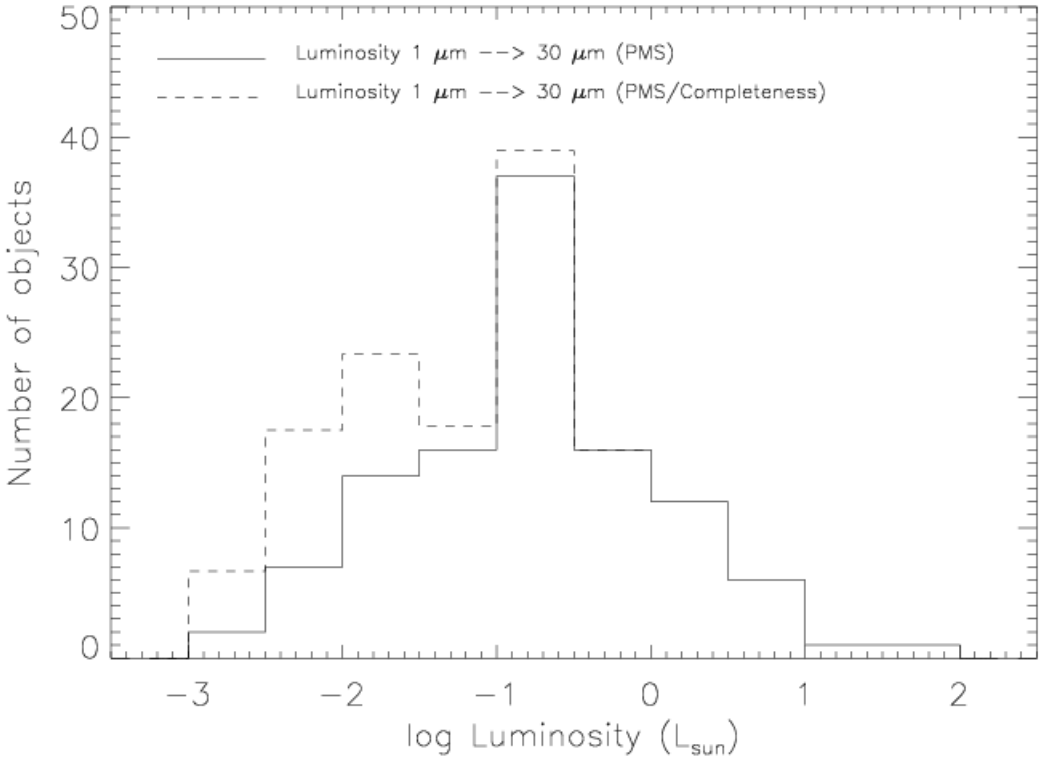

Fig. 13.— Bolometric luminosity function for the Lupus young stellar population (*solid histogram*) and estimated correction for completeness effects (*dashed histogram*).

Figure 13 shows a histogram of the total bolometric luminosities for all YSOs and PMS stars in Lupus as a solid line. Compared to the same figure in Cha II (Alcalá et al. 2008) and

in Serpens (Harvey et al. 2007a), it shows a larger population of low and very-low luminosity objects, which was already noted by previous surveys of the region (see F. Comerón 2008, in prep. and references therein), and a large number of objects with luminosities between 0.3 and 0.1 $L_\odot$. Interestingly, the lowest luminosity members of the population are Lupus3MMS, the Class 0 object in Lupus III (Tachihara et al. 2007), SSTc2d J161027.4-390230, another flat SED object in the same cloud followed by late M-type brown dwarfs from Comerón et al. (2003), Allers et al. (2006) and Allen et al. (2007).

The peak of the luminosity function appears at 0.2 $L_\odot$, which corresponds to a 0.2 $M_\odot$ star (spectral type M5 at an age of 1 Myr) and up to 1.0 $M_\odot$ for objects of 5 Myrs according to the PMS tracks by Baraffe et al. (1998) plus a tail at lower luminosites. Harvey et al. (2007a) made an estimate of the completeness of the c2d catalogs by comparing a trimmed version of the deeper SWIRE catalog of extragalactic sources (Surace et al. 2004), taken to represent 100% completeness by c2d standards, with the number counts of the c2d catalog in Serpens per luminosity bin. Their estimations suggest a 100 % completeness at luminosities $\geq$ 0.3 $L_\odot$ in the c2d catalogs, which corresponds to a 0.3 $M_\odot$ star (spectral type M4.5 at an age of 1 Myr). The dashed line in Figure 13 is the luminosity histogram corrected for completeness effects in each luminosity bin, which suggests that up to 15 additional very low-luminosity objects ($\log L/L_\odot < -1.7$) were missed below the noise level of our c2d observations or were confused in the galactic region of the color-magnitude diagrams. The comparison of both luminosity histograms yields a completeness level in luminosity for our disk study of $\log L/L_\odot \approx -1.0$, which corresponds to a mass of $M \sim 0.1 M_\odot$ for a star of $\sim$ 1 Myr (Baraffe et al. 1998). The lower luminosity limit with respect to that in Serpens stems from the different distances to both clouds and is roughly consistent with the distance squared ratio.

4.4. Disk fractional luminosities

One way to characterize the circumstellar accretion disks around young stars is to compute the disk fractional luminosities $L_{\rm disk}/L_{\rm star}$ and compare them with that of passive reprocessing flaring disks (Kenyon & Hartmann 1987). We computed those ratios by subtracting the stellar fluxes from the observed dereddened fluxes in the SEDs and integrating the IR excess throughout the SED. That was done for all the objects with sufficient data to allow a good fit of the stellar model to the SED, crucial to get a sensible disk luminosity. The resulting flux ratios are also given in Table 11.

The upper panel of Figure 14 shows the stellar luminosity versus the disk fractional luminosity for the sample of YSOs and PMS objects in Lupus. The grey dots correspond

to visual binary systems, as reported in § 2.1, while the black dots represent single stars. In the lower planel, we have collapsed the stellar luminosity axis to get a histogram on disk fractional luminosities for the entire sample. This diagram offers a complete view of the star plus disk population in Lupus and shows several interesting results and trends. The $\log L_{\rm disk}/L_{\rm star}$ ratio of objects in which we could not detect any sizable IR excess were set to -3 so that they appear to the left of both panels. The disk luminosity ratios show a strong dependence on the band used to normalize the dereddened fluxes to the stellar photospheric model and the extinction determination. These are only accurate in those objects with known spectral types, but the deviations are small enough to extract statistical trends from the diagram.

Horizontal dashed lines in the upper panel separate the regions where the luminosities correspond to those of Herbig Ae stars (HAeBe's, spectral types earlier than F0), T Tauri stars (down to M7) and Brown dwarfs (BDs, below M7) of 1 Myr according to Baraffe et al. (1998). The only two known HAeBe's in Lupus, HR 5999 and HR 6000, share the upper region with SSTc2d J161000.1-385401, a intermediate-mass HAeBe candidate in Lupus with small IR excess, which could be a background post-AGB star, given the resemblance of its SED to those of the old field objects found in Serpens (Harvey et al. 2007a). It can be also seen here, as well as in figure 13, that the great majority of the objects in Lupus are M-type T Tauri and very low mass stars.

The vertical lines separate the regimes where the luminosity ratios can be explained by different mechanisms: accretion disks ($L_{\rm disk}/L_{\rm star} > 0.1$), and passive reprocessing disks ($0.02 < L_{\rm disk}/L_{\rm star} < 0.08$ Kenyon & Hartmann 1987), and finally "debris"-like disks ($L_{\rm disk}/L_{\rm star} < 0.02$, which is a conservative upper limit for the fractional disk luminosity of a transitional or young debris disk, Currie et al. 2007). The distribution of points and the histogram in the bottom panel show that the great majority of the disks found in Lupus have luminosities which imply some degree of accretion, similar to what was found in the Cha II cloud (Alcalá et al. 2008). This result contrasts with the 40% of disks with small IR excesses found in § 4.2 and shows that detailed Spitzer SED morphology studies are needed to provide a better description of the inner disks, which are greatly degenerate with the flux ratios in the T Tauri phase.

The grey dots and dashed histogram show the distribution of those YSOs in the plot which were found to be visual binaries in the optical images by Comerón et al (in prep.). It has been suggested that close binaries (< 20 AU) play a central role in the evolution of the disks by dramatically reducing the incidence of disks around multiple stars (Bouwman et al. 2006), while wide (> 100 AU) binaries do not affect significatively the presence and evolution of the circumstellar disks (Pascucci et al. 2007). Here we present further evidence for this

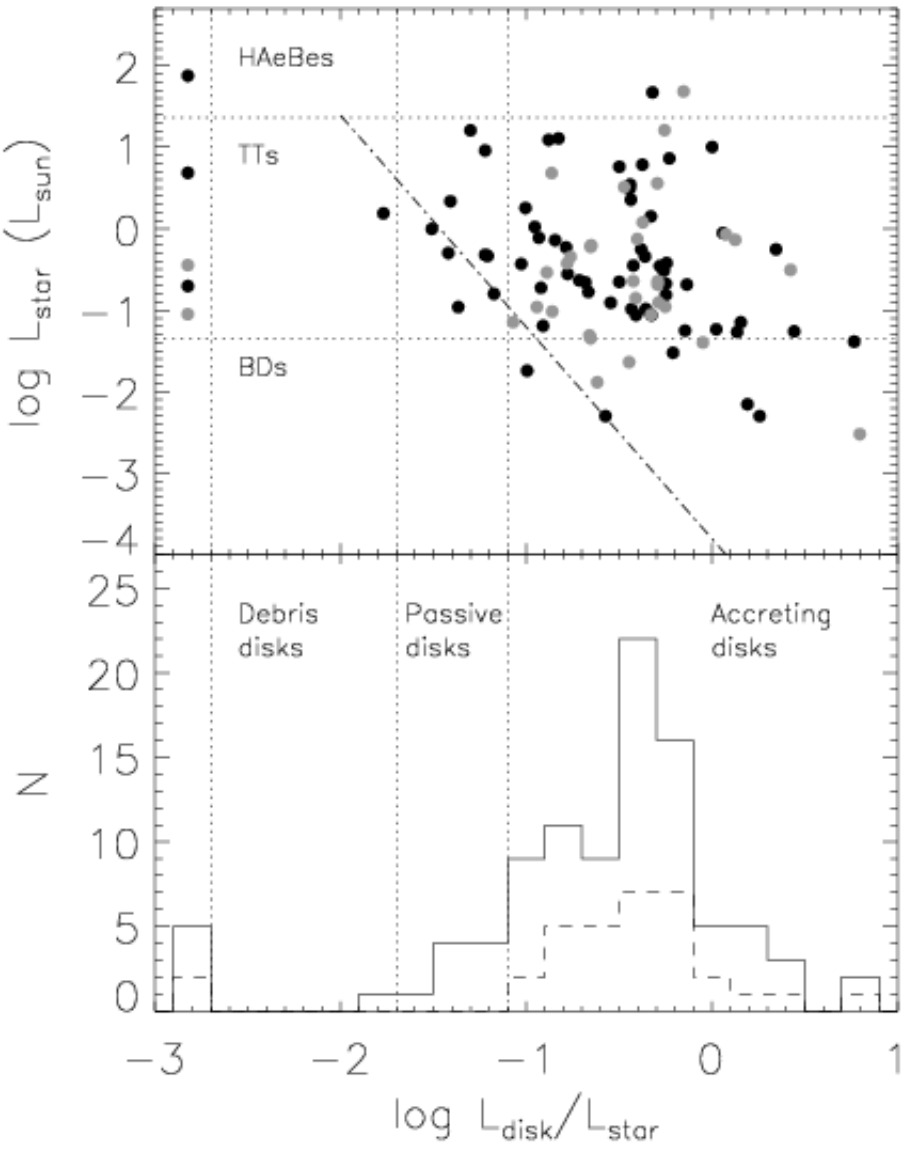

Fig. 14.— *Top*: Correlation plot between the stellar luminosities and the disk fractional luminosities for the PMS stars in Lupus. Solid and grey dots are single and binary stars, respectively and the dot-dashed line marks the approximate 24 μm detection limit. *Bottom*: distribution of disk fractional luminosities for the Lupus sample. The solid and dashed lines show the single and binary stars distributions, respectively. Objects with negligible IR excess are shown in the −3 abscisa for completeness.

lack of correlation between disks and wide orbit companions in Lupus, where binaries and

single stars show the same distribution in terms of luminosity or disk fractional luminosity.

Finally, there seems to be a trend by which lower luminosity objects show higher disk to star luminosity ratios than higher luminosity stars. However, the luminosity distribution of the 'H' and 'T'-type objects only, the least affected by the detection limits in the IR, is statistically equal to the luminosity distribution for the total sample. Therefore, the trend reflects an observational bias caused by the limited detection capability of excesses at longer wavelengths for the faintest sources. The flux sensitivity limit for 24 μm detection with S/N > 3 is ≈ 1 mJy in our observations. This corresponds to photospheric emission of a $\approx 0.2\ L_{\odot}$ ($\log L_{\rm star} \approx -0.7$) star in our sample, which corresponds to a 0.2 $M_{\odot}$ (M5.5) star of 1 Myr. The star Sz 92 is close to the border with 0.47 $L_{\odot}$ ($\log L_{\rm star} \approx -0.3$), a very small excess at 24 μm ($L_{\rm disk}/L_{\rm star} = 0.06$, $\log L_{\rm disk}/L_{\rm star}$ = -1.2) and a flux density at 24 μm of 1.5 mJy. Fainter objects with larger excesses will be detected as soon as their 24 μm is larger than the limiting flux and this number will obviously depend on the level of background emission and crowdedness of the area where a given object is. This limit, shown with a dot-dashed line in the figure, explains the skewness of the data points towards the bottom right of the diagram and illustrates the disk parameter space probed with these observations. The survey is not sensitive to "debris"-like disks around stars less massive than 0.2 $M_{\odot}$ but detects all actively accreting disks down to the substellar regime since those should present detectable IR excess at all IRAC bands which are much more sensitive.

4.5. A Two-Dimensional Classification System

Finally, to explain the diversity in the SEDs, we developed a *second-order* set of parameters to classify the diversity of 2MASS + IRAC + MIPS SEDs that are found in the star-forming regions: $\lambda_{\rm turn-off}$ and $\alpha_{\rm excess}$ (Cieza et al. 2007). In short, $\lambda_{\rm excess}$ is the last wavelength in microns where the observed flux is photospheric and $\alpha_{\rm excess}$ is the slope computed as $\mathrm{dlog}(\lambda F_{\lambda})/\mathrm{dlog}(\lambda)$ starting from $\lambda_{\rm turn-off}$ and up to 70 μm when available. The first parameter gives us an indication of how close the circumstellar matter is to the central object and the second one is a measure of how optically thick and flared it is. Both numbers can be found for all the stars with disks in the sample in Table 11.

Figure 15 shows both values for the sample of YSOs in Lupus for which we could perform a sensible SED fit. Three objects (namely Par-Lup3-3, Par-Lup3-4 and Sz 99) were not included in this analysis since their SEDs did not allow for a good determination of $\lambda_{\rm turn-off}$ due to too much IR excess at short wavelengths in the first two cases and lack of IRAC data in the third one. Cieza et al. (2007) showed that $\lambda_{\rm turn-off}$ is a good "evolutionary" parameter, since it separates efficiently the Classical T Tauri stars from the Weak Line T Tauri stars.

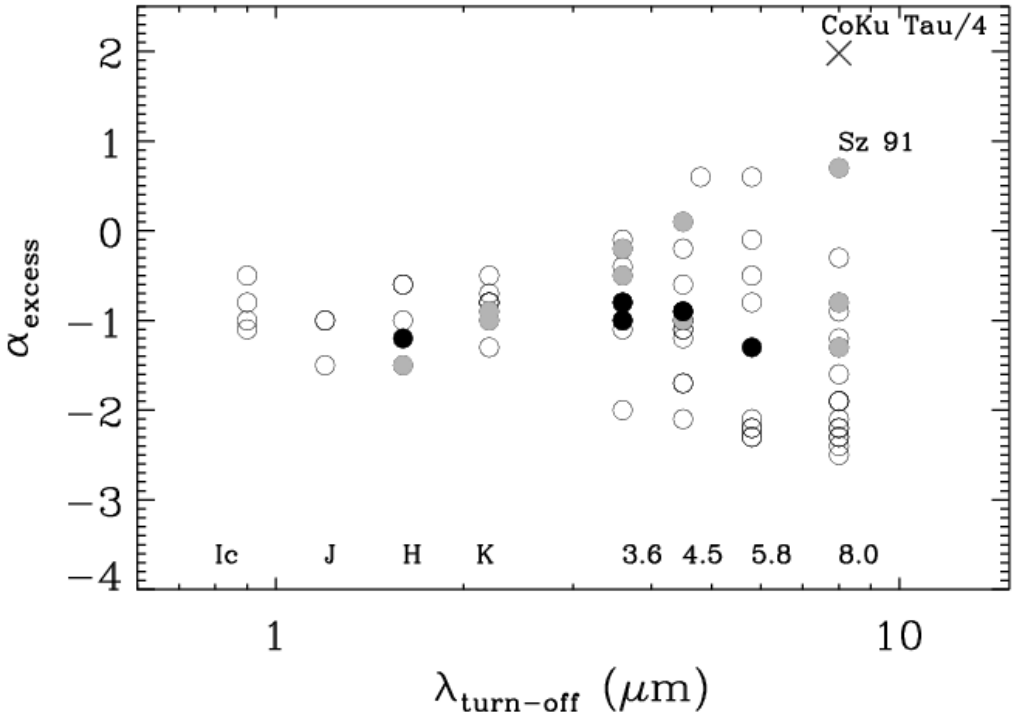

Fig. 15.— Distribution of excess slopes $\alpha_{\rm excess}$ with respect to the wavelength at which the infrared excess begins $\lambda_{\rm turn-off}$ for the Lupus sample (open circles). Solid dots are objects which were detected at 1.3 mm by Nuernberger et al. (1997) and grey dots are objects for which only upper limits were obtained at 1.3 mm. CoKu Tau/4 shows the position of the cold disks in this diagram for comparison.

They also showed that the range of $\alpha_{\rm excess}$ values, which scale with the amount of emitting material in the disk for central objects of similar luminosity, grows with $\lambda_{\rm turn-off}$, which was interpreted by those authors as a signature of multiple "evolutionary paths" of the inner disks of T Tauri stars from the actively accreting phase (with typically $\lambda_{\rm turn-off} < 2\mu$m) to progressively more settled and optically thin disks with larger values of $\lambda_{\rm turn-off}$. The Lupus sample shows a remarkably similar distribution in Figure 15, as also do the Serpens and Cha II samples, suggesting that the result is a common feature of young stellar populations.

The diagram is also useful for identifying transitional disks, or cold disks (Calvet et al. 2005; Brown et al. 2007), i.e. systems with an optically thick outer disk with large inner holes (several AU). These objects appear in the right-upper part of this diagram. For comparison, we show the position of CoKu Tau/4, a well known T Tauri disk with a inner hole of $\sim$ 10 AU devoid of matter (D'Alessio et al. 2005). We also labeled one of the new cold disks

found in Lupus III, Sz 91, which is indeed is the most extreme upper-right object of the whole distribution. The determination of robust cut-offs in this diagram for identifying "bona-fide" disks with holes and their frequency in the full c2d data set is underway and will be presented elsewhere.

In order to compare the inner disk architectures of our sample of Lupus PMS stars with their outer disks, we have marked the 'Sz' stars detected in 1.3 mm continuum observations by Nuernberger et al. (1997) with black dots, and the upper limits with grey dots in Figure 16. As expected, all the millimeter detections and upper limits in the diagram appear at $\alpha_{\rm excess} \geq -1.5$, which imply relatively optically thick inner disks for all values of $\lambda_{\rm turn-off}$.

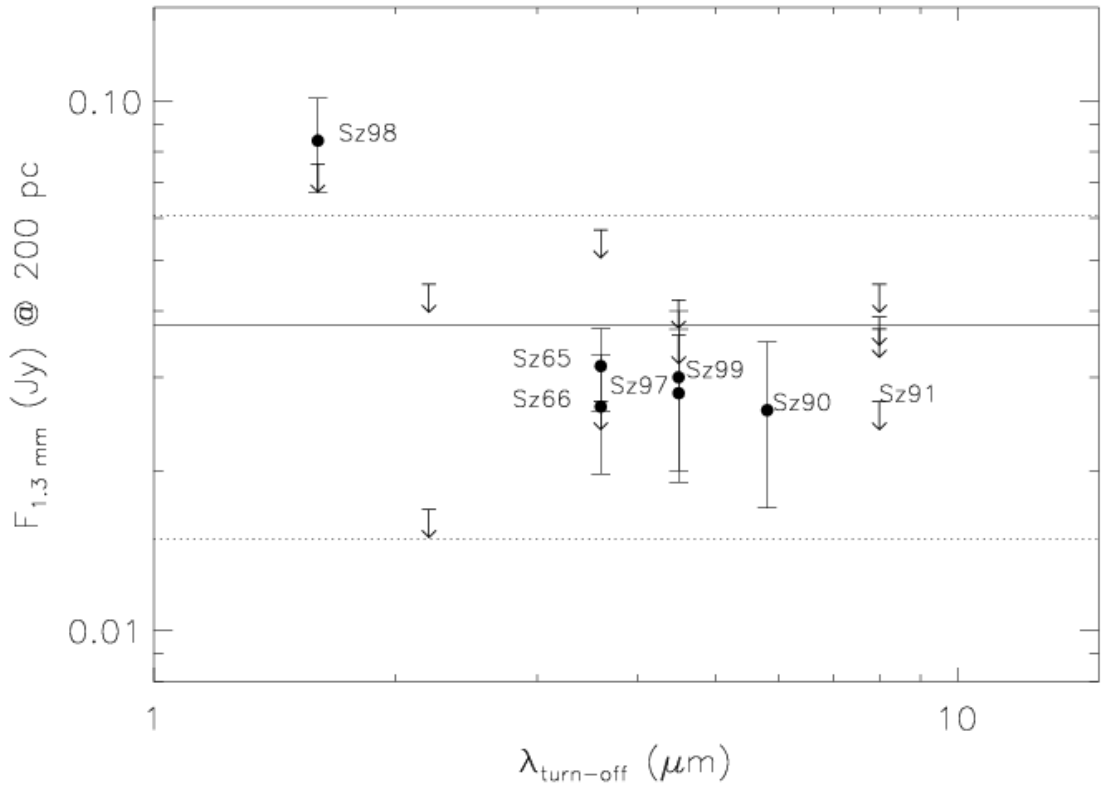

Fig. 16.— Relationship between the continuum flux at 1.3 mm from Nuernberger et al. (1997) and the wavelength $\lambda_{\rm turn-off}$ at which the infrared excess begins for the Classical T Tauri stars in Lupus. The arrow show the positions of the upper limits, including that for the cold disk Sz 91.

However, the really interesting result comes when comparing the millimeter fluxes, which are a proxy for disk total mass (Beckwith & Sargent 1991; Andrews & Williams 2005), with $\lambda_{\rm turn-off}$, which is an indirect indicator of the degree of dust depletion and clearing of the

inner disk. Figure 16 shows the 1.3 mm continuum fluxes and upper limits for the Lupus sample normalized to 200 pc compared to the $\lambda_{\rm turn-off}$. The horizontal line shows the average of the normalized millimeter fluxes and the dotted lines the 1σ error bar of the mean. With the exception of Sz 98, disks with a range of $\lambda_{\rm turn-off}$ or inner disk clearings appear to show quite similar total disk masses, being all well inside the standard deviation of the mean. The case of Sz 98 could be different, since its SED suggests a possible contribution of a remnant envelope, which would contribute to the total millimeter flux. In spite of the low number of detections, the general result is that objects with a range of inner disk configurations show total disk masses in the same order of magnitude. This suggests an inside-out process which empties the inner disk while the outer disk remain unchanged. Alexander & Armitage (2007) show that disk clearing by photoevaporation is more efficient for smaller disk masses while e.g. Edgar (2007) argue that the efficiency of giant planet formation and migration, the main competing mechanism for inner disk dissipation, is proportional to the disk mass. The apparent lack of correlation between inner disk clearing and total disk mass is not compatible with the photoevaporation scenario while it is with the planet formation one. However, the current sample only contains 8 good detections, and several caveats should be taken into account in the interpretation of this figure: apart from the low number statistics, the $\lambda_{\rm turn-off}$ value will be sensitive to the inclination angle, while the millimeter flux is considered roughly insensitive to it (e.g. D'Alessio et al. 1999). More work will be done to quantify the extent of this relation with larger data sets and will be presented elsewhere.

4.6. Outflow sources

Several previous studies have shown the suitability of the IRAC bands, and more specifically IRAC band 2 at 4.5 μm for detecting new high-velocity shocked outflows via the H_2 emission line found in that band (e.g. Noriega-Crespo et al. 2004, Jørgensen et al. 2006). In this section we present the Spitzer data for the known outflow sources in the surveyed Lupus clouds (from the review by Comerón 2008, in prep.) and new emission nebulae found in the IRAC mosaics which could be high velocity outflows and shocks. Table 5 summarizes the results of this effort and Figures 17 and 18 show them.

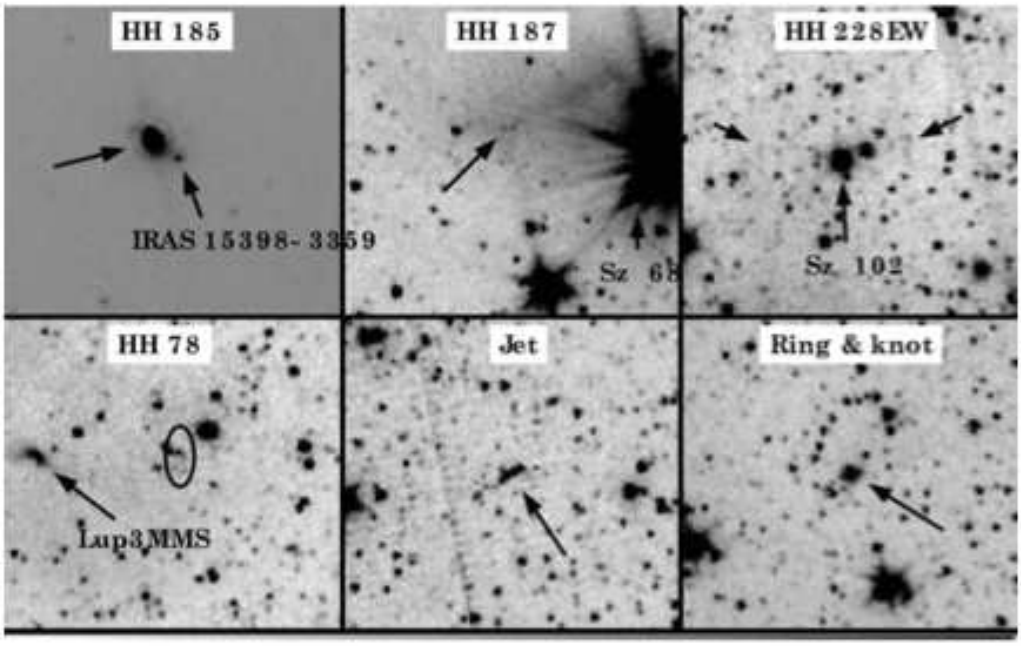

Fig. 17.— Known HH objects detected in Lupus with IRAC, together with a candidate new outflow source in Lupus III and a nebulous object in a ring of stars in Lupus IV. All images have a size of 2′x2′, linear stretch and are from the IRAC1 band at 3.6 μm, except the one showing HH 185, which is IRAC4 at 8.0 μm. North is up and East is to the left. Coordinates are given in Table 5.

The HH 185 object, reported by Heyer & Graham (1989), shows an ellipsoidal shape close to the Flat SED object IRAS 15398-3359 in all IRAC bands. HH 187 (Heyer & Graham 1989) is a faint nebulosity seen at IRAC1 and 2 bands only, and brighter in the latter. HH 228 and HH 78 also appear in the Spitzer bands as small ($\sim 4''$) faint nebulosities around their driving sources. The small [SII] outflow in Par-Lup3-4 reported by Fernández & Comerón

(2005) and the HH 186 36″ [SII] jet around Sz 68 are not detected by the Spitzer observations. Only nebulosities appearing consistently in both epoch images were included to avoid artifacts. All the IRAC images were searched for nebulosities and we report here the detection a jet-like nebulous structure found at all IRAC bands in Lupus III and a nebulous object in a ring of point sources found in Lupus IV. The driving sources of these two objects were not identified.

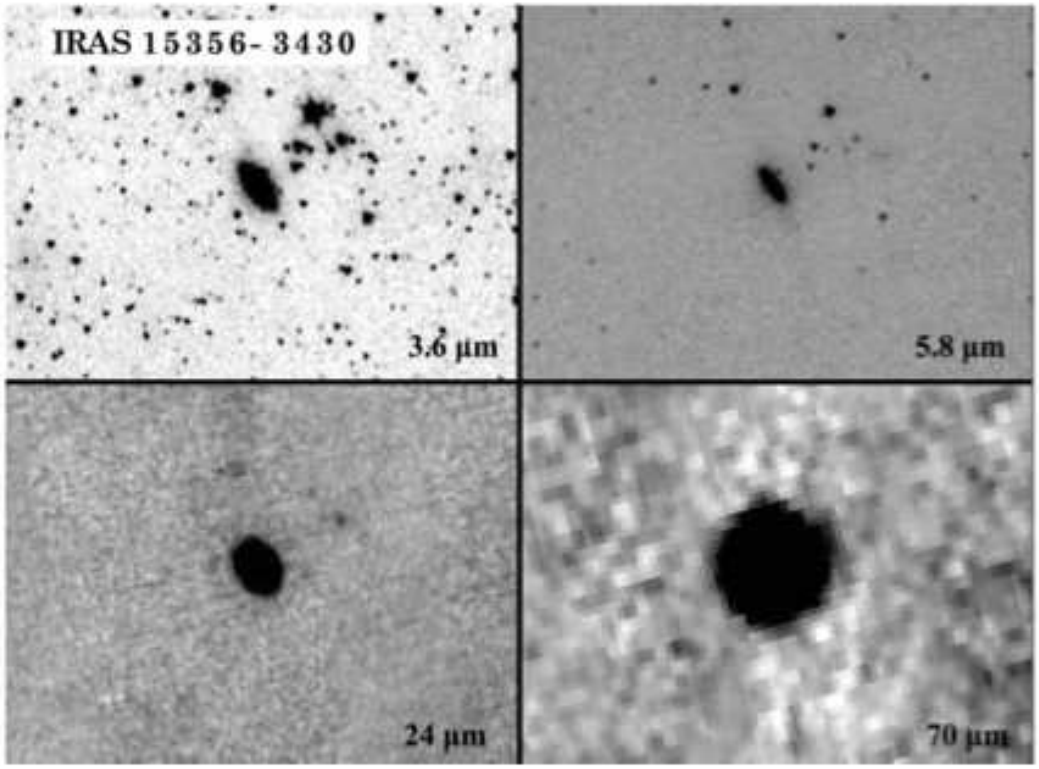

Fig. 18.— IRAC and MIPS images of the extended nebula around the source IRAS 15356-3430. All images have a size of 4′x5′ and linear stretch. North is up and East is to the left. Coordinates are given in Table 5.

Figure 18 shows the remarkable emission around the the bright class I source IRAS 15356-3430. A 40″ elliptical nebulosity is observed in all IRAC bands and also detected in MIPS 24 and 70 μm bands. The nebulosity is also found with a slightly smaller extension in the optical and 2MASS images. Carballo et al. (1992) classified it as a possible YSO or a galaxy based on its IRAS colors and Strauss et al. (1992) confirmed its YSO nature with optical spectroscopy. Its 70 μm flux is as high as that of Lupus3MMS but it has never been observed in the millimeter wavelengths. The SED slope of the object is smaller than that

of Lupus3MMS or IRAS 15398-3359 and that makes it detectable in the near-IR bands. In any case, the Spitzer SEDs of all these sources with extended emission are clearly associated with extremelly embedded and actively accreting objects.

Interestingly, one class II and one class I YSO (Sz 98, Lupus3MMS) happen to have detection quality flag of 'K' only in IRAC2 band at 4.5 μm in the c2d catalog, which means that these sources could not be fitted by a stellar PSF at that wavelength. This suggests the possible presence of unresolved ($< 2''$) outflows detected preferentially through the shocked H_2 line in IRAC band 2 and is consistent with the fact that all three of them are extremely active accretors with large $\alpha_{(K-24\mu m)}$ values and excesses well above the median SED of the T Tauri stars in Taurus. Similarly, in the case of the highly accreting HAeBe star HR 5999, a point source could not be extracted for IRAC bands 1 and 2 so the corresponding fluxes were removed for the SED analysis of that object. This again hints to bright extended emission around 4.5 μm on a scale smaller than the large PSF of the star.

Table 5: Probable high-velocity outflows and nebulae in Lupus

Assoc. YSO ID	R.A. (J2000)	Dec. (J2000)	HH identification / driving source	Ref.	Notes
			Lupus I		
2	15 38 48.36	-34 40 38.2	IRAS 15356-3430	4	a
10	15 43 01.29	-34 09 15.42	HH 185 / IRAS 15398-3359	1	b
15, 16	15 45 19.03	-34 17 32.43	HH 187 / Sz 68 / Sz 69	1	c
			Lupus III		
47	16 08 32.11	-39 03 18.23	HH 228E / Sz 102	2	d
47	16 08 27.18	-39 03 00.68	HH 228W / Sz 102	2	d
87	16 09 12.38	-39 05 00.61	HH 78 / Lupus3 MMS	3	e
...	16 10 57.95	-38 04 37.90	...	4	f
			Lupus IV		
...	16 00 39.04	-42 06 51.51	...	4	h

a Bright 40 $''$ nebula towards the NE in all IRAC and MIPS bands.

b Bright 12 $''$ nebula towards the NE in all IRAC bands.

c Faint 3$''$ nebula knot at 3.6 and 4.5 μm.

d Faint knots at 3.6 and 4.5 μm.

e Faint knots mostly at 3.6 and 4.5 μm.

f 8$''$ jet in all IRAC bands.

h 9$''$ knots at all IRAC bands in a ring of 15 point sources.

References. — 1) Heyer & Graham (1989); 2) Krautter (1986) ; 3) Reipurth & Graham (1988); 4) This work

5. Clouds and Cluster properties

We can use the Spitzer data to also study the star formation history in the Lupus clouds. In particular, we want to estimate the star-formation activity and the clustering properties of the young stellar population in relation to the current cloud structure.

5.1. Extinction maps in Lupus

The structure of the interstellar medium in the direction of the Lupus clouds has been extensively studied with (sub)millimeter molecular line observations (e.g., Murphy et al.

1986; Hara et al. 1999; Vilas-Boas et al. 2000; Tachihara et al. 2001) as well as with optical and infrared star-counts (Cambrésy et al. 1997, 1999) on spatial scales of several arcminutes. These studies reveal a large clumpy structure with a substantial number of overdensities, dominated by the "classical" Lupus I to IV clouds, where star-formation has also been detected. See Comerón 2008 (in prep.) for a complete review of these observations.

The c2d data offer an exceptional tool for producing extinction maps in all the imaged clouds. This is done by estimating the visual extinction towards each source classified as a background star, based on their SED from 1.25 μm to 24 μm. This provides multiple line-of-sight measures, which are then convolved with Gaussian beams of 90″ to 300″ to produce homogeneous extinction maps. These maps are part of the c2d data delivery. In the case of Lupus I, the low number of background stars only allowed reliable construction of an extinction map with a minimum FWHM of 120″. For more information about these maps, see Evans et al. (2007).

The maps with the largest beams (300″) are used to estimate the enclosed cloud masses (§ 5.4) and to compare them with the position of the different YSOs (§ 5.2). They can be seen in Figures 19 to 22. The extinction traces the northern cloud in the Lupus I map with a peak of $A_V \sim 23$ mag and shows two large clumps in Lupus III and IV, with peak extinctions of 33 and 36 mag, respectively. The maximum in Lupus III coincides with the rich star-forming cluster, while it roughly coincides with the Flat SED source SSTc2d J160115.6-415235 in Lupus IV. This is the first report of such a high extinction inactive core in Lupus IV to our knowledge, which was previously unnoticed due to its current lack of activity.

5.2. Spatial distribution and clustering of YSOs in Lupus

Figures 19 to 22 show the spatial distribution of the PMS stars in the three Lupus clouds compared with the c2d extinction maps: In Lupus I, the most striking result is that the majority of the YSOs fall in a ridge of high extinction which extends in the North of the cloud with NE-SW direction. A southern high extinction region contains the pair of T Tauri stars Sz 68 and Sz 69. The majority of the objects, of any SED class but with larger abundance of Class I and Flat SED sources, appear very close to high extinction regions, with the exception of the Class III sources Sz 67 and SSTc2d J153803.1-331358 and the Flat spectrum source IRAS 15398-3359. The close match between the YSO distribution and extinction map in the region and the early class of most of the objects suggests that we are seeing the objects in the places where they were just born.

The sources in Lupus III are dramatically concentrated in the dense star-forming cluster

at RA $\sim 16^h09^m$ and DEC $\sim$ -39°10′, which contains the two bright intermediate mass Herbig Ae/Be stars HR 5999 and HR 6000 in the centre. In this case, objects of all classes are found in the vicinity of the dense cluster and at large distances from it. Figure 21 zooms into the cluster, showing the extraordinary density of PMS objects at the highest extinction area in the whole cloud, where star formation is extremely active. Amongst many Class II and III sources, the cluster contains four Class I sources, including Lupus3MMS, claimed to be the only Class 0 object in the Lupus clouds (Tachihara et al. 2007). Note that only 3 of them appear in Figure 21, while the forth is visible in Figure 20 to the South of the cluster.

Figure 22 shows the distribution of YSOs in Lupus IV around a very dense, yet quite unpopulated, extinction peak at RA $\sim 16^h02m$ and DEC $\sim$ -41°50′ which contains the only Flat spectrum source in the cloud: SSTc2d J160115.6-415235. The rest of the Class II and III sources, together with the Class I source IRAS 15589-4134 are found surrounding the core, but following a different spatial pattern, which suggests that they might have been formed in a different structure. As the contour plot nicely shows, the peak extinction at this clump is higher than that of the star-forming cluster in Lupus III (see also § 5.1). This fact together with the relative Class III predominance in Lupus IV suggests that star-formation may have taken place before in other regions of this cloud and may be about to start in this core. We must note, however, that an object like Lupus3 MMS would have not been detected in this core, since it was only thanks to its millimeter detection that it was identified as a cloud member in Lupus III and such observations are so far not available for Lupus IV.

The observation of these complex extinction structures and YSO distributions has stimulated for many years the discussion on how star-formation takes place, whether it is a hierarchical process or whether it takes place in a centrally-condensed way (see Lada & Lada 2003, LL03 hereafter, and references therein). In order to study the subject with the new Spitzer data, we need to set some standards that will be applied across the c2d observational set. Similar to the other c2d clouds (see, e.g., Alcalá et al. 2008) we identified substructure in the Lupus clouds using the nearest neighbor algorithm applied by Gutermuth et al. (2005) (see Jørgensen et al. 2008, in prep. for details). Following the discussion by Jørgensen et al. we divide concentrations of PMS objects up into "clusters" or "groups" depending on whether they have more or less than 35 members at a given volume density level. We furthermore identify structures with volume densities higher than 1 $M_\odot$ pc^{-3} (the criterion for a cluster by LL03) or 25 $M_\odot$ pc^{-3} as being "loose" or "tight", respectively.

Figure 23 shows the result of the nearest neighbor analysis for the whole Lupus sample. When applied to Lupus this algorithm breaks the complex into three separate entities: two tight concentrations of PMS stars at the 25 M$_\odot$ pc^{-3} level and a loose one at the 1 M$_\odot$ pc^{-3} level (taking into account the difference in distance between Lupus I and IV on one hand

and Lupus III on the other). The Lupus IV cloud has one loose group and Lupus I a tight group. The Lupus III cloud has one tight cluster containing 118 members. Table 8 shows the number of PMS objects of the different classes in the regions identified above. This analysis allows ordering the objects by degree of clustering, with Lupus III being the most clustered region, followed by Lupus I and Lupus IV.

Overall, both the cloud density structure and the distribution of stars in the three regions suggest a centrally-condensed structure dominating the star-formation process only in Lupus III and a more disperse distribution of volume density enhancements in the other two clouds, mostly at Lupus IV, where star-forming cores have formed along a cloud filament in the NE-SW direction. As a whole, the three clouds clearly show a hierarchical structure with separate gas concentrations that evolve independently. This scenario argues in favor of a larger presence of turbulence over gravitational forces (LL03), which is consistent with the Lupus clouds being flanked by the large Scorpius-Centaurus OB associations and therefore subject to their strong high-energy radiation (Comerón 2008).

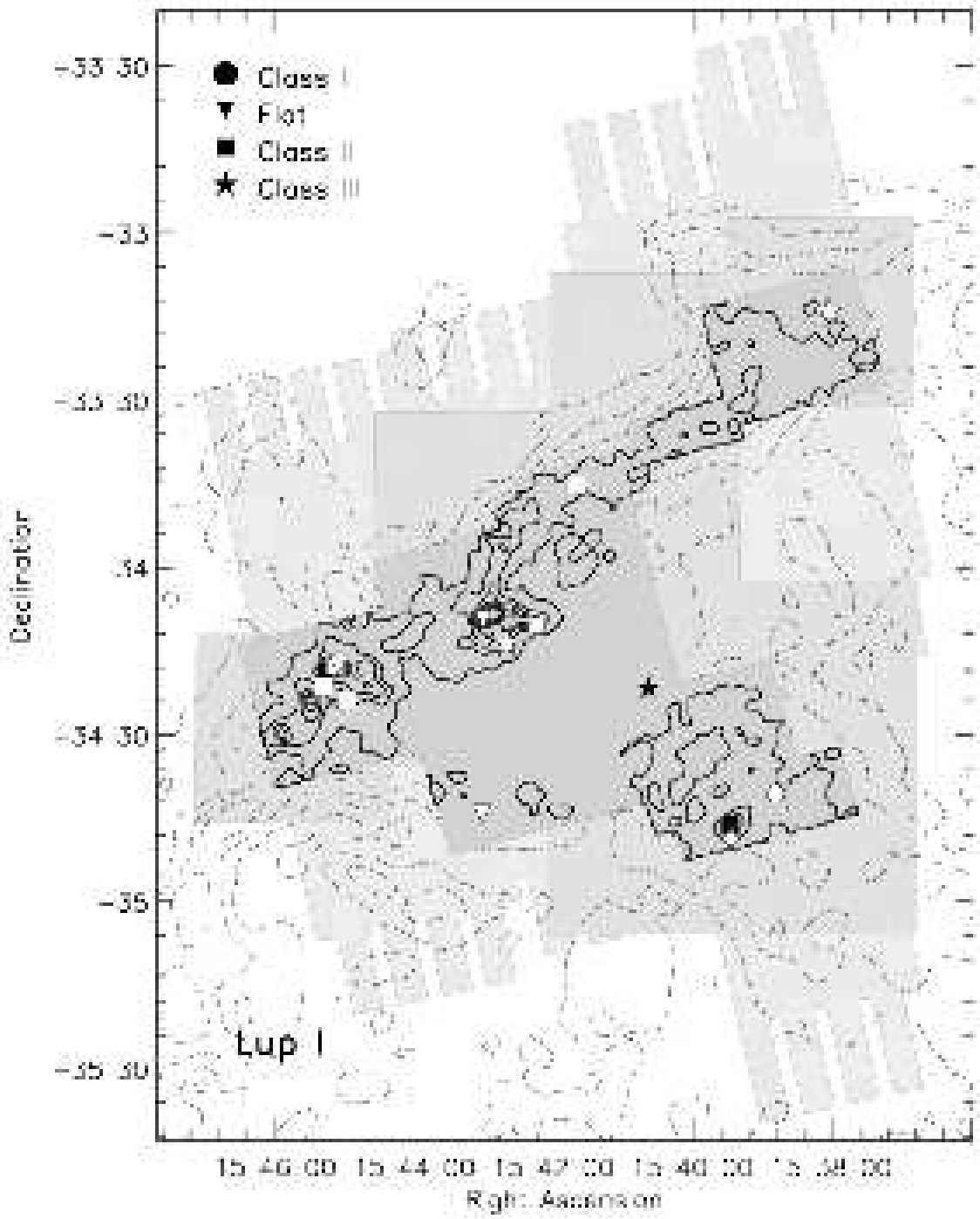

Fig. 19.— Spatial distribution of the spectrally confirmed PMS objects (black symbols) and candidates (white symbols) in Lupus I as function of Lada Class, over-plotted on the contours from the c2d extinction map (continuous lines). The contour levels of extinction are from 2 mag to 20 mag, in steps of 2 mag. The shaded areas, from light to dark-gray, display the regions observed with MIPS, WFI and IRAC, respectively. The dashed lines outside the IRAC area are the contour levels of extinction from Cambrésy (1999), from 1 mag to 6 mag in steps of 0.35 mag. The higher resolution and sensitivity to higher A_V of the c2d extinction map with respect to that of Cambrésy (1999) can be appreciated.

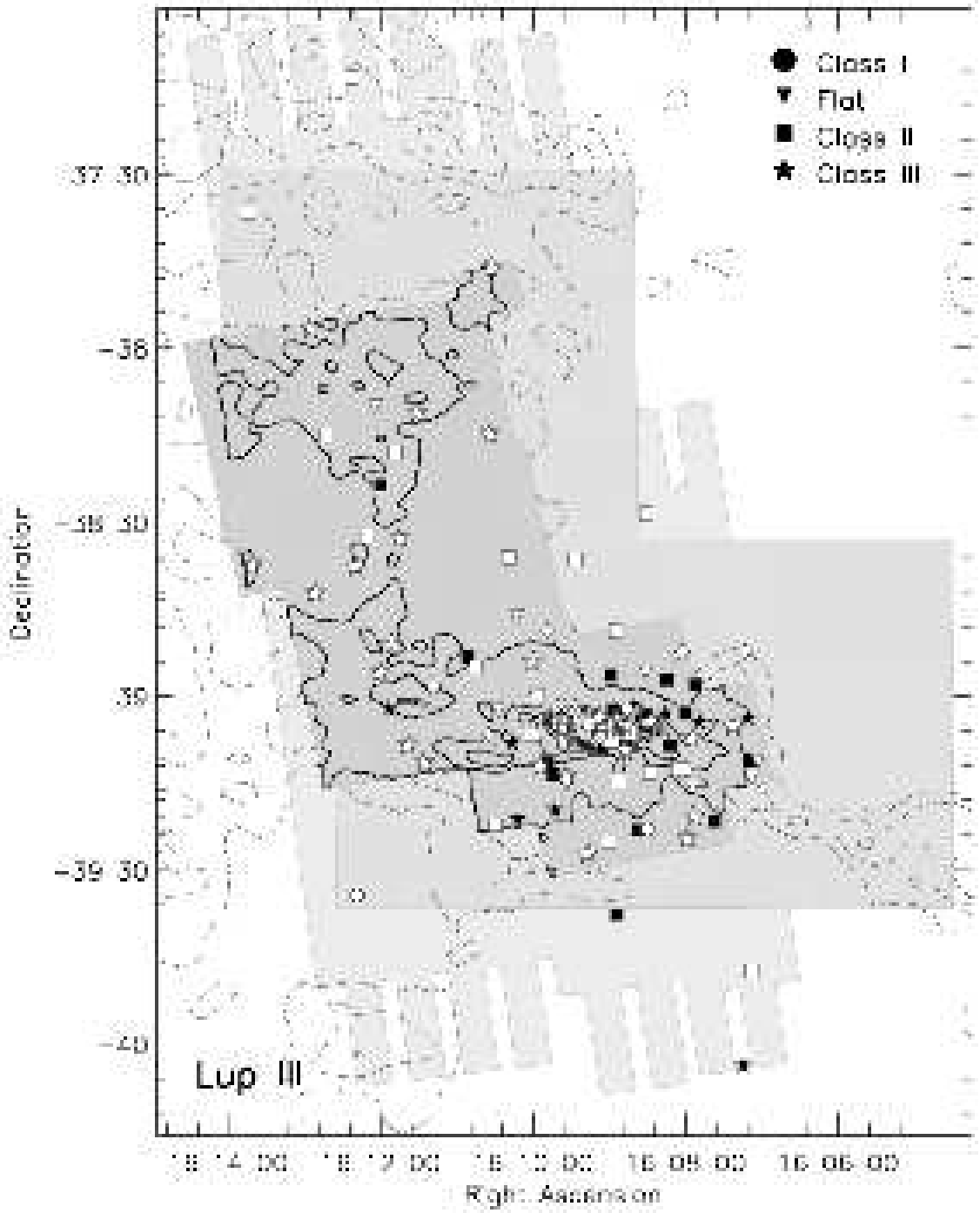

Fig. 20.— Spatial distribution of the PMS objects (filled symbols) and candidates (open symbols) in Lupus III as function of Lada Class, over-plotted on the contours from the c2d extinction map (continuous lines). Symbols as in Figure 19.

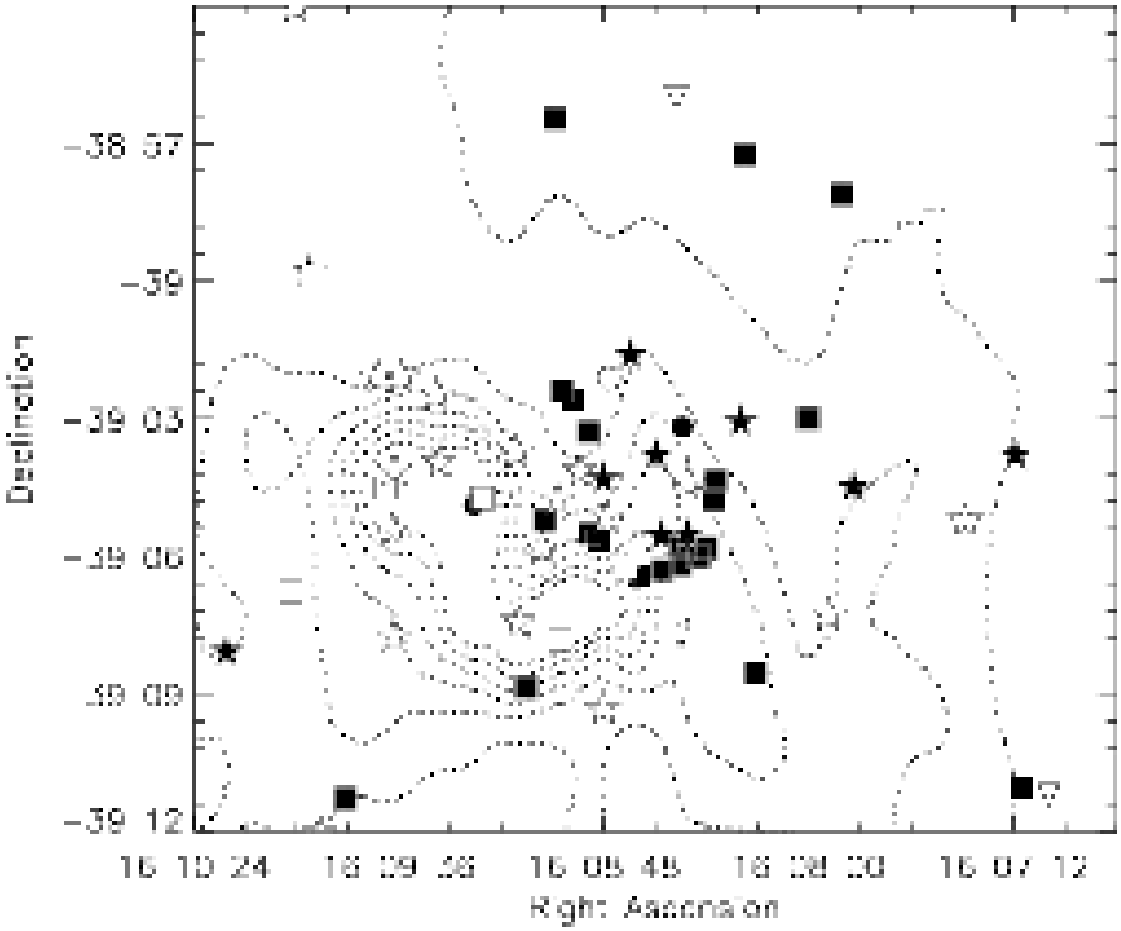

Fig. 21.— Zoom of the dense star-forming cluster in Lupus III. Symbols as in Figure 19, except the dashed lines, which are the 2 to 14 mag contours on the c2d extinction map in steps of 2 magnitudes.

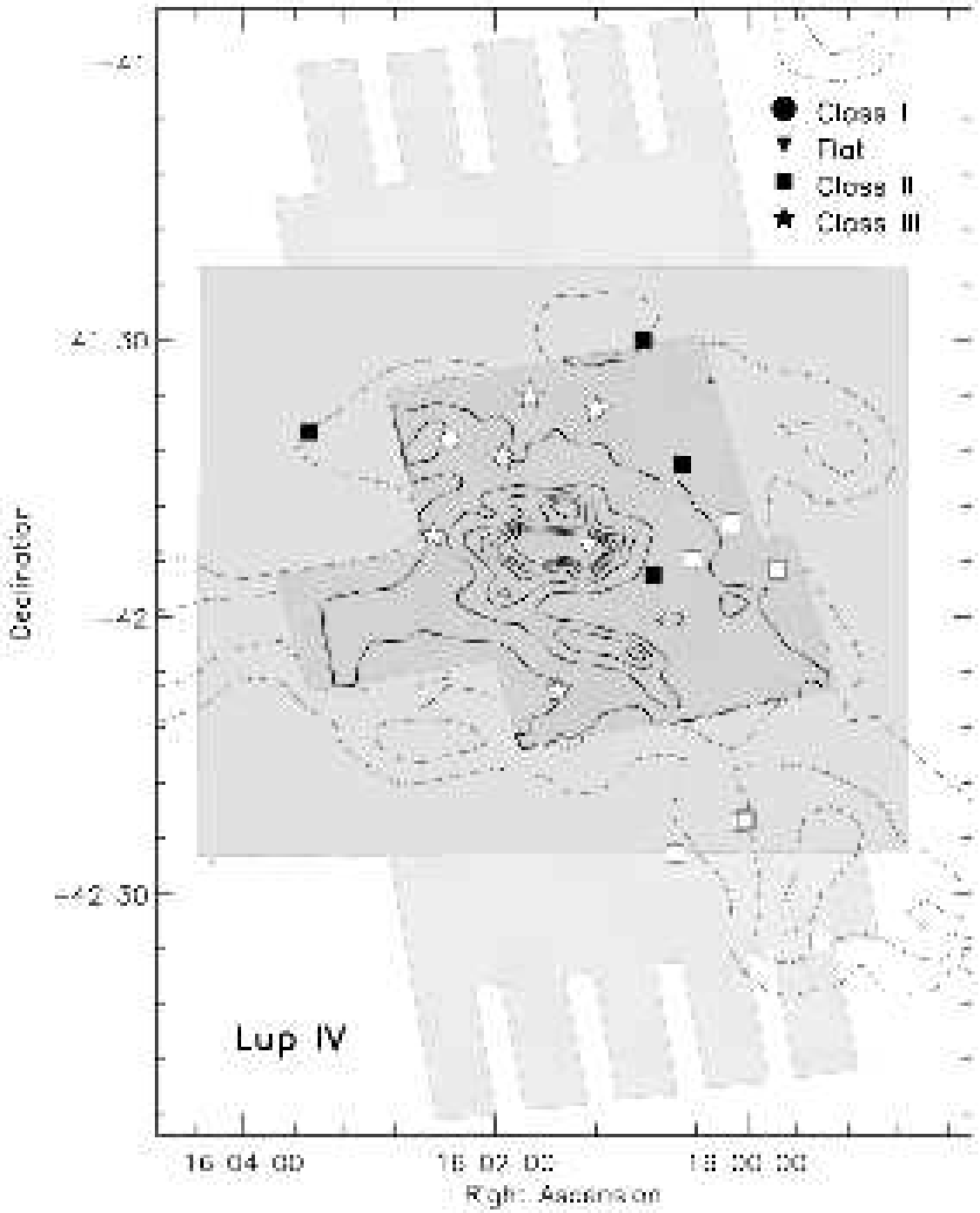

Fig. 22.— Spatial distribution of the PMS objects (filled symbols) and candidates (open symbols) in Lupus IV as function of Lada Class, over-plotted on the contours from the c2d extinction map (continuous lines). Symbols as in Figure 19.

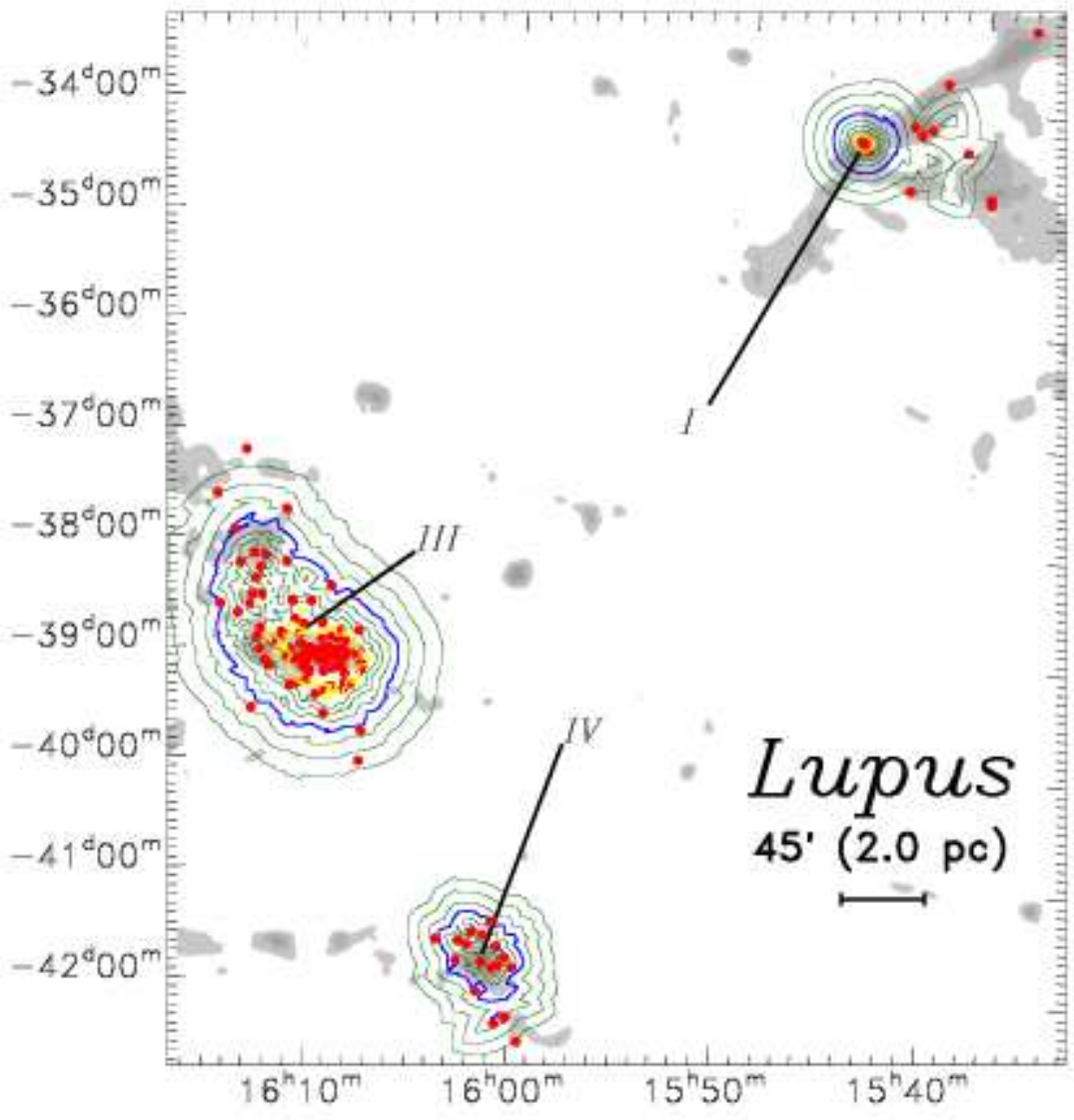

Fig. 23.— Volume density plot for the three Lupus clouds as determined with the nearest-neighbor algorithm by J. Jørgensen et al. (2007, in preparation). The derived contours are compared with extinction map from Cambrésy (1999) in gray scale from 2 to 4.1 in steps of 0.7 mag. The blue contour corresponds to the 1×LL03 level, the yellow to the 25×LL03 level, and the green ones correspond to levels of 0.125, 0.25, 0.5, 2, 4 and 8 times that level. The two groups and the cluster in Lupus III are identified with labels.

5.3. Star Formation Rates

We can also use our complete samples to estimate the star formation rates. In section 3 we computed the total numbers of YSOs and PMS objects for each of the three clouds. The IRAC+MIPS coverage areas reported in § 2.2 were used for the YSOs and the overlapping MIPS areas as given by Chapman et al. (2007) for the PMS stars. Using the typical average mass of 0.5 $M_{\odot}$ for consistency with the other c2d clouds, we find total masses in YSOs of $\sim$ 6, 34, and 6 $M_{\odot}$ in Lupus I, III and IV, respectively. A more appropriate average value for the stellar mass in Lupus of 0.2 $M_{\odot}$ (§ 4.3) would yield total masses in YSOs of $\sim$ 2, 14, and 2 $M_{\odot}$ in Lupus I, III and IV, respectively and therefore it would scale all the results down by $\sim$ 40 % of the quoted values accordingly. These numbers could be slightly underestimated since very embedded objects in the extinction peaks could have not been detected, as it was illustrated by our inability to select Lupus3 MMS based on Spitzer data only. However, given the relative small areas of the very embedded regions, the number of hidden Class 0 of I objects should not be large compared to the total number of stars in the cloud.

Age estimates for the YSOs in Lupus suffer from many the uncertainties in assigning PMS tracks to positions on CMDs (e.g., Mayne et al. 2007), including the uncertain distances to the Lupus clouds. Hughes et al. (1994) use 150 pc for all clouds and obtained an age range from less than 1 to 10 Myr with a peak at 3.2 Myr, however, Comerón et al. (2003) found ages between 1 and 1.5 Myr for objects in Lupus III using a distance of 200 pc (see also the discussion on the ages by Comerón 2008). Detailed determinations of the individual stellar ages for the entired sample will be performed once an optical spectroscopy survey of the sample is completed. This section assumes the average value of 2 Myr for all the stars in Lupus. Table 6 shows the results of these calculations: star formation rates of 3, 17, and 3 $M_{\odot}$ Myr^{-1} are found, or up to two times these values if we include the PMS stars and candidate PMS stars, in the Lupus I, III and IV clouds, respectively.

The numbers are consistent with those found in another low-star forming regions and assume that all stars were formed approximately at the same time. However, it is know that some of these young stellar populations might have appeared at different times, producing a spread in ages (e.g. Hughes et al. 1994). The clusters are clearly young so it is reasonable to assume that new-born stars should be close to the places were they were born. Indeed, early Class objects were found systematically close to the high extinction regions in Lupus I and many Class II objects cluster around the two bright Herbig Ae/Be stars HR 5999 and HR 6000 in the center of the Lupus III cluster. The formation of these latter objects could have been triggered by the strong winds of the two intermediate-mass stars but we found no other evidence for triggered-star formation like clustered populations of objects with the same class in our mosaics. The ages calculated for the PMS stars in the clouds are also in

agreement with the expected cloud removal time-scales of < 5 Myrs after the onset of the star-formation process (Ballesteros-Paredes & Hartmann 2007).

Table 6: Numbers, Densities and Star Formation Rates in Lupus

Type	Ω deg^{-2}	Area pc^2	N	N/Ω deg^{-2}	N/Area pc^{-2}	N/Vol pc^{-3}	SFR $M_\odot$ Myr^{-1}	SFR/Area $M_\odot$ Myr^{-1} pc^{-2}
Lupus I								
YSOs	1.39	9.49	13	9.4	1.4	0.43	3.3	0.35
Total	3.82	26.07	17	4.5	0.6	0.13	4.3	0.16
Lupus III								
YSOs	1.34	16.26	69	51.5	4.2	1.05	17.3	1.06
Total	2.88	34.94	124	43.0	3.5	0.60	31.0	0.89
Lupus IV								
YSOs	0.37	2.52	12	32.4	4.8	3.00	3.0	1.19
Total	1.08	7.37	18	16.7	2.4	0.90	4.5	0.61

Note. — Ω is the solid angle subtended by the cloud, 'Area' is the equivalent in square parsec, 'N' is the number of objects, and 'SFR' stands for Star Forming Rate.

5.4. Cloud Masses and Star Formation Efficiencies

Table 7 summarizes the cloud mass measurements from the literature as cited in the Comerón (2008, in prep.). To those, we add the c2d-derived masses of the clouds from the extinction maps with the lowest spatial resolution ($300''$) as explained in the Delivery Documentation (Evans et al. 2007). The table shows large differences in these mass estimates, most of which are due to the fact that the areas used to compute the total cloud masses differ from the c2d area, whereas both the number of YSOs and c2d cloud mass estimates were obtained from the same area. For this reason, we will use the c2d values (marked with an 'e' in the table) in the following.

Based on these mass estimates and following Alcalá et al. (2008), we derived the Star Formation Efficiency (SFE) as $SFE = \frac{M_{star}}{M_{cloud}+M_{star}}$ where M_{cloud} is the cloud mass and M_{star} is the total mass in YSOs objects, i.e. the sum of the masses over the entire stellar populations, which range from 6 to 34 $M_\odot$ for the YSOs and from 8 to 62 $M_\odot$ if we include

Table 7: Estimates of the cloud masses and Star Formation Efficiencies (SFE) in Lupus

Tracer	Mass[†]	SFE (%)	
	$M_\odot$	YSOs	Total
Lupus I			
^{13}CO	878[a]	0.7	0.9
C^{18}O	326[b]	1.8	2.4
Extinction	22851[c]	0.0	0.0
Extinction	654[d]	0.9	1.2
Extinction	479[e]	1.2	1.6
Lupus III			
^{13}CO	1195[a]	2.8	4.9
C^{18}O	418[b]	7.6	12.9
Extinction	10547[c]	0.3	0.6
Extinction	1666[d]	2.0	3.6
Extinction	846[e]	3.9	6.8
Lupus IV			
C^{18}O	216[b]	2.7	4.0
Extinction	1406[c]	0.4	0.6
Extinction	225[d]	2.6	3.8
Extinction	196[e]	3.0	4.4

[†] All the masses have been normalized to the distances of 150 pc for Lupus I and IV and 200 pc for Lupus III.

[a] Total mass of H_2 derived from the ^{13}CO luminosity (Tachihara et al. 1996).

[b] Total mass of H_2 derived from the C^{18}O luminosity (Hara et al. 1999).

[c] Cloud mass for A_V above 2 (Cambrésy 1999).

[d] Mass in dense condensations as derived from extinction (Andreazza & Vilas-Boas 1996).

[e] Cloud mass for Av > 2 for Lupus III and IV and for Av > 3 for Lupus I using the c2d extinction maps.

the PMS stars (c.f. § 5.3). The average stellar mass (0.5 $M_\odot$) was used here to derive M_{star}. The results on the efficiency of star formation are provided in Table 7. We estimate the SFE in the Lupus clouds to be 0.7 – 2.4 %, 2.0 – 12.9 % and 2.6 – 4.4 % for the three clouds, respectively. The large cloud masses from Cambrésy (1999) were derived for much larger areas and therefore were not considered. In spite of the large differences in total cloud mass estimates, these numbers are consistent the previous estimates in the literature for

Table 8: Star Formation efficiencies (SFE) and class numbers by region in Lupus.

		Total	I	Flat	II	III	$\langle A_V \rangle$	Mass	Volume	SFE
Total		159	8 (4.4%)	12	75	64	...	1501.4	...	5.0%
Extended		23	3 (9.1%)	2	11	20	...	386.1	...	2.8%
I	LG	6	0 (0.0%)	1	5	0	2.75	99.19	1.69	2.9%
...tight	TG	5	0 (0.0%)	1	4	0	6.06	15.72	0.0326	13.7%
III	LC	118	4 (3.4%)	8	53	45	1.47	793.6	98.0	6.9%
...tight	TC	79	4 (5.1%)	5	37	25	3.85	318.9	5.69	11.0%
IV	LG	12	1 (8.3%)	1	6	4	2.96	169.6	3.39	3.4%

Note. — The SFEs and number of objects of per class are presented for different sub-samples according to their spatial distribution: the first two rows show the Total and Extended populations, 'LG' stands for Loose Group, 'TG' is Tight Group, 'LC' is Loose Cluster, and 'TC' is Tight Cluster, defined at § 5.2 and shown in Fig. 23. The $\langle A_V \rangle$, the enclosed masses and volumes were calculated for each of the regions following Jørgensen et al.

Lupus (0.4 – 3.8%, Tachihara et al. 1996) and somewhat higher than estimates for other T associations like e.g. Taurus (1–2%, Mizuno et al. 1999).

We can also calculate the same numbers for the different sub-structures identified in the distribution of the PMS objects. Table 8 gives the number of objects of the different classes in the different groups and clusters described in § 5.2 along with the enclosed cloud masses calculated in the areas subtended by each of the groups and clusters and the c2d extinction maps. The resulting SFE values for each region are also given in the table. All SFEs are larger for the groups and clusters than for the extended population or the global cloud SFEs, as to be expected. The SFEs for the Loose Group (LG) and Tight Group (TG) in Lupus I (see § 5.2) are 2 and 8 times the cloud average SFE in Table 7, while the SFE in the Loose Group in Lupus IV almost matches the global SFE in that cloud. The large numbers in the tight group and cluster in Lupus I and III are due to the relatively small areas containing a moderate numbers of forming stars and seems to suggest again that the star-formation process is more clustered in both clouds, with bigger differences in the SFEs between the clustered and extended population than in Lupus IV, where there is no substantial difference.

The caveat for all these SFE analyses is that the definition of the cloud area used for the cloud mass calculations depends on the surface density of PMS stars and therefore assumes that the remaining cloud outside the chosen area is not related to the formation of the stars inside of it, which is probably correct, but also that a given amount of cloud gas density will always produce a given amount of stars, i.e., it assumes that the star-formation process

is universal and not affected by other characteristics of the cloud like its composition or its initial angular momentum. With this caveat in mind, it is however worth noticing that the SFEs calculated for the bulk of the PMS populations in the three Lupus clouds (i.e. the loose cluster and groups) scale linearly with the enclosed masses in the areas defining the loose clusters or groups. This correlation between SFE and cloud mass is suggestive and was never found when a cutoff in A_V was used to define the cloud boundaries and masses. The result is also interesting since it matches well the dynamical and fast star-formation scenario recently proposed (LL03, Bate et al. 2003): it might help explaining the presence of objects of very different evolutionary stages at small distances as the result of several mild star-formation events in small clouds before a big star-formation event contributes to the bulk of the coeval PMS stars in each of the regions (Ballesteros-Paredes et al. 2007).

6. Summary

We present observations of the Lupus I, III and IV dark clouds at 3.6, 4.5, 5.8 and 8.0 μm made with the Spitzer Space Telescope Infrared Array Camera (IRAC) and discuss them along with optical, near-infrared, observations made with the Multiband Imaging Photometer for Spitzer (MIPS) onboard Spitzer and millimeter flux from the literature to provide a complete description of the three clouds and their young stellar populations. The main results can be summarized as follows:

- We performed a census of the Young Stellar Objects (YSO) applying the c2d Spitzer color criteria in the three clouds and increase the number of cloud members by more than a factor of 4. The PMS population consists of 159 stars in the three clouds with infrared (IR) excess or spectroscopically determined membership, mostly found in the high density regions of the clouds and greatly dominated by low and very low-mass objects. The sample is complete down to M $\approx$ 0.1 $M_\odot$ and probes well down into the sub-stellar regime.

- 30 – 40% of sources are multiple with binary separations between 0.7 and 10″ (100 to 2000 AU). These long period binaries appear not to affect the disk properties.

- A large majority of the YSOs in Lupus are Class II or Class III objects, with only 20 (12%) of Class I or Flat spectrum sources. Objects of all classes appear equally distributed in the clouds and tend to cluster around the cloud high density peaks, except in Lupus IV where they do not follow the extinction distribution.

- The disk survey is complete down to "debris"-like systems in stars as small as M $\approx$ 0.2 $M_\odot$ and includes sub-stellar objects with larger IR excesses. The disk fraction

in Lupus is 70 – 80%, consistent with an age of 1 – 2 Myr. However, the young population contains 20% optically thick accretion disks and 40% relatively less flared disks regarding their Spitzer SEDs.

- A larger variety of inner disk structures is found for larger inner disk clearings, suggesting several possible evolutionary paths for the primordial disks. Similar disk masses are found for a range of inner disk clearings, which provides evidence against a clearing of the inner disks by photoevaporation.

- All previously known Herbig-Haro objects with sizes larger than 3″ were found in the Spitzer images of the clouds and two new sources are reported: a jet-like structure in Lupus III and a nebulous object in Lupus IV.

- Lupus I consist of a filamentary cloud structure with three density enhancements closely followed by early class objects. Lupus III contains a very active star-forming cluster with a very large number of objects of all classes. Lupus IV shows the highest extinction peak in Lupus with few late class objects away from the density peak.

- Clustering analysis of the PMS distribution recovers separate structures in the three clouds, with Lupus III being the most centrally populated and rich, followed by Lupus I and Lupus IV. Overall, the cloud structures are compatible with predictions from the hierarchical star formation scenario.

- We estimate star formation efficiencies of a few percent and a star formation rate of 2 – 10 $M_\odot$ Myr^{-1} in the Lupus clouds. We also find a tentative linear correlation between the star formation efficiencies and the enclosed cloud masses of the three main stellar groups in Lupus.

Table 9. Young Stellar Objects and Pre-Main Sequence stars in Lupus

No.	c2d Name	Object ids.	R.A. (J2000)	DEC. (J2000)	Sel.	PMS status	Lada Class	Refs
		Lupus I						
1	SSTc2d J153803.1-331358	...	15 38 03.10	-33 13 57.7	YSO	Cnd	III	12
2	SSTc2d J153848.2-344041	IRAS 15356-3430	15 38 48.36	-34 40 38.2	YSO	PMS	I	10, 12
3	SSTc2d J153927.3-344844	AKC2006-17	15 39 27.28	-34 48 44.3	(5)	Cnd	III	5
4	SSTc2d J153927.8-344617	Sz 65 / IK Lup / HBC 597	15 39 27.78	-34 46 17.4	YSO	PMS	II	1,12
5	SSTc2d J153928.3-344618	Sz 66	15 39 28.29	-34 46 18.3	YSO	PMS	II	1,12
6	SSTc2d J154038.3-342137	Sz 67 / KWS97 Lup 1-11	15 40 38.27	-34 21 36.7	(1)	PMS	III	1
7	SSTc2d J154140.8-334519	AKC2006-18	15 41 40.82	-33 45 19.0	(5)	Cnd	II	5
8	SSTc2d J154214.6-341026	...	15 42 14.57	-34 10 25.8	YSO	Cnd	I	12
9	SSTc2d J154240.3-341343	...	15 42 40.32	-34 13 43.0	YSO	Cnd	III	12
10	SSTc2d J154301.3-340915	IRAS 15398-3359	15 43 01.29	-34 09 15.4	YSO	Cnd	F	1,12
11	SSTc2d J154302.3-344406	...	15 43 02.29	-34 44 06.2	YSO	Cnd	F	12
12	SSTc2d J154457.9-342340	AKC2006-19	15 44 57.90	-34 23 39.5	YSO	Cnd	II	5,12
13	SSTc2d J154506.3-341738	...	15 45 06.34	-34 17 38.2	YSO	Cnd	F	12
14	SSTc2d J154508.9-341734	...	15 45 08.88	-34 17 33.7	YSO	Cnd	II	12
15	SSTc2d J154512.9-341731	Sz 68 / HT Lup / HBC 248	15 45 12.87	-34 17 30.8	(1)	PMS	II	1
16	SSTc2d J154517.4-341829	Sz 69 / HW Lup / HBC 598	15 45 17.42	-34 18 28.5	YSO	PMS	II	1,12
17	SSTc2d J154518.5-342125	...	15 45 18.53	-34 21 24.8	YSO	Cnd	II	12
		Lupus III						
18	SSTc2d J160703.9-391112	...	16 07 03.85	-39 11 11.6	YSO	Cnd	F	12
19	SSTc2d J160708.6-391407	...	16 07 08.57	-39 14 07.7	YSO	Cnd	F	12
20	SSTc2d J160708.6-394723	...	16 07 08.64	-39 47 22.7	(7)	Cnd	II	7
21	SSTc2d J160710.1-391104	Sz 90 / HBC 613 / KWS97 Lup 3-23	16 07 10.08	-39 11 03.5	YSO	PMS	II	1,12
22	SSTc2d J160711.6-390348	Sz 91 / HBC 614 / KWS97 Lup 3-24	16 07 11.60	-39 03 47.7	YSO	PMS	III	1,12
23	SSTc2d J160714.0-385238	Lup 605	16 07 14.00	-38 52 37.9	(4)	Cnd	III	4
24	SSTc2d J160715.2-400342	Sz 92 / Th 22	16 07 15.20	-40 03 42.0	(1)	PMS	III	1
25	SSTc2d J160723.4-390510	Lup 654	16 07 23.44	-39 05 10.1	(4)	Cnd	III	4

Table 9—Continued

No.	c2d Name	Object ids.	R.A. (J2000)	DEC. (J2000)	Sel.	PMS status	Lada Class	Refs
26	SSTc2d J160737.7-392139	Lup 713	16 07 37.72	-39 21 38.8	YSO	PMS	II	4,12
27	SSTc2d J160749.6-390429	Sz 94 / KWS97 Lup 3-28	16 07 49.60	-39 04 29.0	(1)	PMS	III	1, 11
28	SSTc2d J160752.3-385806	Sz 95	16 07 52.32	-38 58 06.3	YSO	PMS	II	1, 11,12
29	SSTc2d J160754.1-392046	...	16 07 54.09	-39 20 46.2	YSO	Cnd	III	12
30	SSTc2d J160754.7-391545	2MASS J16075475-3915446	16 07 54.75	-39 15 44.6	YSO	Cnd	F	6,12
31	SSTc2d J160755.3-390718	...	16 07 55.29	-39 07 17.8	YSO	Cnd	III	12
32	SSTc2d J160758.9-392435	Lup 714	16 07 58.90	-39 24 34.9	(4)	Cnd	III	4
33	SSTc2d J160800.2-390300	Lup 604s	16 08 00.20	-39 02 59.7	YSO	PMS	II	4,6,12
34	SSTc2d J160801.7-391231	2MASS J16080175-3912316	16 08 01.75	-39 12 31.6	(2)	Cnd	II	6
35	SSTc2d J160803.0-385229	...	16 08 03.02	-38 52 29.3	YSO	Cnd	III	12
36	SSTc2d J160806.2-391223	2MASS J16080618-3912225	16 08 06.17	-39 12 22.5	YSO	Cnd	II	6,12
37	SSTc2d J160812.6-390834	Sz 96	16 08 12.62	-39 08 33.5	YSO	PMS	II	1,11,12
38	SSTc2d J160815.0-385715	2MASS J16081497-3857145	16 08 14.96	-38 57 14.5	YSO	PMS	II	6,12
39	SSTc2d J160816.0-390304	Par-Lup3-1	16 08 16.03	-39 03 04.2	(1)	PMS	III	3
40	SSTc2d J160821.8-390422	Sz 97 / Th 24	16 08 21.79	-39 04 21.5	YSO	PMS	II	1,12
41	SSTc2d J160822.5-390446	Sz 98 / HK Lup / HBC 616	16 08 22.50	-39 04 46.0	YSO	PMS	II	1, 11,12
42	SSTc2d J160824.0-390549	Sz 99 / Th 25	16 08 24.04	-39 05 49.4	YSO	PMS	II	1,12
43	SSTc2d J160825.8-390601	Sz 100 / Th 26	16 08 25.76	-39 06 01.1	YSO	PMS	II	1, 11,12
44	SSTc2d J160828.1-391310	Lup 607	16 08 28.10	-39 13 10.0	(3)	Cnd	II	4
45	SSTc2d J160828.2-390425	NTO2000-0526.9-5630	16 08 28.16	-39 04 24.6	(6)	Cnd	III	2
46	SSTc2d J160828.4-390532	Sz 101 / Th 27	16 08 28.43	-39 05 32.4	YSO	PMS	III	1, 11,12
47	SSTc2d J160829.7-390311	Sz 102 / Krautter's star	16 08 29.73	-39 03 11.0	YSO	PMS	I	1, 11,12
48	SSTc2d J160830.1-392259	IRAC J16083010-3922592	16 08 30.10	-39 22 59.2	(6)	Cnd	I	6
49	SSTc2d J160830.3-390611	Sz 103 / Th 29 / HBC 618	16 08 30.26	-39 06 11.1	YSO	PMS	II	1,12
50	SSTc2d J160830.7-382827	...	16 08 30.70	-38 28 26.8	(7)	Cnd	II	7
51	SSTc2d J160830.8-390549	Sz 104 / Th 30	16 08 30.81	-39 05 48.8	YSO	PMS	II	1,12
52	SSTc2d J160831.1-385600	IRAC J16083110-3856000	16 08 31.10	-38 56 00.0	(2)	Cnd	F	6

Table 9—Continued

No.	c2d Name	Object ids.	R.A. (J2000)	DEC. (J2000)	Sel.	PMS status	Lada Class	Refs
53	SSTc2d J160834.3-390618	HR 5999 / V856 Sco / HBC 619	16 08 34.30	-39 06 18.0	(1)	PMS	II	1,11
54	SSTc2d J160834.6-390534	HR 6000 / KWS97 Lup 3-40 / V1027 Sco	16 08 34.60	-39 05 34.0	(1)	PMS	III	1
55	SSTc2d J160835.8-390348	Par-Lup3-2	16 08 35.78	-39 03 47.9	(3)	PMS	III	3, 11
56	SSTc2d J160837.3-392311	Lup 706	16 08 37.30	-39 23 10.8	(4)	PMS	II	4
57	SSTc2d J160839.8-390625	Sz 106	16 08 39.76	-39 06 25.3	YSO	PMS	II	1,12
58	SSTc2d J160841.8-390137	Sz 107 / KWS97 Lup 3-44	16 08 41.79	-39 01 37.0	YSO	PMS	III	1, 11,12
59	SSTc2d J160842.7-390618	Sz 108 / HBC 620 / KWS97 Lup 3-45	16 08 42.73	-39 06 18.3	(1)	PMS	III	1, 11
60	SSTc2d J160842.7-390615	Sz 108B	16 08 42.87	-39 06 14.7	YSO	Cnd	II	1,12
61	SSTc2d J160846.8-390207	IRAC J16084679-3902074	16 08 46.79	-39 02 07.4	(2)	Cnd	I	6
62	SSTc2d J160847.5-390509	2MASSJ16084747-3905087	16 08 47.47	-39 05 08.7	(2)	Cnd	III	6
63	SSTc2d J160848.2-390419	Sz 109	16 08 48.16	-39 04 19.2	(1)	PMS	III	1, 11
64	SSTc2d J160848.2-390920	Lup 617	16 08 48.17	-39 09 19.9	(3)	Cnd	III	4
65	SSTc2d J160849.4-390539	Par-Lup3-3	16 08 49.40	-39 05 39.3	YSO	PMS	II	3, 11,12
66	SSTc2d J160851.4-390530	Par-Lup3-4	16 08 51.43	-39 05 30.4	YSO	PMS	II	3,12
67	SSTc2d J160851.6-390318	Sz 110 / Th 32 / HBC 621	16 08 51.57	-39 03 17.7	YSO	PMS	II	1, 11,12
68	SSTc2d J160853.2-391440	2MASS J16085324-3914401	16 08 53.23	-39 14 40.3	YSO	Cnd	II	6, 12
69	SSTc2d J160853.7-390410	NTO2000-0532.1-5616	16 08 53.68	-39 04 09.6	(6)	Cnd	III	2
70	SSTc2d J160853.7-391437	2MASS J16085373-3914367	16 08 53.73	-39 14 36.7	YSO	PMS	II	6,12
71	SSTc2d J160854.7-393744	Sz 111 / Th 33 / HBC 622	16 08 54.68	-39 37 43.9	(1)	PMS	II	1
72	SSTc2d J160855.3-384848	2MASS J16085529-3848481	16 08 55.29	-38 48 48.1	YSO	Cnd	II	6
73	SSTc2d J160855.5-390234	Sz 112	16 08 55.52	-39 02 33.9	YSO	PMS	II	1, 11,12
74	SSTc2d J160857.8-390223	Sz 113 / Th 34	16 08 57.80	-39 02 22.7	YSO	PMS	II	1,12
75	SSTc2d J160858.3-390736	NTO2000-0536.7-5943	16 08 58.27	-39 07 35.5	YSO	Cnd	II	2,12
76	SSTc2d J160858.3-390749	NTO2000-0536.7-5956	16 08 58.30	-39 07 49.4	(2)	Cnd	II	2
77	SSTc2d J160858.9-390446	NTO2000-0537.4-5653	16 08 58.92	-39 04 46.0	(2)	Cnd	III	2
78	SSTc2d J160859.5-385628	2MASS J16085953-3856275	16 08 59.53	-38 56 27.6	YSO	PMS	II	6, 12
79	SSTc2d J160901.4-392512	...	16 09 01.40	-39 25 11.9	YSO	Cnd	II	12

Table 9—Continued

No.	c2d Name	Object ids.	R.A. (J2000)	DEC. (J2000)	Sel.	PMS status	Lada Class	Refs
80	SSTc2d J160901.8-390513	Sz 114 / V908 Sco / HBC 623	16 09 01.84	-39 05 12.5	YSO	PMS	II	1, 11,12
81	SSTc2d J160902.4-390549	NTO2000-0540.9-5757	16 09 02.44	-39 05 49.4	(2)	Cnd	III	2
82	SSTc2d J160906.2-390852	Sz 115	16 09 06.21	-39 08 51.8	YSO	PMS	II	1, 11
83	SSTc2d J160908.0-390726	NTO2000-0546.4-5934	16 09 07.98	-39 07 26.4	(2)	Cnd	III	2
84	SSTc2d J160908.5-390343	Lup 608s	16 09 08.50	-39 03 43.1	(4)	Cnd	III	4, 11
85	SSTc2d J160916.4-390444	NTO2000-0554.9-5651	16 09 16.43	-39 04 43.7	(2)	Cnd	II	2
86	SSTc2d J160917.1-392710	Lup 710	16 09 17.13	-39 27 09.7	(4)	Cnd	III	4
87	SSTc2d J160918.1-390453	Lupus3 MMS	16 09 18.07	-39 04 53.4	YSO	PMS	I	8, 12
88	SSTc2d J160920.3-390402	NTO2000-0558.8-5610	16 09 20.30	-39 04 01.6	(2)	Cnd	II	2
89	SSTc2d J160923.2-390407	NTO2000-0601.7-5616	16 09 23.15	-39 04 07.4	(2)	Cnd	II	2
90	SSTc2d J160926.6-390358	NTO2000-0605.1-5606	16 09 26.61	-39 03 57.7	(6)	Cnd	III	2
91	SSTc2d J160927.0-383628	...	16 09 26.98	-38 36 27.6	(7)	Cnd	II	7
92	SSTc2d J160927.1-390228	NTO2000-0605.6-5437	16 09 27.08	-39 02 28.4	(2)	Cnd	III	2
93	SSTc2d J160934.1-391342	...	16 09 34.11	-39 13 42.1	YSO	Cnd	III	12
94	SSTc2d J160934.2-391513	IRAC J16093418-3915127	16 09 34.18	-39 15 12.7	(6)	Cnd	F	6
95	SSTc2d J160935.4-390205	NTO2000-0614.0-5414	16 09 35.37	-39 02 05.4	(2)	Cnd	III	2
96	SSTc2d J160937.2-390407	NTO2000-0615.6-5616	16 09 37.15	-39 04 06.9	(2)	Cnd	III	2
97	SSTc2d J160937.2-390745	NTO2000-0615.6-5953	16 09 37.19	-39 07 44.7	(2)	Cnd	III	2
98	SSTc2d J160937.4-390526	NTO2000-0615.8-5734	16 09 37.38	-39 05 25.7	(2)	Cnd	III	2
99	SSTc2d J160939.3-390432	NTO2000-0617.7-5641	16 09 39.29	-39 04 31.8	(2)	Cnd	II	2
100	SSTc2d J160941.1-390206	NTO2000-0619.6-5414	16 09 41.08	-39 02 05.6	(2)	Cnd	III	2
101	SSTc2d J160942.6-391941	Sz 116 / Th 36 / HBC 625	16 09 42.57	-39 19 40.8	(1)	PMS	III	1
102	SSTc2d J160944.3-391330	Sz 117 / Th 37 / HBC 626	16 09 44.34	-39 13 30.3	YSO	PMS	II	1,12
103	SSTc2d J160948.6-391117	Sz 118	16 09 48.64	-39 11 16.9	YSO	PMS	II	1,12
104	SSTc2d J160949.9-384903	Lup 650	16 09 49.87	-38 49 03.3	(4)	Cnd	III	4
105	SSTc2d J160954.5-391204	Lup 810s	16 09 54.49	-39 12 03.5	(4)	Cnd	III	4
106	SSTc2d J160956.3-385952	Lup 818s	16 09 56.29	-38 59 51.7	YSO	Cnd	II	4,12

Table 9—Continued

No.	c2d Name	Object ids.	R.A. (J2000)	DEC. (J2000)	Sel.	PMS status	Lada Class	Refs
107	SSTc2d J160957.1-385948	Sz 119	16 09 57.07	-38 59 47.9	(1)	PMS	III	1
108	SSTc2d J161000.1-385401	...	16 10 00.11	-38 54 01.1	YSO	Cnd	III	12
109	SSTc2d J161001.3-390645	2MASS J16100133-3906449	16 10 01.32	-39 06 44.9	YSO	Cnd	II	4,12
110	SSTc2d J161012.2-392118	Sz 121 / Th 40 / KWS97 Lup 3-63	16 10 12.21	-39 21 18.3	(1)	PMS	III	1
111	SSTc2d J161013.1-384617	...	16 10 13.06	-38 46 16.8	YSO	Cnd	F	12
112	SSTc2d J161016.4-390805	Sz 122 / Th 41 / KWS97 Lup 3-64	16 10 16.44	-39 08 05.4	(1)	PMS	III	1
113	SSTc2d J161018.6-383613	...	16 10 18.56	-38 36 13.0	YSO	Cnd	II	12
114	SSTc2d J161019.8-383607	...	16 10 19.84	-38 36 06.8	YSO	Cnd	II	12
115	SSTc2d J161027.4-390230	...	16 10 27.43	-39 02 30.2	YSO	Cnd	F	12
116	SSTc2d J161029.6-392215	...	16 10 29.57	-39 22 14.7	YSO	Cnd	II	12
117	SSTc2d J161032.6-374615	IRAS 16072-3738	16 10 32.59	-37 46 14.9	YSO	Cnd	III	12
118	SSTc2d J161034.5-381450	...	16 10 34.51	-38 14 50.3	YSO	Cnd	III	12
119	SSTc2d J161035.0-390655	...	16 10 34.97	-39 06 54.6	YSO	Cnd	III	12
120	SSTc2d J161045.4-385455	...	16 10 45.38	-38 54 54.9	YSO	Cnd	II	12
121	SSTc2d J161051.6-385314	Sz 123 / Th 42 / HBC 629	16 10 51.60	-38 53 14.0	YSO	PMS	II	1,12
122	SSTc2d J161118.7-385824	...	16 11 18.69	-38 58 23.6	YSO	Cnd	III	12
123	SSTc2d J161126.0-391123	...	16 11 25.98	-39 11 23.2	YSO	Cnd	III	12
124	SSTc2d J161131.9-381110	...	16 11 31.93	-38 11 10.4	YSO	Cnd	III	12
125	SSTc2d J161138.6-390828	Lup 831s	16 11 38.61	-39 08 27.5	(4)	Cnd	III	4
126	SSTc2d J161144.9-383245	...	16 11 44.86	-38 32 44.7	YSO	Cnd	III	12
127	SSTc2d J161148.7-381758	...	16 11 48.67	-38 17 58.3	YSO	Cnd	II	12
128	SSTc2d J161151.2-385104	Lup 802s	16 11 51.20	-38 51 04.2	(4)	Cnd	III	4
129	SSTc2d J161153.4-390216	Sz 124 / Th 43 / HBC 631	16 11 53.35	-39 02 16.1	(1)	PMS	III	1
130	SSTc2d J161159.8-382339	SST-Lup3-1	16 11 59.81	-38 23 38.5	YSO	PMS	II	9,12
131	SSTc2d J161200.1-385557	...	16 12 00.06	-38 55 56.9	YSO	Cnd	III	12
132	SSTc2d J161204.5-380959	...	16 12 04.48	-38 09 59.0	YSO	Cnd	F	12
133	SSTc2d J161211.2-383220	...	16 12 11.22	-38 32 19.8	YSO	Cnd	II	12

Table 9—Continued

No.	c2d Name	Object ids.	R.A. (J2000)	DEC. (J2000)	Sel.	PMS status	Lada Class	Refs
134	SSTc2d J161218.5-393418	...	16 12 18.47	-39 34 18.3	(7)	Cnd	I	7
135	SSTc2d J161219.6-383742	...	16 12 19.60	-38 37 42.2	YSO	Cnd	III	12
136	SSTc2d J161222.7-371328	...	16 12 22.73	-37 13 27.6	(7)	Cnd	II	7
137	SSTc2d J161243.8-381503	...	16 12 43.75	-38 15 03.3	YSO	Cnd	II	12
138	SSTc2d J161251.7-384216	...	16 12 51.72	-38 42 16.0	YSO	Cnd	III	12
139	SSTc2d J161256.0-375643	...	16 12 55.96	-37 56 43.8	YSO	Cnd	III	12
140	SSTc2d J161341.0-383724	...	16 13 40.95	-38 37 23.7	YSO	Cnd	III	12
141	SSTc2d J161344.1-373646	...	16 13 44.11	-37 36 46.4	(7)	Cnd	II	7
		Lupus IV						
142	SSTc2d J155925.2-423507	...	15 59 25.24	-42 35 07.1	(7)	Cnd	II	7
143	SSTc2d J155945.3-415457	...	15 59 45.28	-41 54 57.2	YSO	Cnd	II	12
144	SSTc2d J160000.6-422158	...	16 00 00.62	-42 21 57.5	(7)	Cnd	II	7
145	SSTc2d J160002.4-422216	...	16 00 02.37	-42 22 15.5	(7)	Cnd	II	7
146	SSTc2d J160007.4-414949	IRAS 15567-4141	16 00 07.43	-41 49 48.9	YSO	Cnd	II	12
147	SSTc2d J160026.1-415356	...	16 00 26.13	-41 53 55.6	YSO	Cnd	II	12
148	SSTc2d J160031.1-414337	Sz 130 / HBC 610	16 00 31.05	-41 43 37.2	YSO	PMS	II	1,12
149	SSTc2d J160034.4-422540	...	16 00 34.39	-42 25 39.5	(7)	Cnd	II	7
150	SSTc2d J160044.5-415531	F 403 / MY Lup / IRAS 15573-4147	16 00 44.53	-41 55 31.2	YSO	PMS	II	1,12
151	SSTc2d J160049.4-413004	Sz 131	16 00 49.42	-41 30 04.1	(1)	PMS	II	1
152	SSTc2d J160111.6-413730	...	16 01 11.55	-41 37 30.1	YSO	Cnd	III	12
153	SSTc2d J160115.6-415235	...	16 01 15.55	-41 52 35.3	YSO	Cnd	F	12
154	SSTc2d J160129.7-420804	...	16 01 29.69	-42 08 03.6	YSO	Cnd	III	12
155	SSTc2d J160143.3-413606	...	16 01 43.28	-41 36 05.7	YSO	Cnd	III	12
156	SSTc2d J160157.0-414244	IRAS 15585-4134	16 01 57.04	-41 42 43.9	YSO	Cnd	III	12
157	SSTc2d J160221.6-414054	IRAS 15589-4132	16 02 21.61	-41 40 53.7	YSO	Cnd	I	12
158	SSTc2d J160229.9-415111	...	16 02 29.91	-41 51 11.1	YSO	Cnd	III	12
159	SSTc2d J160329.4-414003	Sz 133	16 03 29.41	-41 40 02.7	(1)	PMS	II	1

Table 9—Continued

No.	c2d Name	Object ids.	R.A. (J2000)	DEC. (J2000)	Sel.	PMS status	Lada Class	Refs

Note. — Column 1 gives an identification number. Columns 2 and 3 give the c2d and previous names when available. Note that the c2d names are slightly different from those in Chapman et al. (2007) due to a change in the naming convention. Columns 4 and 5 give the coordinates as in the Spitzer catalog. Column 6: 'YSO' means that satisfies the c2d YSO selection criteria (§ 3), otherwise it gives reference to a previous survey. Column 7: 'PMS' means that the object has been spectroscopically confirmed as a Pre-Main Sequence and 'Cnd' means that it is still a candidate. Column 8 gives the SED class from the slope computed from K to 24 μm with the Spitzer data. Column 9 gives other references to the object.

References. — 1) Comerón (2008); 2) Nakajima et al. (2000) ; 3) Comerón et al. (2003); 4) López Martí et al. (2005); 5) Allers et al. (2006); 6) Allen et al. (2007); 7) Chapman et al. (2007); 8) Tachihara et al. (2007); 9) Merín et al. (2007); 10) Strauss et al. (1992) 11) Gondoin (2006); 12) This work

Table 10. Visual binary objects in Lupus

No.	Object Id.	Separation (")	Notes
		In Lupus I	
1	SSTc2d J153803.1-331358	6	
4	Sz 65	6.5	with Sz 66
5	Sz 66	6.5	with Sz 65
7	AKC2006-18	8.4	NW
		8.5	E
15	Sz 68	2.5	from Reipurth & Zinnecker (1993)
16	Sz 69	6.6	SW
17	SSTc2d J154518.5-342125	6.1	NE
		6.2	SW, only in Z
		In Lupus III	
18	SSTc2d J160703.9-391112	12	SE
19	SSTc2d J160708.6-391407	2.2	SE, merged in MIPS
20	SSTc2d J160708.6-394723	2.9	SE
22	Sz 91	5.0	SE
26	Lup713	3.2	N, merged in MIPS
28	Sz 95	3.0	NW, faint
30	2MASS J16075475-3915446	2.2	SE, faint
31	SSTc2d J160755.3-390718	2.7	NE, IRAC eliptical
35	SSTc2d J160803.0-385229	6.0	E
43	Sz 100	4.0	SW
44	Lup607	2.5	E
53	HR 5999	1.5	from Ghez et al. (1997)
59	Sz 108	3.8	with Sz108B
60	Sz 108B	3.8	with Sz108
61	IRAC J16084679-3902074	4.0	SE
62	2MASS J16084747-3905087	2.2	E
		5.2	SE
66	Par-Lup3-4	4.5	SE
70	2MASS J16085373-3914367	5.0	SW, separated in IRAC
72	2MASS J16085529-3848481	3.0	SW, merged in IRAC and MIPS
73	Sz 112	2.8	SE, faint
77	NTO2000-0537.4-5653	5.0	N
78	2MASS J16085953-3856275	2.0	SW
81	NTO2000-0540.9-5757	2.4	NE
		2.4	NW
86	Lup710	3.4	W

Table 10—Continued

No.	Object Id.	Separation (")	Notes
89	NTO2000-0601.7-5616	7.0	N, from IRAC images
95	NTO2000-614.0-5414	0.8	N
		1.5	SE
		2.3	NW
101	Sz 116	1.5	complex shape
105	Lup810s	2.2	SW
		2.0	E
106	Lup818s	1.9	SE, faint
111	SSTc2d J161013.1-384617	3.0	SW
		3.0	S, not merged in IRAC
113	SSTc2d J161018.6-383613	2.7	S, very faint
114	SSTc2d J161019.8-383607	3.9	S
121	Sz 123	1.7	merged
122	SSTc2d J161118.7-385824	10.0	not merged
130	SST-Lup3-1	10.0	NE, not merged
131	SSTc2d J161200.1-385557	4.0	W
133	SSTc2d J161211.2-383220	2.7	S, faint
134	SSTc2d J161218.5-393418	1.7	E, faint
141	SSTc2d J161344.1-373646	4.2	NW
	In Lupus IV		
143	SSTc2d J155945.3-415457	4.0	W
144	SSTc2d J160000.6-422158	6.0	SE
145	SSTc2d J160002.4-422216	9.0	SW
147	SSTc2d J160026.1-415356	2.8	W, merged
		3.9	NE, not merged
148	Sz 130	3.7	SW, faint
		6.8	NE
154	SSTc2d J160129.7-420804	2.3	NW, faint
157	IRAS 15589-4132	2.6	SE, merged
159	Sz 133	3.6	E

Table 11. SED analysis results for the Class II and III objects in Lupus

No.	Object Id.	SpT	Ref.	A_V (mag)	L_* ($L_\odot$)	L_{disk}/L_*	$\lambda_{turn-off}$ (μm)	α_{excess}	YSOc	PMS	Bin.	SED type
					Lupus I							
1	SSTc2d J153803.1-331358	M5	6	3.0	1.192	0.424	8.0	-2.2	YSOc	Cnd	Y	L
3	AKC2006-17	L2	3	0.0	0.00046	0.288	2.2	-1.8	(5)	Cnd	N	L
4	Sz 65	M0	4	1.0	0.849	1.190	3.6	-1.0	YSOc	PMS	Y	T
5	Sz 66	M3	4	2.0	0.311	2.653	3.6	-0.8	YSOc	PMS	Y	T
6	Sz 67	M4	4	0.0	0.278	0.167	8.0	-0.8	(1)	PMS	N	E
7	AKC2006-18	M9	3	1.0	0.004	0.323	4.5	-1.4	(5)	Cnd	Y	L
9	SSTc2d J154240.3-341343	K6	6	9.0	2.163	0.039	8.0	-1.9	YSOc	Cnd	N	L
12	AKC2006-19	M7.5	3	0.0	0.018	0.101	5.8	0.6	YSOc	Cnd	N	L
14	SSTc2d J154508.9-341734	K0	6	10.0	1.049	0.111	2.2	-0.7	YSOc	Cnd	N	LU
15	Sz 68	K2	4	1.5	4.824	0.137	1.6	-1.5	(1)	PMS	Y	T
16	Sz 69	M1	4	4.0	0.375	0.166	2.2	-1.0	YSOc	PMS	Y	L
17	SSTc2d J154518.5-342125	M9	6	2.0	0.096	0.138	4.5	-1.0	YSOc	Cnd	Y	T
					Lupus III							
20	SSTc2d J160708.6-394723	K4	6	1.0	0.300	0.261	1.6	-1.3	(7)	Cnd	Y	L
21	Sz 90	K8	4	3.0	1.538	0.017	5.8	-1.3	YSOc	PMS	N	L
22	Sz 91	M0.5	4	1.0	0.206	0.510	8.0	0.7	YSOc	PMS	Y	LU
23	Lup 605	M6.5	2	1.0	0.014	0.016	8.0	...	(4)	Cnd	N	E
24	Sz 92	K0	6	1.0	0.478	0.060	2.2	-2.5	(1)	PMS	N	L
25	Lup 654	L1	2	0.0	0.002	0.151	8.0	...	(4)	Cnd	N	E
26	Lup 713	M6	2	0.0	0.023	0.358	3.6	-1.1	YSOc	PMS	Y	T
27	Sz 94	M4	4	0.0	0.103	0.369	8.0	...	(1)	PMS	N	E
28	Sz 95	M1.5	4	1.0	0.289	0.129	4.5	-1.0	YSOc	PMS	Y	L
29	SSTc2d J160754.1-392046	M2	6	5.0	4.834	-0.188	24.0	...	YSOc	Cnd	N	E
31	SSTc2d J160755.3-390718	M4	6	10.0	3.591	0.508	5.8	-2.1	YSOc	Cnd	Y	L
32	Lup 714	M5	2	1.0	0.052	0.227	8.0	...	(4)	Cnd	N	E
33	Lup 604s	M5.5	2	1.0	0.056	0.716	3.6	-1.0	YSOc	PMS	N	T

Table 11—Continued

No.	Object Id.	SpT	Ref.	A_V (mag)	L_* ($L_\odot$)	L_{disk}/L_*	$\lambda_{turn-off}$ (μm)	α_{excess}	YSOc	PMS	Bin.	SED type
34	2MASS J16080175-3912316	K6	6	6.0	0.010	0.208	3.6	-0.4	(2)	Cnd	N	T
35	SSTc2d J160803.0-385229	M1	6	4.0	0.450	0.173	24.0	...	YSOc	Cnd	Y	L
36	2MASS J16080618-3912225	K7	6	7.0	3.092	0.360	4.5	-1.7	YSOc	Cnd	N	L
37	Sz 96	M1.5	4	0.0	0.556	0.416	2.2	-0.9	YSOc	PMS	N	T
38	2MASS J16081497-3857145	M4.7	4	1.0	0.005	1.806	1.6	-0.6	YSOc	PMS	N	H
39	Par-Lup3-1	M7.5	4	1.0	0.064	0.123	8.0	...	(1)	PMS	N	E
40	Sz 97	M3	4	1.0	0.219	0.208	4.5	-0.9	YSOc	PMS	N	L
41	Sz 98	M0	4	0.0	0.555	2.214	1.6	-1.2	YSOc	PMS	N	H
42	Sz 99	M3.3	4	0.0	0.058	1.056	4.5	-0.9	YSOc	PMS	N	L
43	Sz 100	M5	4	1.0	0.226	0.511	3.6	-0.5	YSOc	PMS	Y	T
44	Lup 607	M5	2	2.0	0.038	0.003	5.8	0.1	(3)	Cnd	Y	T
45	NTO2000-0526.9-5630	G8	6	10.0	0.014	0.082	2.2	-2.8	(6)	Cnd	N	L
46	Sz 101	M4	4	2.0	0.993	0.031	8.0	-1.3	YSOc	PMS	N	L
49	Sz 103	M4	4	1.0	0.154	0.565	3.6	-0.2	YSOc	PMS	N	T
50	SSTc2d J160830.7-382827	K1	6	1.0	3.026	0.215	2.2	-0.2	(7)	Cnd	N	L
51	Sz 104	M5	4	0.0	0.123	0.285	4.5	0.1	YSOc	PMS	N	H
53	HR 5999	A7	4	0.0	48.288	0.704	0.9	-1.1	(1)	PMS	Y	T
54	HR 6000	A3	4	0.0	75.295	0.001	24.0	...	(1)	PMS	N	E
55	Par-Lup3-2	M6	4	0.0	0.158	0.067	8.0	...	(3)	PMS	N	E
56	Lup 706	L0	2	0.0	0.005	0.267	2.2	-1.3	(4)	PMS	N	H
57	Sz 106	M0	4	0.0	0.055	2.775	0.9	-0.5	YSOc	PMS	N	H
58	Sz 107	M5.5	4	1.0	0.188	0.120	8.0	-0.9	YSOc	PMS	N	L
59	Sz 108	M1	4	0.0	0.624	0.224	24.0	...	(1)	PMS	Y	E
60	Sz 108B	M6	6	4.0	0.356	0.001	8.0	-0.3	YSOc	Cnd	Y	L
63	Sz 109	M5.5	4	1.0	0.197	0.001	8.0	...	(1)	PMS	N	E
64	Lup 617	M6	2	0.0	0.038	0.044	8.0	...	(3)	Cnd	N	E
65	Par-Lup3-3	M4.5	4	0.0	0.041	5.843	0.7	-0.2	YSOc	PMS	N	H

Table 11—Continued

No.	Object Id.	SpT	Ref.	A_V (mag)	L_* ($L_\odot$)	L_{disk}/L_*	$\lambda_{turn-off}$ (μm)	α_{excess}	YSOc	PMS	Bin.	SED type
66	Par-Lup3-4	M5	4	0.0	0.003	6.262	1.2	0.3	YSOc	PMS	Y	H
67	Sz 110	M2	4	0.0	0.210	0.565	2.2	-0.5	YSOc	PMS	N	T
68	2MASS J16085324-3914401	M1	6	2.0	0.206	0.732	2.2	-0.8	YSOc	Cnd	N	T
69	NTO2000-0532.1-5616	K5	6	3.0	0.004	0.167	5.8	-0.5	(6)	Cnd	N	L
70	2MASS J16085373-3914367	M5.5	4	8.0	0.045	0.222	4.5	-1.1	YSOc	PMS	Y	L
71	Sz 111	M1.5	4	0.0	0.348	0.524	4.8	0.6	(1)	PMS	N	LU
72	2MASS J16085529-3848481	M2	6	3.0	0.088	0.469	4.5	-1.2	YSOc	Cnd	Y	T
73	Sz 112	M4	4	1.0	0.222	0.317	4.5	-1.7	YSOc	PMS	N	L
74	Sz 113	M4	4	2.0	0.087	0.390	3.6	-0.4	YSOc	PMS	N	T
77	NTO2000-0537.4-5653	K7	6	4.0	0.002	0.457	8.0	...	(2)	Cnd	Y	E
78	2MASS J16085953-3856275	M8	4	0.0	0.013	0.241	0.9	-0.8	YSOc	PMS	Y	T
79	SSTc2d J160901.4-392512	M3	6	0.0	0.071	1.431	0.9	-0.8	YSOc	Cnd	N	T
80	Sz 114	M4	4	2.0	0.719	0.143	4.5	-0.6	YSOc	PMS	N	T
81	NTO2000-0540.9-5757	K2	6	5.0	0.010	0.018	8.0	-0.9	(2)	Cnd	Y	E
82	Sz 115	M4	4	1.0	0.167	0.216	8.0	-1.2	YSOc	PMS	N	L
83	NTO2000-0546.4-5934	K7	6	13.0	0.047	0.257	2.2	-2.6	(2)	Cnd	N	E
84	Lup 608s	M5	2	1.0	0.059	0.351	8.0	...	(4)	Cnd	N	E
86	Lup 710	M5	2	2.0	0.038	0.001	8.0	...	(4)	Cnd	Y	E
91	SSTc2d J160927.0-383628	K7	6	3.0	0.139	0.371	2.2	-0.4	(7)	Cnd	N	T
92	NTO2000-0605.6-5437	G9	2	6.0	0.005	0.078	5.8	...	(2)	Cnd	N	E
93	SSTc2d J160934.1-391342	M4	6	6.0	6.082	0.422	24.0	...	YSOc	Cnd	N	L
95	NTO2000-0614.0-5414	K0	6	5.0	0.004	0.075	5.8	...	(2)	Cnd	Y	E
100	NTO2000-0619.6-5414	G9	6	4.0	0.004	0.054	4.5	-1.4	(2)	Cnd	N	L
101	Sz 116	M1.5	4	0.0	0.227	0.377	24.0	...	(1)	PMS	Y	L
102	Sz 117	M2	4	1.0	0.303	0.550	3.6	-0.8	YSOc	PMS	N	T
103	Sz 118	K6	4	6.0	0.881	1.146	0.9	-1.0	YSOc	PMS	N	T
104	Lup 650	M4	2	2.0	0.005	0.260	24.0	...	(4)	Cnd	N	E

Table 11—Continued

No.	Object Id.	SpT	Ref.	A_V (mag)	L_* ($L_\odot$)	L_{disk}/L_*	$\lambda_{turn-off}$ (μm)	α_{excess}	YSOc	PMS	Bin.	SED type
105	Lup 810s	M5	2	1.0	0.054	0.270	8.0	...	(4)	Cnd	Y	E
106	Lup 818s	M6	2	1.0	0.089	0.001	24.0	...	YSOc	Cnd	Y	T
107	Sz 119	M4	4	1.0	0.501	0.038	24.0	...	(1)	PMS	N	E
108	SSTc2d J161000.1-385401	A0	6	12.0	47.066	0.4784	8.0	-1.9	YSOc	Cnd	N	L
109	2MASS J16100133-3906449	G0	6	7.0	0.774	0.117	4.5	-1.1	YSOc	Cnd	N	L
110	Sz 121	M3	4	1.0	0.453	0.436	24.0	...	(1)	PMS	N	E
112	Sz 122	M2	4	0.0	0.232	0.193	24.0	...	(1)	PMS	N	E
113	SSTc2d J161018.6-383613	M1	6	2.0	0.071	0.085	5.8	-0.8	YSOc	Cnd	Y	L
114	SSTc2d J161019.8-383607	M4	6	2.0	0.049	0.219	4.5	-1.0	YSOc	Cnd	Y	L
116	SSTc2d J161029.6-392215	M4	6	1.0	0.087	0.472	5.8	-0.1	YSOc	Cnd	N	T
117	IRAS 16072-3738	M5	6	6.0	12.788	0.149	24.0	...	YSOc	Cnd	N	E
118	SSTc2d J161034.5-381450	M4	6	5.0	7.277	0.590	8.0	-2.4	YSOc	Cnd	N	L
119	SSTc2d J161035.0-390655	M5	6	6.0	1.413	0.469	8.0	-2.5	YSOc	Cnd	N	L
120	SSTc2d J161045.4-385455	K9	6	0.0	0.007	1.555	1.2	-1.0	YSOc	Cnd	N	H
121	Sz 123	M3	4	0.0	0.124	0.516	24.0	...	YSOc	PMS	Y	T
122	SSTc2d J161118.7-385824	M8	6	3.0	16.142	0.556	8.0	-2.1	YSOc	Cnd	Y	L
123	SSTc2d J161126.0-391123	K5	6	6.0	16.114	0.050	5.8	-2.2	YSOc	Cnd	N	L
124	SSTc2d J161131.9-381110	K9	6	2.0	0.103	0.440	4.5	-2.1	YSOc	Cnd	N	L
125	Lup 831s	K7	6	4.0	0.133	0.424	8.0	...	(4)	Cnd	N	E
126	SSTc2d J161144.9-383245	M3	6	3.0	0.109	0.043	8.0	-1.6	YSOc	Cnd	N	L
127	SSTc2d J161148.7-381758	K4	6	1.0	0.030	0.617	1.6	-0.6	YSOc	Cnd	N	T
128	Lup 802s	M4	2	1.0	0.025	0.361	8.0	...	(4)	Cnd	N	E
129	Sz 124	M0	4	0.0	0.462	0.062	24.0	...	(1)	PMS	N	E
130	SST-Lup3-1	M5.5	5	0.0	0.040	0.894	2.2	-0.8	YSOc	PMS	Y	T
131	SSTc2d J161200.1-385557	M2	6	2.0	3.247	0.337	5.8	-2.3	YSOc	Cnd	Y	L
133	SSTc2d J161211.2-383220	K7	6	6.0	0.598	0.222	3.6	-0.1	YSOc	Cnd	Y	T
135	SSTc2d J161219.6-383742	M5	6	4.0	3.474	0.363	24.0	...	YSOc	Cnd	N	L

Table 11—Continued

No.	Object Id.	SpT	Ref.	A_V (mag)	L_* ($L_\odot$)	L_{disk}/L_*	$\lambda_{turn-off}$ (μm)	α_{excess}	YSOc	PMS	Bin.	SED type
136	SSTc2d J161222.7-371328	G8	6	6.0	2.871	0.126	2.2	-1.8	(7)	Cnd	N	L
137	SSTc2d J161243.8-381503	K0	6	0.0	0.378	0.570	1.2	-1.0	YSOc	Cnd	N	T
138	SSTc2d J161251.7-384216	M8	6	1.0	2.263	0.366	8.0	-1.9	YSOc	Cnd	N	L
139	SSTc2d J161256.0-375643	K6	6	3.0	12.288	0.132	8.0	-2.3	YSOc	Cnd	N	L
140	SSTc2d J161341.0-383724	K1	6	5.0	9.096	0.060	24.0	...	YSOc	Cnd	N	L
141	SSTc2d J161344.1-373646	K9	6	2.0	0.067	0.374	2.2	-1.0	(7)	Cnd	Y	L
					Lupus IV							
142	SSTc2d J155925.2-423507	M2	6	0.0	0.019	0.222	2.2	-1.4	(7)	Cnd	N	L
143	SSTc2d J155945.3-415457	M0	6	2.0	0.729	1.336	1.2	-1.5	YSOc	Cnd	Y	T
144	SSTc2d J160000.6-422158	M2	6	1.0	0.065	0.589	2.2	-1.5	(7)	Cnd	Y	L
145	SSTc2d J160002.4-422216	K7	6	2.0	0.122	0.551	1.6	-1.3	(7)	Cnd	N	T
146	IRAS 15567-4141	M9	6	6.0	5.739	0.317	5.8	-2.2	YSOc	Cnd	N	L
147	SSTc2d J160026.1-415356	M1	6	3.0	0.109	0.114	5.8	-0.5	YSOc	Cnd	Y	L
148	Sz 130	M1.5	4	0.0	0.140	0.388	2.2	-0.8	YSOc	PMS	Y	T
149	SSTc2d J160034.4-422540	M8	6	2.0	1.450	0.813	2.2	-2.4	(7)	Cnd	N	L
150	F 403	K0	6	0.0	1.788	0.099	4.5	-0.2	YSOc	PMS	N	L
151	Sz 131	M2	4	0.0	0.054	1.368	1.6	-1.0	(1)	PMS	N	T
152	SSTc2d J160111.6-413730	M1	6	3.0	0.352	0.377	5.8	-2.3	YSOc	Cnd	N	L
154	SSTc2d J160129.7-420804	K6	6	4.0	0.746	0.396	8.0	...	YSOc	Cnd	Y	L
155	SSTc2d J160143.3-413606	M2	6	3.0	0.589	0.164	8.0	-2.2	YSOc	Cnd	N	L
156	IRAS 15585-4134	K7	6	6.0	10.027	1.002	3.6	-2.0	YSOc	Cnd	N	L
158	SSTc2d J160229.9-415111	M0	6	6.0	0.368	0.094	8.0	-2.3	YSOc	Cnd	N	L
159	Sz 133	K2	1	4.0	0.110	0.560	1.2	-99.	(1)	PMS	Y	H

Note. — Columns 3 and 4 give the spectral types and their corresponding references. In cases without a previous reference, the value was calculated with the optical and near-IR photometry (see § 4.2). Column 5 gives the extinction from the best fit of the photometry to the stellar model. Columns 6 and 7 show the stellar and disk fractional luminosities (§ 4.3 and 4.4). Columns 8 and 9 list the 2-dimensional parameters (§ 4.5) and Columns 10, 11 and 12 repeat the information in Tables 9 and 10.

References. — 1) Comerón (2008) 2) López Martí et al. (2005) 3) Allers et al. (2006) 4) Allen et al. (2007) 5) Merín et al. (2007) 6) This work

Table 12. Optical and Near-Infrared magnitudes of the Lupus sample

No.	Object Id.	B 0.44 μm	V 0.55 μm	R_c 0.64 μm	I_c 0.79 μm	Z 0.96 μm	J 1.23 μm	H 1.66 μm	Ks 2.16 μm
				Lupus I					
1	SSTc2dJ153803.1-331358	17.76 ± 0.05	16.44 ± 0.05	14.24 ± 0.22	11.84 ± 0.00	10.98 ± 0.00	9.03 ± 0.02	7.93 ± 0.02	7.47 ± 0.02
2	IRAS15356-3430	...	...	...	...	...	14.68 ± 0.05	13.56 ± 0.05	12.51 ± 0.05
3	AKC2006-17	...	...	23.86 ± 0.27	21.27 ± 0.59	19.14 ± 0.13	17.19 ± 0.03	16.27 ± 0.03	15.69 ± 0.03
4	Sz65	13.11 ± 0.05	12.13 ± 0.05	11.33 ± 0.05	10.76 ± 0.00	10.48 ± 0.00	9.19 ± 0.04	8.41 ± 0.04	7.98 ± 0.04
5	Sz66	...	...	14.51 ± 0.00	12.56 ± 0.00	11.66 ± 0.00	10.89 ± 0.03	9.88 ± 0.03	9.29 ± 0.03
6	Sz67	...	...	...	11.40 ± 0.00	11.34 ± 0.00	10.00 ± 0.02	9.36 ± 0.02	9.12 ± 0.02
7	AKC2006-18	...	...	19.45 ± 0.04	17.12 ± 0.03	16.00 ± 0.03	14.67 ± 0.03	14.02 ± 0.03	13.56 ± 0.03
8	SSTc2dJ154214.6-341026	...	...	...	19.33 ± 0.08	18.42 ± 0.07	15.99 ± 0.10	14.59 ± 0.10	13.56 ± 0.10
9	SSTc2dJ154240.3-341343	19.74 ± 0.05	...	18.17 ± 0.32	14.64 ± 0.01	13.20 ± 0.01	10.72 ± 0.02	9.05 ± 0.02	8.32 ± 0.02
10	IRAS15398-3359	...	...	18.38 ± 0.05	21.72 ± 0.25	20.86 ± 0.23	...	...	...
11	SSTc2dJ154302.3-344406	18.76 ± 0.05	...	18.35 ± 0.05	...	...	16.58 ± 0.12	15.59 ± 0.12	14.62 ± 0.12
12	AKC2006-19	18.38 ± 0.05	17.74 ± 0.05	17.29 ± 0.05	15.28 ± 0.05	...	12.98 ± 0.02	12.41 ± 0.02	12.13 ± 0.02
13	SSTc2dJ154506.3-341738	...	...	...	...	...	15.56 ± 0.07	13.52 ± 0.07	12.10 ± 0.07
14	SSTc2dJ154508.9-341734	...	...	18.73 ± 0.05	...	...	12.20 ± 0.03	10.64 ± 0.03	9.71 ± 0.03
15	Sz68	11.53 ± 0.05	10.35 ± 0.05	...	...	...	7.57 ± 0.02	6.86 ± 0.02	6.48 ± 0.02
16	Sz69	17.41 ± 0.06	16.25 ± 0.06	...	...	...	11.18 ± 0.03	10.16 ± 0.03	9.41 ± 0.03
17	SSTc2dJ154518.5-342125	17.95 ± 0.05	...	17.35 ± 0.05	...	...	11.64 ± 0.03	10.95 ± 0.03	10.48 ± 0.03
				Lupus III					
18	SSTc2dJ160703.9-391112	...	...	18.79 ± 0.06	16.80 ± 0.02	16.16 ± 0.02	14.68 ± 0.04	13.77 ± 0.04	13.11 ± 0.05
19	SSTc2dJ160708.6-391407	17.85 ± 0.05	...	18.67 ± 0.76	17.86 ± 0.04	17.05 ± 0.04	15.22 ± 0.05	13.13 ± 0.05	11.56 ± 0.02
20	SSTc2dJ160708.6-394723	15.38 ± 0.05	14.04 ± 0.05	13.50 ± 0.05	...	...	11.51 ± 0.02	10.65 ± 0.02	10.11 ± 0.02
21	Sz90	15.28 ± 0.05	13.70 ± 0.05	13.70 ± 0.68	12.49 ± 0.00	11.80 ± 0.00	10.35 ± 0.02	9.32 ± 0.02	8.72 ± 0.02
22	Sz91	16.25 ± 0.05	14.58 ± 0.05	14.11 ± 0.27	12.92 ± 0.00	12.39 ± 0.01	11.06 ± 0.02	10.12 ± 0.02	9.85 ± 0.02
23	Lup605	...	...	18.84 ± 0.20	16.49 ± 0.02	15.67 ± 0.02	14.21 ± 0.03	13.57 ± 0.03	13.20 ± 0.04
24	Sz92	...	12.98 ± 0.05	...	...	...	11.27 ± 0.02	10.57 ± 0.02	10.41 ± 0.02
25	Lup654	17.95 ± 0.05	...	18.25 ± 0.52	17.54 ± 0.04	17.13 ± 0.04	15.75 ± 0.23	14.88 ± 0.23	14.60 ± 0.27
26	Lup713	18.38 ± 0.05	...	17.12 ± 0.67	15.68 ± 0.02	14.82 ± 0.01	13.24 ± 0.03	12.57 ± 0.03	12.13 ± 0.03
27	Sz94	16.31 ± 0.05	16.00 ± 0.05	14.76 ± 0.05	13.00 ± 0.00	12.49 ± 0.01	11.45 ± 0.02	10.80 ± 0.02	10.56 ± 0.02
28	Sz95	16.39 ± 0.05	14.57 ± 0.05	14.25 ± 0.28	12.71 ± 0.00	12.33 ± 0.01	11.01 ± 0.02	10.28 ± 0.02	10.01 ± 0.02
29	SSTc2dJ160754.1-392046	17.15 ± 0.05	15.32 ± 0.05	14.58 ± 0.26	12.26 ± 0.00	11.09 ± 0.00	9.45 ± 0.02	8.41 ± 0.02	7.91 ± 0.03
30	2MASSJ16075475-3915446	...	...	21.91 ± 0.11	19.92 ± 0.11	18.76 ± 0.08	17.20 ± 0.22	16.12 ± 0.22	14.46 ± 0.08
31	SSTc2dJ160755.3-390718	...	...	19.39 ± 0.36	15.70 ± 0.02	13.60 ± 0.01	10.32 ± 0.02	8.56 ± 0.02	7.61 ± 0.03
32	Lup714	17.34 ± 0.05	...	16.58 ± 0.32	14.74 ± 0.01	14.06 ± 0.01	12.57 ± 0.02	11.92 ± 0.02	11.59 ± 0.02

Table 12—Continued

No.	Object Id.	B 0.44 μm	V 0.55 μm	R_c 0.64 μm	I_c 0.79 μm	Z 0.96 μm	J 1.23 μm	H 1.66 μm	Ks 2.16 μm
33	Lup604s	16.94 ± 0.05	17.01 ± 0.05	16.72 ± 0.23	14.31 ± 0.01	13.48 ± 0.01	12.15 ± 0.03	11.45 ± 0.03	11.07 ± 0.02
34	2MASSJ16080175-3912316	...	...	19.69 ± 1.16	19.37 ± 0.08	18.29 ± 0.07	16.40 ± 0.14	15.06 ± 0.14	14.25 ± 0.09
35	SSTc2dJ160803.0-385229	15.78 ± 0.05	13.52 ± 0.05	13.88 ± 0.41	12.00 ± 0.00	11.04 ± 0.00	9.52 ± 0.02	8.51 ± 0.02	8.10 ± 0.03
36	2MASSJ16080618-3912225	...	...	18.00 ± 1.12	13.76 ± 0.01	12.50 ± 0.01	10.03 ± 0.02	8.53 ± 0.02	7.67 ± 0.02
37	Sz96	14.80 ± 0.05	13.43 ± 0.05	13.69 ± 0.08	11.83 ± 0.00	12.33 ± 0.00	10.13 ± 0.02	9.35 ± 0.02	8.96 ± 0.02
38	2MASSJ16081497-3857145	...	...	18.93 ± 0.57	17.42 ± 0.03	16.73 ± 0.04	15.21 ± 0.05	14.20 ± 0.05	13.13 ± 0.03
39	Par-Lup3-1	17.74 ± 0.05	...	18.15 ± 0.19	15.28 ± 0.01	14.19 ± 0.01	12.52 ± 0.02	11.75 ± 0.02	11.25 ± 0.02
40	Sz97	16.18 ± 0.05	14.61 ± 0.05	14.67 ± 0.11	12.92 ± 0.00	12.38 ± 0.01	11.24 ± 0.02	10.55 ± 0.02	10.22 ± 0.02
41	Sz98	14.99 ± 0.05	13.66 ± 0.05	11.70 ± 0.05	11.21 ± 0.00	10.74 ± 0.00	9.53 ± 0.02	8.65 ± 0.02	8.01 ± 0.02
42	Sz99	15.49 ± 0.05	16.00 ± 0.05	15.39 ± 0.35	14.17 ± 0.01	13.42 ± 0.01	11.93 ± 0.02	11.21 ± 0.02	10.74 ± 0.02
43	Sz100	16.62 ± 0.05	15.43 ± 0.05	14.97 ± 0.25	13.12 ± 0.01	12.32 ± 0.00	10.98 ± 0.02	10.35 ± 0.02	9.91 ± 0.02
44	Lup607	17.45 ± 0.05	...	17.76 ± 0.67	16.13 ± 0.02	15.34 ± 0.02	13.74 ± 0.09	...	12.44 ± 0.11
45	NTO2000-0526.9-5630	...	...	24.17 ± 0.33	21.31 ± 0.18	20.29 ± 0.19	17.19 ± 0.17	16.14 ± 0.08	15.35 ± 0.07
46	Sz101	...	...	14.00 ± 0.52	12.35 ± 0.00	11.65 ± 0.00	10.40 ± 0.02	9.72 ± 0.02	9.39 ± 0.02
47	Sz102	16.26 ± 0.05	15.91 ± 0.05	15.38 ± 0.51	15.69 ± 0.02	15.64 ± 0.02	14.56 ± 0.04	13.65 ± 0.04	12.58 ± 0.03
48	IRACJ16083010-3922592	...	...	22.46 ± 0.14	20.72 ± 0.15	20.28 ± 0.17	...	...	...
49	Sz103	...	11.14 ± 0.05	15.18 ± 0.01	13.15 ± 0.01	12.53 ± 0.01	11.38 ± 0.02	10.62 ± 0.02	10.23 ± 0.02
50	SSTc2dJ160830.7-382827	11.89 ± 0.05	11.15 ± 0.05	10.67 ± 0.05	...	...	8.97 ± 0.02	8.39 ± 0.02	8.22 ± 0.03
51	Sz104	...	15.25 ± 0.05	13.96 ± 1.68	13.57 ± 0.01	12.92 ± 0.01	11.66 ± 0.02	11.00 ± 0.02	10.65 ± 0.02
52	IRACJ16083110-3856000	...	...	21.60 ± 0.09	20.74 ± 0.17	21.06 ± 0.26	...	...	...
53	HR5999	7.38 ± 0.05	7.10 ± 0.05	6.92 ± 0.05	...	...	5.91 ± 0.02	5.22 ± 0.02	4.39 ± 0.04
54	HR6000	6.55 ± 0.05	6.62 ± 0.05	6.66 ± 0.05	...	...	6.67 ± 0.02	6.71 ± 0.02	6.67 ± 0.02
55	Par-Lup3-2	16.88 ± 0.05	15.49 ± 0.05	15.02 ± 0.10	13.09 ± 0.00	12.47 ± 0.01	11.24 ± 0.03	10.73 ± 0.03	10.34 ± 0.02
56	Lup706	...	...	20.70 ± 0.06	18.44 ± 0.05	16.82 ± 0.03	15.17 ± 0.06	14.24 ± 0.06	13.83 ± 0.04
57	Sz106	...	...	15.00 ± 0.98	14.66 ± 0.01	14.28 ± 0.01	11.65 ± 0.03	10.66 ± 0.03	10.15 ± 0.02
58	Sz107	17.31 ± 0.05	16.06 ± 0.05	15.42 ± 0.10	13.20 ± 0.01	12.45 ± 0.01	11.25 ± 0.03	10.62 ± 0.03	10.31 ± 0.02
59	Sz108	14.68 ± 0.01	11.78 ± 0.05	11.72 ± 0.05	11.68 ± 0.00	10.86 ± 0.00	9.79 ± 0.03	9.04 ± 0.03	8.84 ± 0.03
60	Sz108B	...	...	17.71 ± 0.02	14.39 ± 0.01	13.30 ± 0.01	...	...	...
61	IRACJ16084679-3902074	...	...	22.28 ± 0.13	21.04 ± 0.18	20.94 ± 0.25	...	...	...
62	2MASSJ16084747-3905087	...	...	20.93 ± 0.07	19.32 ± 0.08	18.48 ± 0.07	16.45 ± 0.14	15.37 ± 0.14	14.83 ± 0.11
63	Sz109	18.23 ± 0.05	16.43 ± 0.05	15.71 ± 0.19	13.57 ± 0.01	12.72 ± 0.01	11.40 ± 0.02	10.82 ± 0.02	10.50 ± 0.02
64	Lup617	17.27 ± 0.05	17.41 ± 0.05	17.29 ± 0.05	15.02 ± 0.01	14.21 ± 0.01	12.87 ± 0.03	12.26 ± 0.03	11.97 ± 0.02
65	Par-Lup3-3	16.76 ± 0.05	...	15.89 ± 0.39	14.24 ± 0.01	13.33 ± 0.01	11.45 ± 0.03	10.17 ± 0.03	9.55 ± 0.02
66	Par-Lup3-4	...	...	18.97 ± 0.59	18.18 ± 0.05	17.88 ± 0.06	15.46 ± 0.06	14.26 ± 0.06	13.30 ± 0.04

Table 12—Continued

No.	Object Id.	B 0.44 μm	V 0.55 μm	R_c 0.64 μm	I_c 0.79 μm	Z 0.96 μm	J 1.23 μm	H 1.66 μm	Ks 2.16 μm
67	Sz110	15.27 ± 0.05	14.58 ± 0.05	13.72 ± 0.05	12.28 ± 0.00	12.09 ± 0.00	10.97 ± 0.02	10.22 ± 0.02	9.75 ± 0.02
68	2MASSJ16085324-3914401	17.53 ± 0.05	16.35 ± 0.05	15.35 ± 0.09	13.52 ± 0.01	12.93 ± 0.01	11.33 ± 0.03	10.28 ± 0.03	9.80 ± 0.02
69	NTO2000-0532.1-5616	...	...	19.19 ± 0.51	18.39 ± 0.05	17.94 ± 0.06	16.62 ± 0.12	15.49 ± 0.12	14.90 ± 0.11
70	2MASSJ16085373-3914367	...	...	21.73 ± 0.10	18.76 ± 0.06	17.39 ± 0.04	14.97 ± 0.07	13.44 ± 0.07	12.52 ± 0.04
71	Sz111	15.34 ± 0.05	13.98 ± 0.05	13.29 ± 0.05	...	...	10.62 ± 0.02	9.80 ± 0.02	9.54 ± 0.02
72	2MASSJ16085529-3848481	17.36 ± 0.05	...	17.24 ± 0.23	15.24 ± 0.01	14.44 ± 0.01	12.98 ± 0.03	12.39 ± 0.03	12.02 ± 0.02
73	Sz112	16.62 ± 0.05	15.39 ± 0.05	14.78 ± 0.15	12.93 ± 0.00	12.26 ± 0.01	11.00 ± 0.02	10.29 ± 0.02	9.96 ± 0.02
74	Sz113	17.46 ± 0.05	16.50 ± 0.05	16.64 ± 0.11	14.65 ± 0.01	13.83 ± 0.01	12.46 ± 0.02	11.73 ± 0.02	11.26 ± 0.02
75	NTO2000-0536.7-5943	...	...	...	...	...	< 17.39	16.51 ± 0.17	12.56 ± 0.03
76	NTO2000-0536.7-5956	...	...	...	...	...	< 17.53	< 16.62	15.15 ± 0.13
77	NTO2000-0537.4-5653	...	...	21.76 ± 0.10	19.79 ± 0.10	18.92 ± 0.10	< 17.02	15.65 ± 0.00	15.27 ± 0.16
78	2MASSJ16085953-3856275	...	...	19.25 ± 0.58	16.91 ± 0.02	15.70 ± 0.02	13.90 ± 0.03	13.29 ± 0.03	12.83 ± 0.03
79	SSTc2dJ160901.4-392512	16.92 ± 0.05	15.31 ± 0.05	15.04 ± 0.20	13.48 ± 0.01	13.37 ± 0.01	11.61 ± 0.02	10.68 ± 0.02	10.29 ± 0.02
80	Sz114	15.33 ± 0.05	14.12 ± 0.05	14.35 ± 0.39	12.54 ± 0.00	11.72 ± 0.00	10.41 ± 0.03	9.70 ± 0.03	9.32 ± 0.02
81	NTO2000-0540.9-5757	...	...	19.53 ± 0.54	18.60 ± 0.06	17.96 ± 0.06	16.17 ± 0.08	15.22 ± 0.08	14.86 ± 0.11
82	Sz115	16.88 ± 0.05	15.48 ± 0.05	15.09 ± 0.09	13.12 ± 0.01	12.57 ± 0.01	11.33 ± 0.03	10.65 ± 0.03	10.45 ± 0.03
83	NTO2000-0546.4-5934	...	...	...	21.65 ± 0.24	19.85 ± 0.14	16.58 ± 0.13	14.24 ± 0.13	12.94 ± 0.04
84	Lup608s	18.00 ± 0.05	16.60 ± 0.05	16.43 ± 0.16	14.16 ± 0.01	13.42 ± 0.01	12.20 ± 0.03	11.64 ± 0.03	11.36 ± 0.03
85	NTO2000-0554.9-5651	...	...	...	...	...	< 17.79	< 16.44	15.16 ± 0.15
86	Lup710	17.66 ± 0.05	...	17.76 ± 0.26	15.67 ± 0.02	14.92 ± 0.01	13.55 ± 0.03	13.04 ± 0.03	12.66 ± 0.03
87	Lupus3MMS	...	...	...	...	...	...	...	0.00 ± 0.00
88	NTO2000-0558.8-5610	...	...	...	...	...	< 18.21	< 16.02	14.90 ± 0.11
89	NTO2000-0601.7-5616	...	...	...	...	...	< 16.92	15.23 ± 0.00	13.12 ± 0.03
90	NTO2000-0605.1-5606	...	...	...	...	...	18.57 ± 0.27	17.57 ± 0.13	15.33 ± 0.08
91	SSTc2dJ160927.0-383628	17.55 ± 0.05	...	16.31 ± 0.14	14.74 ± 0.01	14.05 ± 0.01	12.55 ± 0.03	11.69 ± 0.03	10.95 ± 0.02
92	NTO2000-0605.6-5437	...	...	21.03 ± 0.07	19.48 ± 0.09	19.03 ± 0.10	17.29 ± 0.11	16.56 ± 0.10	15.67 ± 0.08
93	SSTc2dJ160934.1-391342	18.32 ± 0.05	16.44 ± 0.05	15.42 ± 0.18	12.24 ± 0.00	10.80 ± 0.00	8.68 ± 0.02	7.33 ± 0.02	6.67 ± 0.02
94	IRACJ16093418-3915127	...	...	...	...	...	...	...	...
95	NTO2000-0614.0-5414	...	...	21.23 ± 0.08	19.64 ± 0.09	19.04 ± 0.10	17.30 ± 0.12	16.54 ± 0.10	15.75 ± 0.09
96	NTO2000-0615.6-5616	...	...	...	...	...	...	18.41 ± 0.40	15.38 ± 0.10
97	NTO2000-0615.6-5953	...	...	...	...	...	< 17.59	15.57 ± 0.00	14.87 ± 0.11
98	NTO2000-0615.8-5734	...	...	...	...	...	< 18.30	14.16 ± 0.00	11.21 ± 0.02
99	NTO2000-0617.7-5641	...	...	...	...	...	< 17.69	< 15.67	13.38 ± 0.04
100	NTO2000-0619.6-5414	...	...	19.73 ± 0.71	19.12 ± 0.08	18.49 ± 0.08	17.09 ± 0.09	16.40 ± 0.09	15.73 ± 0.08

Table 12—Continued

No.	Object Id.	B 0.44 μm	V 0.55 μm	R_c 0.64 μm	I_c 0.79 μm	Z 0.96 μm	J 1.23 μm	H 1.66 μm	Ks 2.16 μm
101	Sz116	14.79 ± 0.05	13.23 ± 0.05	13.05 ± 0.05	12.20 ± 0.00	11.84 ± 0.00	10.47 ± 0.03	9.77 ± 0.03	9.53 ± 0.03
102	Sz117	15.84 ± 0.05	14.59 ± 0.05	14.20 ± 0.16	12.38 ± 0.00	12.19 ± 0.00	10.68 ± 0.02	9.85 ± 0.02	9.43 ± 0.02
103	Sz118	18.32 ± 0.05	16.90 ± 0.05	16.61 ± 0.05	15.00 ± 0.01	12.98 ± 0.01	10.45 ± 0.03	9.35 ± 0.03	8.68 ± 0.02
104	Lup650	...	...	19.85 ± 0.04	17.62 ± 0.03	16.87 ± 0.04	15.39 ± 0.06	14.76 ± 0.06	14.38 ± 0.07
105	Lup810s	16.61 ± 0.05	16.38 ± 0.05	16.16 ± 0.51	15.20 ± 0.01	14.69 ± 0.01	12.84 ± 0.04	11.68 ± 0.04	11.26 ± 0.03
106	Lup818s	17.37 ± 0.05	...	16.49 ± 1.11	15.28 ± 0.01	14.38 ± 0.01	13.01 ± 0.03	12.39 ± 0.03	11.99 ± 0.03
107	Sz119	15.35 ± 0.05	13.71 ± 0.05	13.49 ± 0.61	12.10 ± 0.00	11.54 ± 0.00	10.39 ± 0.02	9.67 ± 0.02	9.42 ± 0.02
108	SSTc2dJ161000.1-385401	...	...	17.41 ± 0.11	13.55 ± 0.01	11.33 ± 0.00	9.63 ± 0.02	8.49 ± 0.02	7.70 ± 0.02
109	2MASSJ16100133-3906449	18.38 ± 0.05	17.42 ± 0.05	17.90 ± 0.11	15.27 ± 0.01	14.10 ± 0.01	12.20 ± 0.03	11.15 ± 0.03	10.52 ± 0.02
110	Sz121	15.70 ± 0.05	14.06 ± 0.05	13.88 ± 0.13	11.90 ± 0.00	11.57 ± 0.00	10.07 ± 0.02	9.31 ± 0.02	9.03 ± 0.02
111	SSTc2dJ161013.1-384617	...	...	19.15 ± 0.24	17.42 ± 0.03	16.94 ± 0.04	15.87 ± 0.08	15.03 ± 0.08	13.92 ± 0.05
112	Sz122	15.33 ± 0.05	13.73 ± 0.05	13.28 ± 0.05	12.18 ± 0.00	11.97 ± 0.00	10.87 ± 0.03	10.12 ± 0.03	9.93 ± 0.02
113	SSTc2dJ161018.6-383613	18.37 ± 0.05	16.63 ± 0.05	16.67 ± 0.18	14.70 ± 0.01	13.91 ± 0.01	12.66 ± 0.02	12.09 ± 0.02	11.76 ± 0.02
114	SSTc2dJ161019.8-383607	17.39 ± 0.05	...	16.76 ± 1.26	15.57 ± 0.01	14.70 ± 0.01	13.28 ± 0.04	< 12.65	12.32 ± 0.04
115	SSTc2dJ161027.4-390230	...	...	21.73 ± 0.10	19.26 ± 0.07	18.31 ± 0.07	16.59 ± 0.12	15.29 ± 0.12	14.73 ± 0.09
116	SSTc2dJ161029.6-392215	17.51 ± 0.05	16.31 ± 0.05	15.79 ± 0.05	13.90 ± 0.01	13.42 ± 0.01	11.94 ± 0.02	11.27 ± 0.02	10.91 ± 0.02
117	IRAS16072-3738	18.38 ± 0.05	17.15 ± 0.05	15.07 ± 0.21	11.70 ± 0.00	10.39 ± 0.00	8.01 ± 0.03	6.87 ± 0.03	6.29 ± 0.02
118	SSTc2dJ161034.5-381450	17.49 ± 0.05	15.72 ± 0.05	14.38 ± 0.18	11.65 ± 0.00	10.51 ± 0.00	8.01 ± 0.02	6.85 ± 0.02	6.31 ± 0.02
119	SSTc2dJ161035.0-390655	18.20 ± 0.05	...	17.22 ± 0.07	13.96 ± 0.01	12.56 ± 0.01	10.38 ± 0.02	8.82 ± 0.02	8.21 ± 0.02
120	SSTc2dJ161045.4-385455	17.51 ± 0.05	...	17.13 ± 0.13	16.05 ± 0.02	15.74 ± 0.02	14.31 ± 0.03	13.40 ± 0.03	12.96 ± 0.03
121	Sz123	15.89 ± 0.05	14.48 ± 0.05	14.44 ± 0.17	12.98 ± 0.00	12.49 ± 0.01	11.09 ± 0.02	10.21 ± 0.02	9.78 ± 0.02
122	SSTc2dJ161118.7-385824	17.68 ± 0.05	15.53 ± 0.05	13.97 ± 0.05	...	...	6.79 ± 0.02	5.51 ± 0.02	4.84 ± 0.02
123	SSTc2dJ161126.0-391123	18.18 ± 0.05	17.52 ± 0.05	16.09 ± 0.25	12.43 ± 0.00	11.51 ± 0.00	8.40 ± 0.02	7.14 ± 0.02	6.48 ± 0.02
124	SSTc2dJ161131.9-381110	18.76 ± 0.05	...	15.90 ± 0.34	14.56 ± 0.01	13.97 ± 0.01	12.28 ± 0.03	11.09 ± 0.03	10.69 ± 0.02
125	Lup831s	18.00 ± 0.05	...	17.21 ± 0.18	15.37 ± 0.01	14.53 ± 0.01	12.51 ± 0.02	11.19 ± 0.02	10.69 ± 0.02
126	SSTc2dJ161144.9-383245	17.49 ± 0.05	...	17.12 ± 0.10	14.73 ± 0.01	13.90 ± 0.01	12.44 ± 0.02	11.82 ± 0.02	11.47 ± 0.03
127	SSTc2dJ161148.7-381758	17.04 ± 0.05	15.64 ± 0.05	15.72 ± 0.09	14.99 ± 0.01	14.84 ± 0.01	13.71 ± 0.03	13.04 ± 0.03	12.35 ± 0.02
128	Lup802s	17.54 ± 0.05	17.31 ± 0.05	17.15 ± 0.05	15.18 ± 0.01	14.54 ± 0.01	13.25 ± 0.03	12.56 ± 0.03	12.25 ± 0.03
129	Sz124	14.44 ± 0.05	13.04 ± 0.05	12.33 ± 0.05	11.41 ± 0.00	11.36 ± 0.00	10.29 ± 0.02	9.63 ± 0.02	9.44 ± 0.02
130	SST-Lup3-1	18.17 ± 0.05	16.55 ± 0.05	16.24 ± 0.05	14.26 ± 0.01	13.60 ± 0.01	12.20 ± 0.02	11.51 ± 0.02	11.20 ± 0.02
131	SSTc2dJ161200.1-385557	18.29 ± 0.05	15.88 ± 0.05	14.94 ± 0.05	11.41 ± 0.00	10.87 ± 0.00	8.77 ± 0.02	7.43 ± 0.02	6.90 ± 0.02
132	SSTc2dJ161204.5-380959	...	...	19.17 ± 0.65	18.68 ± 0.06	17.72 ± 0.05	16.55 ± 0.17	15.38 ± 0.17	14.83 ± 0.13
133	SSTc2dJ161211.2-383220	18.03 ± 0.05	...	17.25 ± 0.30	14.76 ± 0.01	14.13 ± 0.01	11.84 ± 0.02	10.28 ± 0.02	9.41 ± 0.02
134	SSTc2dJ161218.5-393418	...	...	18.58 ± 0.10	16.84 ± 0.03	16.24 ± 0.02	14.89 ± 0.04	13.73 ± 0.04	12.77 ± 0.03

Table 12—Continued

No.	Object Id.	B 0.44 μm	V 0.55 μm	R_c 0.64 μm	I_c 0.79 μm	Z 0.96 μm	J 1.23 μm	H 1.66 μm	Ks 2.16 μm
135	SSTc2dJ161219.6-383742	17.24 ± 0.05	15.57 ± 0.05	14.55 ± 0.05	11.82 ± 0.00	10.77 ± 0.00	8.72 ± 0.02	7.62 ± 0.02	7.19 ± 0.02
136	SSTc2dJ161222.7-371328	17.63 ± 0.05	15.63 ± 0.05	15.76 ± 0.05	...	...	10.63 ± 0.02	9.60 ± 0.02	8.96 ± 0.02
137	SSTc2dJ161243.8-381503	15.00 ± 0.05	13.44 ± 0.05	13.39 ± 0.05	11.61 ± 0.00	11.74 ± 0.00	10.54 ± 0.02	9.77 ± 0.02	9.54 ± 0.02
138	SSTc2dJ161251.7-384216	17.22 ± 0.05	15.45 ± 0.05	14.06 ± 0.05	...	...	8.57 ± 0.02	7.48 ± 0.02	6.99 ± 0.02
139	SSTc2dJ161256.0-375643	17.47 ± 0.05	15.45 ± 0.05	14.22 ± 0.29	10.98 ± 0.00	10.43 ± 0.00	7.77 ± 0.02	6.64 ± 0.02	6.11 ± 0.02
140	SSTc2dJ161341.0-383724	16.21 ± 0.05	13.68 ± 0.05	13.22 ± 0.05	...	...	8.91 ± 0.04	7.75 ± 0.04	7.27 ± 0.02
141	SSTc2dJ161344.1-373646	17.97 ± 0.05	...	16.37 ± 0.01	14.66 ± 0.01	14.09 ± 0.01	12.76 ± 0.09	12.09 ± 0.09	11.61 ± 0.02
				Lupus IV					
142	SSTc2dJ155925.2-423507	17.42 ± 0.05	16.82 ± 0.05	...	...	...	13.18 ± 0.05	12.58 ± 0.05	12.26 ± 0.05
143	SSTc2dJ155945.3-415457	18.27 ± 0.05	14.41 ± 0.05	13.42 ± 0.29	11.56 ± 0.00	11.02 ± 0.00	9.10 ± 0.05	7.78 ± 0.05	7.19 ± 0.05
144	SSTc2dJ160000.6-422158	17.29 ± 0.05	15.85 ± 0.05	15.25 ± 0.05	13.43 ± 0.01	13.02 ± 0.01	11.63 ± 0.05	10.98 ± 0.05	10.66 ± 0.05
145	SSTc2dJ160002.4-422216	16.86 ± 0.05	15.46 ± 0.05	14.98 ± 0.17	13.59 ± 0.01	13.09 ± 0.01	11.45 ± 0.05	10.59 ± 0.05	10.14 ± 0.05
146	IRAS15567-4141	...	...	16.30 ± 0.05	...	...	8.16 ± 0.05	7.06 ± 0.05	6.12 ± 0.05
147	SSTc2dJ160026.1-415356	16.57 ± 0.05	16.45 ± 0.05	15.70 ± 0.21	13.80 ± 0.01	13.10 ± 0.01	11.82 ± 0.05	11.10 ± 0.05	10.78 ± 0.05
148	Sz130	15.82 ± 0.05	14.71 ± 0.05	13.56 ± 0.54	12.46 ± 0.00	12.26 ± 0.00	10.73 ± 0.05	9.93 ± 0.05	9.62 ± 0.05
149	SSTc2dJ160034.4-422540	16.92 ± 0.05	17.39 ± 0.05	15.56 ± 0.05	...	...	8.71 ± 0.05	7.53 ± 0.05	6.90 ± 0.05
150	F403	12.64 ± 0.05	12.17 ± 0.05	11.06 ± 0.05	...	...	9.46 ± 0.05	8.68 ± 0.05	8.35 ± 0.05
151	Sz131	17.51 ± 0.05	16.13 ± 0.05	14.60 ± 0.05	12.92 ± 0.00	13.26 ± 0.01	11.47 ± 0.05	10.61 ± 0.05	10.10 ± 0.05
152	SSTc2dJ160111.6-413730	18.38 ± 0.05	16.66 ± 0.05	15.46 ± 0.06	12.98 ± 0.00	12.27 ± 0.00	10.48 ± 0.05	9.37 ± 0.05	8.96 ± 0.05
153	SSTc2dJ160115.6-415235	...	...	...	...	...	16.44 ± 0.05	14.47 ± 0.05	12.85 ± 0.05
154	SSTc2dJ160129.7-420804	18.26 ± 0.05	16.48 ± 0.05	15.67 ± 0.12	13.34 ± 0.01	12.63 ± 0.01	10.78 ± 0.05	9.54 ± 0.05	9.05 ± 0.05
155	SSTc2dJ160143.3-413606	18.01 ± 0.05	16.26 ± 0.05	15.17 ± 0.40	12.43 ± 0.00	11.70 ± 0.00	10.15 ± 0.05	9.07 ± 0.05	8.60 ± 0.05
156	IRAS15585-4134	17.99 ± 0.05	16.07 ± 0.05	14.24 ± 0.08	11.11 ± 0.00	9.97 ± 0.00	7.10 ± 0.05	5.71 ± 0.05	5.09 ± 0.05
157	IRAS15589-4132	17.84 ± 0.05	...	17.98 ± 1.27	17.74 ± 0.04	17.19 ± 0.04	14.98 ± 0.05	13.71 ± 0.05	12.89 ± 0.05
158	SSTc2dJ160229.9-415111	...	...	17.69 ± 0.10	14.69 ± 0.01	13.53 ± 0.01	11.52 ± 0.05	10.26 ± 0.05	9.71 ± 0.05
159	Sz133	17.77 ± 0.05	16.60 ± 0.05	15.78 ± 0.23	15.04 ± 0.01	14.06 ± 0.01	12.11 ± 0.05	10.55 ± 0.05	9.53 ± 0.05

Note. — B and V magnitudes from the NOMAD catalog (Zacharias et al. 2005).

Note. — R_c, I_c, and z magnitudes from F. Comeron et al. (in prep.).

Note. — J, H, and Ks magnitudes from the 2MASS catalog (Cutri et al. 2003).

Table 13. IRAC and MIPS fluxes in mJy of the Lupus sample

No.	Object Id.	IRAC 3.6 μm	IRAC 4.5 μm	IRAC 5.8 μm	IRAC 8.0 μm	MIPS 24 μm	MIPS 70 μm	MIPS 160 μm
				Lupus I				
1	SSTc2dJ153803.1-331358	347.00 ± 18.80	220.00 ± 18.80	182.00 ± 9.44	126.00 ± 6.43	35.60 ± 3.30	< 50.00	...
2	IRAS15356-3430	3.95 ± 0.40	2.76 ± 0.40	9.58 ± 0.75	42.70 ± 3.11	114.00 ± 11.20	2920.00 ± 279.00	...
3	AKC2006-17	0.49 ± 0.03	0.37 ± 0.03	0.35 ± 0.04	0.25 ± 0.06	0.41 ± 0.46	< 50.00	...
4	Sz65	255.00 ± 14.30	225.00 ± 14.30	231.00 ± 12.50	284.00 ± 14.00	483.00 ± 44.60	468.00 ± 47.30	...
5	Sz66	95.80 ± 4.98	81.50 ± 4.98	82.50 ± 3.99	100.00 ± 4.84	167.00 ± 15.50	< 50.00	...
6	Sz67	79.10 ± 4.08	50.10 ± 4.08	35.10 ± 1.70	21.30 ± 1.03	2.68 ± 0.37	< 50.00	...
7	AKC2006-18	1.81 ± 0.10	1.75 ± 0.10	1.56 ± 0.10	1.40 ± 0.08	0.40 ± 0.33	< 50.00	...
8	SSTc2dJ154214.6-341026	2.18 ± 0.14	1.78 ± 0.14	3.52 ± 0.23	16.40 ± 0.92	56.10 ± 5.20	593.00 ± 56.20	...
9	SSTc2dJ154240.3-341343	178.00 ± 11.00	120.00 ± 11.00	99.80 ± 5.06	68.80 ± 3.28	13.00 ± 1.22	< 50.00	...
10	IRAS15398-3359	...	25.20 ± 2.00	35.80 ± 3.00	118.00 ± 18.00	991000.00 ± 99.00	15400.00 ± 1540.00	57.20 ± 11.44
11	SSTc2dJ154302.3-344406	2.45 ± 0.12	3.25 ± 0.12	4.23 ± 0.21	5.89 ± 0.28	21.50 ± 1.99	89.70 ± 15.40	...
12	AKC2006-19	5.48 ± 0.27	4.06 ± 0.27	3.29 ± 0.16	3.73 ± 0.18	3.44 ± 0.38	< 50.00	...
13	SSTc2dJ154506.3-341738	14.10 ± 0.68	15.40 ± 0.68	16.20 ± 0.77	19.10 ± 0.90	69.90 ± 6.46	204.00 ± 23.20	...
14	SSTc2dJ154508.9-341734	101.00 ± 5.12	104.00 ± 5.12	100.00 ± 4.73	94.30 ± 4.66	137.00 ± 12.70	702.00 ± 67.80	...
15	Sz68[a]	1580.00 ± 132.00	1420.00 ± 132.00	1690.00 ± 97.90	2170.00 ± 130.00	286.00 ± 270.00	4900.00 ± 459.00	52000.00 ± 10400.00
16	Sz69	111.00 ± 5.84	120.00 ± 5.84	94.60 ± 4.59	83.00 ± 4.12	100.00 ± 9.72	154.00 ± 20.10	...
17	SSTc2dJ154518.5-342125	37.70 ± 1.89	37.90 ± 1.89	35.80 ± 1.71	40.30 ± 1.91	38.50 ± 3.56	< 50.00	...
				Lupus III				
18	SSTc2dJ160703.9-391112	4.02 ± 0.20	5.08 ± 0.20	6.92 ± 0.34	11.70 ± 0.56	33.60 ± 3.16	99.20 ± 17.20	...
19	SSTc2dJ160708.6-391407	32.90 ± 1.64	48.30 ± 1.64	60.60 ± 2.89	89.30 ± 4.44	196.00 ± 18.20	189.00 ± 22.50	...
20	SSTc2dJ160708.6-394723	...	...	...	...	34.80 ± 3.31	< 50.00	...
21	Sz90	185.00 ± 9.56	154.00 ± 9.56	127.00 ± 6.33	123.00 ± 5.93	258.00 ± 24.00	335.00 ± 34.70	...
22	Sz91[a]	38.60 ± 1.93	24.70 ± 1.93	17.20 ± 0.83	10.90 ± 0.52	9.72 ± 0.98	502.00 ± 53.20	...
23	Lup605	...	< 1.54	...	0.61 ± 0.05	...	< 50.00	...
24	Sz92	...	...	...	...	1.54 ± 0.50	< 50.00	...
25	Lup654	0.50 ± 0.03	0.31 ± 0.03	0.20 ± 0.03	0.15 ± 0.04	0.47 ± 0.49	< 50.00	...
26	Lup713[a]	6.96 ± 0.46	6.12 ± 0.46	5.65 ± 0.31	6.69 ± 0.33	6.39 ± 0.64	< 50.00	...
27	Sz94	19.60 ± 1.00	13.50 ± 1.00	9.35 ± 0.44	5.69 ± 0.27	0.80 ± 0.45	< 50.00	...
28	Sz95	42.10 ± 2.53	31.80 ± 2.53	27.30 ± 1.41	29.60 ± 1.42	30.00 ± 2.82	< 50.00	...
29	SSTc2dJ160754.1-392046	112.00 ± 12.20	131.00 ± 12.20	103.00 ± 5.19	66.00 ± 3.26	16.30 ± 1.55	< 50.00	...
30	2MASSJ16075475-3915446[a]	2.71 ± 0.15	3.62 ± 0.15	4.13 ± 0.21	3.94 ± 0.19	16.50 ± 1.56	91.50 ± 16.40	...
31	SSTc2dJ160755.3-390718[a]	372.00 ± 28.10	272.00 ± 28.10	271.00 ± 13.90	180.00 ± 9.06	73.20 ± 6.84	< 50.00	...
32	Lup714	9.30 ± 0.48	6.30 ± 0.48	4.33 ± 0.24	2.60 ± 0.14	0.06 ± 0.43	< 50.00	...

Table 13—Continued

No.	Object Id.	IRAC 3.6 μm	IRAC 4.5 μm	IRAC 5.8 μm	IRAC 8.0 μm	MIPS 24 μm	MIPS 70 μm	MIPS 160 μm
33	Lup604s	16.30 ± 0.90	15.10 ± 0.90	12.80 ± 0.64	14.40 ± 0.69	16.60 ± 1.57	< 50.00	...
34	2MASSJ16080175-3912316	1.07 ± 0.06	1.06 ± 0.06	1.00 ± 0.06	1.32 ± 0.08	3.51 ± 0.40	< 50.00	...
35	SSTc2dJ160803.0-385229	217.00 ± 12.10	118.00 ± 12.10	102.00 ± 5.13	67.50 ± 3.53	16.20 ± 1.55	< 50.00	...
36	2MASSJ16080618-3912225	323.00 ± 38.20	249.00 ± 38.20	253.00 ± 15.00	339.00 ± 17.50	99.50 ± 9.44	< 50.00	...
37	Sz96	168.00 ± 12.60	113.00 ± 12.60	138.00 ± 7.99	173.00 ± 9.38	241.00 ± 22.90	157.00 ± 21.90	...
38	2MASSJ16081497-3857145	4.55 ± 0.25	5.35 ± 0.25	5.78 ± 0.29	5.80 ± 0.28	7.88 ± 0.77	< 50.00	...
39	Par-Lup3-1	12.70 ± 0.74	9.77 ± 0.74	6.86 ± 0.34	4.22 ± 0.21	0.55 ± 0.46	< 50.00	...
40	Sz97	27.90 ± 1.73	25.20 ± 1.73	23.70 ± 1.14	25.70 ± 1.23	31.20 ± 2.97	88.60 ± 16.90	...
41	Sz98	373.00 ± 30.40	477.00 ± 30.40	429.00 ± 25.40	693.00 ± 39.90	1200.00 ± 114.00	540.00 ± 55.10	...
42	Sz99	23.80 ± 1.39	22.90 ± 1.39	20.10 ± 1.01	21.10 ± 1.00	26.20 ± 2.45	< 50.00	...
43	Sz100	53.10 ± 3.21	50.40 ± 3.21	48.70 ± 2.48	61.70 ± 3.04	130.00 ± 12.10	223.00 ± 28.50	...
44	Lup607[a]	3.40 ± 0.19	2.91 ± 0.19	2.53 ± 0.14	3.56 ± 0.18	7.15 ± 0.70	< 50.00	...
45	NTO2000-0526.9-5630	0.62 ± 0.03	0.47 ± 0.03	0.33 ± 0.04	0.18 ± 0.08	0.25 ± 0.61	< 50.00	...
46	Sz101	79.80 ± 4.11	55.50 ± 4.11	41.60 ± 2.03	32.90 ± 1.60	24.10 ± 2.29	< 50.00	...
47	Sz102	14.40 ± 0.82	24.10 ± 0.83	34.00 ± 1.68	67.00 ± 3.26	347.00 ± 32.60	257.00 ± 30.20	...
48	IRACJ16083010-3922592	0.23 ± 0.02	0.27 ± 0.02	0.39 ± 0.07	0.62 ± 0.05	2.68 ± 0.34	< 50.00	...
49	Sz103	32.10 ± 1.97	28.10 ± 1.97	30.00 ± 1.81	33.80 ± 1.77	81.20 ± 7.66	317.00 ± 40.00	...
50	SSTc2dJ160830.7-382827	...	...	...	...	473.00 ± 45.80	2200.00 ± 219.00	2209.00 ± 441.80
51	Sz104	25.50 ± 1.47	22.50 ± 1.47	20.00 ± 1.01	21.30 ± 1.10	47.90 ± 4.62	441.00 ± 53.20	...
52	IRACJ16083110-3856000	0.27 ± 0.02	0.37 ± 0.02	0.49 ± 0.05	0.68 ± 0.05	2.22 ± 0.32	< 50.00	...
53	HR5999[b]	35.50 ± 17.20	...	12100.00 ± 1270.00	3490.00 ± 590.00	2890.00 ± 720.00	3780.00 ± 360.00	...
54	HR6000	650.00 ± 47.60	262.00 ± 47.60	256.00 ± 13.30	134.00 ± 7.64	19.20 ± 2.11	< 50.00	...
55	Par-Lup3-2	25.90 ± 1.37	18.60 ± 1.37	13.00 ± 0.62	7.64 ± 0.38	0.76 ± 0.43	< 50.00	...
56	Lup706	2.23 ± 0.15	2.01 ± 0.15	1.77 ± 0.11	1.93 ± 0.11	1.29 ± 0.54	< 50.00	...
57	Sz106	60.10 ± 4.42	81.30 ± 4.42	72.10 ± 3.58	73.80 ± 3.86	69.50 ± 6.56	< 50.00	...
58	Sz107	26.50 ± 1.51	20.20 ± 1.51	14.10 ± 0.68	9.24 ± 0.44	10.70 ± 1.03	< 50.00	...
59	Sz108	86.70 ± 4.35	58.20 ± 4.35	36.50 ± 1.96	25.60 ± 1.24	3.79 ± 1.30	< 50.00	...
60	Sz108B	32.60 ± 1.84	27.00 ± 1.84	23.60 ± 1.19	22.30 ± 1.18	53.50 ± 5.06	< 50.00	...
61	IRACJ16084679-3902074	0.31 ± 0.02	0.40 ± 0.02	0.55 ± 0.05	0.89 ± 0.07	3.75 ± 0.42	< 50.00	...
62	2MASSJ16084747-3905087	0.06 ± 0.09	0.11 ± 0.09	0.31 ± 0.14	0.31 ± 0.29	0.28 ± 2.32	< 50.00	...
63	Sz109	21.80 ± 1.30	17.10 ± 1.30	12.10 ± 0.59	7.15 ± 0.38	0.94 ± 0.93	< 50.00	...
64	Lup617	6.52 ± 0.35	4.67 ± 0.35	3.31 ± 0.17	2.03 ± 0.11	0.29 ± 0.52	< 50.00	...
65	Par-Lup3-3	69.40 ± 4.79	79.00 ± 4.79	77.60 ± 3.75	127.00 ± 6.39	191.00 ± 18.10	< 50.00	...
66	Par-Lup3-4	2.80 ± 0.15	2.88 ± 0.15	2.24 ± 0.13	1.73 ± 0.10	26.60 ± 2.55	492.00 ± 53.60	...

Table 13—Continued

No.	Object Id.	IRAC 3.6 μm	IRAC 4.5 μm	IRAC 5.8 μm	IRAC 8.0 μm	MIPS 24 μm	MIPS 70 μm	MIPS 160 μm
67	Sz110	69.90 ± 3.61	67.80 ± 3.61	58.80 ± 2.82	70.50 ± 3.45	171.00 ± 16.20	< 50.00	...
68	2MASSJ16085324-3914401	57.10 ± 3.13	46.70 ± 3.13	43.70 ± 2.14	45.50 ± 2.22	54.90 ± 5.15	119.00 ± 20.40	...
69	NTO2000-0532.1-5616	0.44 ± 0.03	0.29 ± 0.03	0.17 ± 0.04	0.10 ± 0.08	0.36 ± 0.53	< 50.00	...
70	2MASSJ16085373-3914367	7.30 ± 0.38	6.52 ± 0.38	5.79 ± 0.29	5.07 ± 0.25	5.90 ± 0.86	< 50.00	...
71	Sz111[c]	...	...	...	...	41.50 ± 3.86	< 50.00	1678.00 ± 335.60
72	2MASSJ16085529-3848481[a]	7.60 ± 0.38	7.76 ± 0.38	5.85 ± 0.30	6.97 ± 0.35	7.05 ± 0.70	< 50.00	...
73	Sz112[a]	48.70 ± 2.96	38.00 ± 2.96	30.40 ± 1.49	24.80 ± 1.22	124.00 ± 11.70	120.00 ± 25.20	...
74	Sz113	15.40 ± 0.89	15.00 ± 0.89	14.90 ± 0.72	20.50 ± 0.99	56.10 ± 5.35	88.30 ± 16.00	...
75	NTO2000-0536.7-5943	32.80 ± 1.82	40.70 ± 1.82	45.10 ± 2.16	28.10 ± 1.36	3.91 ± 0.48	< 50.00	...
76	NTO2000-0536.7-5956	1.85 ± 0.10	2.28 ± 0.10	2.09 ± 0.11	1.30 ± 0.08	0.09 ± 0.49	< 50.00	...
77	NTO2000-0537.4-5653	0.35 ± 0.02	0.23 ± 0.02	0.13 ± 0.02	0.09 ± 0.06	0.14 ± 0.40	< 50.00	...
78	2MASSJ16085953-3856275[a]	3.89 ± 0.21	3.69 ± 0.21	3.77 ± 0.23	4.31 ± 0.21	5.40 ± 0.57	< 50.00	...
79	SSTc2dJ160901.4-392512	44.70 ± 2.95	34.00 ± 2.95	30.60 ± 1.61	25.80 ± 1.29	42.20 ± 3.96	114.00 ± 15.00	...
80	Sz114	95.70 ± 5.43	101.00 ± 5.43	97.20 ± 4.66	121.00 ± 6.02	347.00 ± 32.30	257.00 ± 30.50	...
81	NTO2000-0540.9-5757[a]	0.43 ± 0.03	0.32 ± 0.03	0.16 ± 0.05	0.14 ± 0.04	0.18 ± 0.52	< 50.00	...
82	Sz115	22.20 ± 1.36	18.40 ± 1.36	14.80 ± 0.72	12.40 ± 0.59	10.50 ± 1.01	< 50.00	...
83	NTO2000-0546.4-5934	4.76 ± 0.25	3.36 ± 0.26	2.57 ± 0.14	1.54 ± 0.09	0.22 ± 0.44	< 50.00	...
84	Lup608s	10.70 ± 0.61	7.74 ± 0.61	5.45 ± 0.27	3.28 ± 0.16	0.69 ± 0.43	< 50.00	...
85	NTO2000-0554.9-5651	0.75 ± 0.04	0.65 ± 0.04	0.54 ± 0.04	0.38 ± 0.04	0.31 ± 0.30	< 50.00	...
86	Lup710	3.58 ± 0.20	2.40 ± 0.20	1.73 ± 0.12	1.00 ± 0.07	0.02 ± 0.45	< 50.00	...
87	Lupus3MMS	0.25 ± 0.03	1.00 ± 0.03	0.99 ± 0.07	0.55 ± 0.05	32.40 ± 3.04	2610.00 ± 252.00	8708.00 ± 1742.00
88	NTO2000-0558.8-5610	1.53 ± 0.08	1.44 ± 0.08	1.31 ± 0.07	0.84 ± 0.06	0.08 ± 0.30	< 50.00	...
89	NTO2000-0601.7-5616	5.72 ± 0.31	5.18 ± 0.31	4.84 ± 0.24	2.95 ± 0.15	0.21 ± 0.41	< 50.00	...
90	NTO2000-0605.1-5606	0.68 ± 0.04	0.61 ± 0.04	0.55 ± 0.04	0.30 ± 0.03	0.17 ± 0.44	< 50.00	...
91	SSTc2dJ160927.0-383628	...	...	...	...	36.30 ± 3.39	73.60 ± 11.40	...
92	NTO2000-0605.6-5437	0.17 ± 0.01	0.12 ± 0.01	0.08 ± 0.02	0.03 ± 0.05	0.02 ± 0.44	< 50.00	...
93	SSTc2dJ160934.1-391342	533.00 ± 55.00	399.00 ± 55.00	466.00 ± 26.00	283.00 ± 14.90	53.50 ± 5.02	< 50.00	...
94	IRACJ16093418-3915127	0.22 ± 0.01	0.29 ± 0.01	0.36 ± 0.04	0.46 ± 0.04	1.65 ± 0.28	< 50.00	...
95	NTO2000-0614.0-5414	0.25 ± 0.02	0.11 ± 0.02	0.11 ± 0.03	0.01 ± 0.05	0.12 ± 0.46	< 50.00	...
96	NTO2000-0615.6-5616	1.16 ± 0.06	1.09 ± 0.06	0.97 ± 0.06	0.61 ± 0.05	0.04 ± 0.31	< 50.00	...
97	NTO2000-0615.6-5953	0.55 ± 0.03	0.40 ± 0.03	0.24 ± 0.04	0.15 ± 0.05	0.19 ± 0.34	< 50.00	...
98	NTO2000-0615.8-5734	49.30 ± 3.10	50.70 ± 3.10	54.50 ± 2.64	35.00 ± 1.67	6.43 ± 0.64	< 50.00	...
99	NTO2000-0617.7-5641	6.31 ± 0.34	5.84 ± 0.34	5.60 ± 0.27	3.55 ± 0.18	0.35 ± 0.32	< 50.00	...
100	NTO2000-0619.6-5414	0.16 ± 0.01	0.10 ± 0.01	0.06 ± 0.05	0.07 ± 0.05	0.05 ± 0.30	< 50.00	...

Table 13—Continued

No.	Object Id.	IRAC 3.6 μm	IRAC 4.5 μm	IRAC 5.8 μm	IRAC 8.0 μm	MIPS 24 μm	MIPS 70 μm	MIPS 160 μm
101	Sz116[a]	50.00 ± 3.47	30.40 ± 3.47	20.90 ± 1.26	14.10 ± 0.77	1.70 ± 0.33	< 50.00	...
102	Sz117	65.20 ± 4.38	61.50 ± 4.38	56.90 ± 2.74	55.30 ± 2.67	91.50 ± 8.51	122.00 ± 20.50	...
103	Sz118	212.00 ± 16.20	255.00 ± 16.20	238.00 ± 12.20	302.00 ± 22.80	355.00 ± 33.60	322.00 ± 38.80	...
104	Lup650	0.70 ± 0.04	0.47 ± 0.04	0.32 ± 0.03	0.19 ± 0.04	0.27 ± 0.35	< 50.00	...
105	Lup810s	9.56 ± 0.61	6.55 ± 0.61	4.54 ± 0.23	2.78 ± 0.14	0.47 ± 0.33	< 50.00	...
106	Lup818s[a]	7.44 ± 0.39	6.50 ± 0.39	5.81 ± 0.29	7.63 ± 0.37	11.70 ± 1.12	96.90 ± 22.10	...
107	Sz119	49.20 ± 3.12	37.70 ± 3.12	25.90 ± 1.23	15.30 ± 0.77	2.01 ± 0.32	< 50.00	...
108	SSTc2dJ161000.1-385401	366.00 ± 23.90	176.00 ± 23.90	268.00 ± 14.00	206.00 ± 10.60	97.20 ± 9.14	< 50.00	...
109	2MASSJ16100133-3906449	27.20 ± 1.58	24.00 ± 1.58	21.00 ± 1.01	18.80 ± 0.89	24.10 ± 2.28	< 50.00	...
110	Sz121	81.70 ± 4.34	55.40 ± 4.34	38.10 ± 1.85	23.20 ± 1.10	2.82 ± 0.36	< 50.00	...
111	SSTc2dJ161013.1-384617[a]	1.89 ± 0.11	2.78 ± 0.11	2.35 ± 0.14	2.36 ± 0.13	12.80 ± 1.21	< 50.00	...
112	Sz122	34.50 ± 1.71	21.80 ± 1.71	15.30 ± 0.75	8.96 ± 0.43	0.99 ± 0.25	< 50.00	...
113	SSTc2dJ161018.6-383613[a]	7.03 ± 0.47	6.30 ± 0.47	4.67 ± 0.29	4.97 ± 0.25	4.01 ± 0.44	< 50.00	...
114	SSTc2dJ161019.8-383607	5.41 ± 0.30	5.47 ± 0.30	4.17 ± 0.27	4.92 ± 0.25	5.29 ± 0.55	< 50.00	...
115	SSTc2dJ161027.4-390230	0.67 ± 0.04	0.61 ± 0.04	0.48 ± 0.04	0.44 ± 0.05	8.29 ± 0.82	< 50.00	...
116	SSTc2dJ161029.6-392215	19.10 ± 0.93	14.20 ± 0.93	11.50 ± 0.56	10.90 ± 0.53	33.70 ± 3.18	110.00 ± 18.00	...
117	IRAS16072-3738	1200.00 ± 67.10	667.00 ± 67.10	633.00 ± 30.90	412.00 ± 21.90	107.00 ± 10.20	< 50.00	...
118	SSTc2dJ161034.5-381450	1210.00 ± 64.20	616.00 ± 64.20	672.00 ± 32.60	463.00 ± 22.90	109.00 ± 10.20	< 50.00	...
119	SSTc2dJ161035.0-390655	234.00 ± 12.30	154.00 ± 12.30	125.00 ± 6.33	82.60 ± 3.98	18.40 ± 1.76	< 50.00	...
120	SSTc2dJ161045.4-385455	4.93 ± 0.24	5.55 ± 0.24	6.30 ± 0.31	6.90 ± 0.33	3.21 ± 0.37	< 50.00	...
121	Sz123[a]	59.90 ± 3.08	50.40 ± 3.08	42.60 ± 2.07	44.90 ± 2.12	61.00 ± 5.76	327.00 ± 35.60	...
122	SSTc2dJ161118.7-385824	2820.00 ± 258.00	2530.00 ± 258.00	2390.00 ± 123.00	1600.00 ± 91.20	518.00 ± 49.70	< 50.00	...
123	SSTc2dJ161126.0-391123	1010.00 ± 54.60	599.00 ± 54.60	556.00 ± 27.00	362.00 ± 17.10	105.00 ± 9.76	< 50.00	...
124	SSTc2dJ161131.9-381110	18.80 ± 0.92	11.80 ± 0.92	8.99 ± 0.45	6.38 ± 0.32	1.86 ± 0.33	< 50.00	...
125	Lup831s	20.20 ± 0.98	11.20 ± 0.98	8.80 ± 0.42	5.04 ± 0.25	0.45 ± 0.32	< 50.00	...
126	SSTc2dJ161144.9-383245	10.40 ± 0.52	7.24 ± 0.52	5.03 ± 0.25	3.01 ± 0.15	1.60 ± 0.28	< 50.00	...
127	SSTc2dJ161148.7-381758	11.60 ± 0.57	11.40 ± 0.57	10.80 ± 0.56	12.20 ± 0.58	22.90 ± 2.22	< 50.00	...
128	Lup802s	4.79 ± 0.24	3.30 ± 0.24	2.26 ± 0.12	1.30 ± 0.08	0.10 ± 0.33	< 50.00	...
129	Sz124	50.80 ± 2.49	32.40 ± 2.49	22.10 ± 1.05	13.70 ± 0.64	1.67 ± 0.26	< 50.00	...
130	SST-Lup3-1	15.80 ± 0.84	13.10 ± 0.84	11.00 ± 0.53	12.90 ± 0.61	21.00 ± 1.98	< 50.00	...
131	SSTc2dJ161200.1-385557	615.00 ± 33.10	346.00 ± 33.10	291.00 ± 15.60	182.00 ± 8.80	48.80 ± 4.59	< 50.00	...
132	SSTc2dJ161204.5-380959	1.98 ± 0.10	2.84 ± 0.10	3.68 ± 0.19	4.70 ± 0.23	11.30 ± 1.09	< 50.00	...
133	SSTc2dJ161211.2-383220[a]	50.50 ± 2.60	54.20 ± 2.60	65.10 ± 3.09	113.00 ± 5.47	77.90 ± 7.25	< 50.00	...
134	SSTc2dJ161218.5-393418[a]	...	...	...	...	134.00 ± 12.60	< 50.00	...

Table 13—Continued

No.	Object Id.	IRAC 3.6 μm	IRAC 4.5 μm	IRAC 5.8 μm	IRAC 8.0 μm	MIPS 24 μm	MIPS 70 μm	MIPS 160 μm
135	SSTc2dJ161219.6-383742	463.00 ± 26.00	288.00 ± 26.00	251.00 ± 12.30	167.00 ± 8.39	40.90 ± 3.85	< 50.00	...
136	SSTc2dJ161222.7-371328	...	...	...	...	46.50 ± 4.32	< 50.00	...
137	SSTc2dJ161243.8-381503	90.30 ± 4.46	75.30 ± 4.46	69.80 ± 3.29	74.80 ± 3.57	92.50 ± 8.68	116.00 ± 16.50	...
138	SSTc2dJ161251.7-384216	637.00 ± 34.20	349.00 ± 34.20	306.00 ± 15.10	202.00 ± 10.90	74.30 ± 7.04	< 50.00	...
139	SSTc2dJ161256.0-375643	1330.00 ± 72.70	738.00 ± 72.70	684.00 ± 33.40	439.00 ± 20.80	116.00 ± 10.80	< 50.00	...
140	SSTc2dJ161341.0-383724	392.00 ± 20.60	219.00 ± 20.60	177.00 ± 9.04	112.00 ± 5.38	25.10 ± 2.38	...	...
141	SSTc2dJ161344.1-373646	...	...	...	...	10.10 ± 0.97	< 50.00	...
				Lupus IV				
142	SSTc2dJ155925.2-423507	...	...	...	...	5.59 ± 0.59	< 50.00	...
143	SSTc2dJ155945.3-415457	578.00 ± 31.00	335.00 ± 31.00	323.00 ± 16.00	380.00 ± 18.70	268.00 ± 24.80	< 50.00	...
144	SSTc2dJ160000.6-422158	...	...	...	...	16.50 ± 1.54	< 50.00	...
145	SSTc2dJ160002.4-422216	...	...	...	...	41.00 ± 3.79	< 50.00	...
146	IRAS15567-4141	1380.00 ± 145.00	2000.00 ± 145.00	1680.00 ± 113.00	1620.00 ± 87.30	780.00 ± 73.40	91.60 ± 14.80	...
147	SSTc2dJ160026.1-415356[a]	21.50 ± 1.05	16.80 ± 1.05	14.20 ± 0.67	16.30 ± 0.78	24.00 ± 2.23	< 50.00	...
148	Sz130[a]	59.00 ± 3.02	53.50 ± 3.02	53.30 ± 2.53	70.10 ± 3.35	115.00 ± 10.60	165.00 ± 22.10	...
149	SSTc2dJ160034.4-422540	...	...	...	...	483.00 ± 44.60	108.00 ± 17.00	...
150	F403	177.00 ± 9.40	141.00 ± 9.40	140.00 ± 6.81	213.00 ± 11.20	590.00 ± 55.20	1050.00 ± 103.00	2272.00 ± 454.40
151	Sz131	...	< 55.70	...	58.20 ± 2.78	64.40 ± 5.95	52.90 ± 10.20	...
152	SSTc2dJ160111.6-413730	96.90 ± 4.79	61.30 ± 4.79	49.10 ± 2.34	34.30 ± 1.64	7.82 ± 0.76	< 50.00	...
153	SSTc2dJ160115.6-415235	8.36 ± 0.44	9.92 ± 0.44	8.98 ± 0.44	7.70 ± 0.37	75.90 ± 7.03	1220.00 ± 123.00	5386.00 ± 1077.00
154	SSTc2dJ160129.7-420804[a]	91.10 ± 4.43	58.60 ± 4.43	48.90 ± 2.31	38.00 ± 1.85	17.90 ± 1.67	< 50.00	...
155	SSTc2dJ160143.3-413606	121.00 ± 6.02	69.90 ± 6.02	56.40 ± 2.68	36.60 ± 1.76	10.20 ± 0.97	< 50.00	...
156	IRAS15585-4134	1400.00 ± 182.00	1860.00 ± 182.00	1710.00 ± 88.20	1170.00 ± 58.20	263.00 ± 24.40	< 50.00	...
157	IRAS15589-4132[a]	5.10 ± 0.30	4.87 ± 0.30	12.60 ± 0.62	42.10 ± 2.03	144.00 ± 13.40	1030.00 ± 107.00	2336.00 ± 467.20
158	SSTc2dJ160229.9-415111	49.90 ± 2.60	30.10 ± 2.60	25.50 ± 1.22	18.20 ± 0.85	5.15 ± 0.51	< 50.00	...
159	Sz133[a]	...	...	...	...	142.00 ± 13.20	< 50.00	...

Note. — [a] Binary star inside IRAC or MIPS PSFs, corresponding fluxes transformed to upper limits in SED plots.

Note. — [b] Flux from IRAC bands 1 and 2 saturated.

Note. — [c] MIPS-1 non-detection likely due to high background.

Note. — MIPS-2 non-detections were transformed to 50 mJy upper limits, which is a good estimate of the 70 μm background around most sources.

Table 14. IRAS and 1.3 mm fluxes in mJy of the Lupus sample

No.	Object Id.	IRAS 12 μm	IRAS 25 μm	IRAS 60 μm	IRAS 100 μm	Cont. 1300 μm
			Lupus I			
1	SSTc2dJ153803.1-331358	...	...	...	...	...
2	IRAS15356-3430	332.00 ± 33.20	299.00 ± 29.90	2620.00 ± 262.00	18000.00 ± 1800.00	...
3	AKC2006-17	...	...	...	...	...
4	Sz65	548.00 ± 54.80	756.00 ± 75.60	692.00 ± 69.20	...	56.00 ± 10.00
5	Sz66	548.00 ± 54.80	756.00 ± 75.60	692.00 ± 69.20	...	47.00 ± 12.00
6	Sz67	...	...	...	...	< 66.00
7	AKC2006-18	...	...	...	...	...
8	SSTc2dJ154214.6-341026	...	...	...	...	...
9	SSTc2dJ154240.3-341343	...	...	...	...	...
10	IRAS15398-3359[a]	250.00 ± 250.00	1280.00 ± 128.00	15200.00 ± 1520.00	41300.00 ± 4130.00	365.00 ± 10.00
11	SSTc2dJ154302.3-344406	...	...	...	...	...
12	AKC2006-19	...	...	...	...	...
13	SSTc2dJ154506.3-341738	...	...	...	...	...
14	SSTc2dJ154508.9-341734	...	...	...	...	...
15	Sz68	2590.00 ± 259.00	3990.00 ± 399.00	7920.00 ± 792.00	24400.00 ± 2440.00	135.00 ± 15.00
16	Sz69	...	...	...	...	< 30.00
17	SSTc2dJ154518.5-342125	...	...	...	...	...
			Lupus III			
18	SSTc2dJ160703.9-391112	...	...	...	...	...
19	SSTc2dJ160708.6-391407	...	...	...	...	...
20	SSTc2dJ160708.6-394723	...	...	...	...	...
21	Sz90	...	...	...	...	26.00 ± 9.00
22	Sz91	...	...	...	...	< 27.00
23	Lup605	...	...	...	...	...
24	Sz92	...	...	...	...	...
25	Lup654	...	...	...	...	...
26	Lup713	...	...	...	...	...
27	Sz94	...	...	...	...	< 45.00
28	Sz95	...	...	...	...	< 36.00
29	SSTc2dJ160754.1-392046	...	...	...	...	...
30	2MASSJ16075475-3915446	...	...	...	...	...
31	SSTc2dJ160755.3-390718	...	...	...	...	...
32	Lup714	...	...	...	...	...

Table 14—Continued

No.	Object Id.	IRAS 12 μm	IRAS 25 μm	IRAS 60 μm	IRAS 100 μm	Cont. 1300 μm
33	Lup604s	...	...	...	...	...
34	2MASSJ16080175-3912316	...	...	...	...	...
35	SSTc2dJ160803.0-385229	...	...	...	...	...
36	2MASSJ16080618-3912225	...	...	...	...	...
37	Sz96	...	...	...	...	< 45.00
38	2MASSJ16081497-3857145	...	...	...	...	...
39	Par-Lup3-1	...	...	...	...	...
40	Sz97	...	...	...	...	28.00 ± 9.00
41	Sz98	...	...	...	...	84.00 ± 17.00
42	Sz99	...	...	...	...	< 30.00
43	Sz100	...	...	...	...	< 27.00
44	Lup607	...	...	...	...	...
45	NTO2000-0526.9-5630	...	...	...	...	...
46	Sz101	...	...	...	...	< 39.00
47	Sz102	...	...	...	...	< 30.00
48	IRACJ16083010-3922592	...	...	...	...	...
49	Sz103	...	...	...	...	< 57.00
50	SSTc2dJ160830.7-382827	...	...	...	...	...
51	Sz104	...	...	...	...	< 42.00
52	IRACJ16083110-3856000	...	...	...	...	...
53	HR5999	18000.00 ± 1800.00	14500.00 ± 1450.00	14400.00 ± 2880.00	< 63200.00	...
54	HR6000	...	...	...	...	...
55	Par-Lup3-2	...	...	...	...	...
56	Lup706	...	...	...	...	...
57	Sz106	...	...	...	...	...
58	Sz107	...	...	...	...	...
59	Sz108	...	...	...	...	...
60	Sz108B	...	...	...	...	...
61	IRACJ16084679-3902074	...	...	...	...	...
62	2MASSJ16084747-3905087	...	...	...	...	...
63	Sz109	...	...	...	...	...
64	Lup617	...	...	...	...	...
65	Par-Lup3-3	...	...	...	...	...
66	Par-Lup3-4	...	...	...	...	...

Table 14—Continued

No.	Object Id.	IRAS 12 μm	IRAS 25 μm	IRAS 60 μm	IRAS 100 μm	Cont. 1300 μm
67	Sz110	...	...	...	...	...
68	2MASSJ16085324-3914401	...	...	...	...	...
69	NTO2000-0532.1-5616	...	...	...	...	...
70	2MASSJ16085373-3914367	...	...	...	...	...
71	Sz111	...	110.00 ± 70.00	1120.00 ± 70.00	4580.00 ± 70.00	...
72	2MASSJ16085529-3848481	...	...	...	...	...
73	Sz112	...	...	...	...	...
74	Sz113	...	...	...	...	...
75	NTO2000-0536.7-5943	...	...	...	...	...
76	NTO2000-0536.7-5956	...	...	...	...	...
77	NTO2000-0537.4-5653	...	...	...	...	...
78	2MASSJ16085953-3856275	...	...	...	...	...
79	SSTc2dJ160901.4-392512	...	...	...	...	...
80	Sz114	...	...	...	...	...
81	NTO2000-0540.9-5757	...	...	...	...	...
82	Sz115	...	...	...	...	...
83	NTO2000-0546.4-5934	...	...	...	...	...
84	Lup608s	...	...	...	...	...
85	NTO2000-0554.9-5651	...	...	...	...	...
86	Lup710	...	...	...	...	...
87	Lupus3MMS	...	...	...	< 25500.00	...
88	NTO2000-0558.8-5610	...	...	...	...	...
89	NTO2000-0601.7-5616	...	...	...	...	...
90	NTO2000-0605.1-5606	...	...	...	...	...
91	SSTc2dJ160927.0-383628	...	...	...	...	...
92	NTO2000-0605.6-5437	...	...	...	...	...
93	SSTc2dJ160934.1-391342	...	...	...	...	...
94	IRACJ16093418-3915127	...	...	...	...	...
95	NTO2000-0614.0-5414	...	...	...	...	...
96	NTO2000-0615.6-5616	...	...	...	...	...
97	NTO2000-0615.6-5953	...	...	...	...	...
98	NTO2000-0615.8-5734	...	...	...	...	...
99	NTO2000-0617.7-5641	...	...	...	...	...
100	NTO2000-0619.6-5414	...	...	...	...	...

Table 14—Continued

No.	Object Id.	IRAS 12 μm	IRAS 25 μm	IRAS 60 μm	IRAS 100 μm	Cont. 1300 μm
101	Sz116	...	...	...	...	...
102	Sz117	...	...	...	...	...
103	Sz118	...	...	...	...	...
104	Lup650	...	...	...	...	...
105	Lup810s	...	...	...	...	...
106	Lup818s	...	...	...	...	...
107	Sz119	...	...	...	...	...
108	SSTc2dJ161000.1-385401	...	...	...	...	...
109	2MASSJ16100133-3906449	...	...	...	...	...
110	Sz121	...	...	...	...	...
111	SSTc2dJ161013.1-384617	...	...	...	...	...
112	Sz122	...	...	...	...	...
113	SSTc2dJ161018.6-383613	...	...	...	...	...
114	SSTc2dJ161019.8-383607	...	...	...	...	...
115	SSTc2dJ161027.4-390230	...	...	...	...	...
116	SSTc2dJ161029.6-392215	...	...	...	...	...
117	IRAS16072-3738	287.00 $\pm$ 28.10	$<$ 449.00	$<$ 444.00	$<$ 22100.00	...
118	SSTc2dJ161034.5-381450	...	...	...	...	...
119	SSTc2dJ161035.0-390655	...	...	...	...	...
120	SSTc2dJ161045.4-385455	...	...	...	...	...
121	Sz123	...	...	...	...	...
122	SSTc2dJ161118.7-385824	...	...	...	...	...
123	SSTc2dJ161126.0-391123	...	...	...	...	...
124	SSTc2dJ161131.9-381110	...	...	...	...	...
125	Lup831s	...	...	...	...	...
126	SSTc2dJ161144.9-383245	...	...	...	...	...
127	SSTc2dJ161148.7-381758	...	...	...	...	...
128	Lup802s	...	...	...	...	...
129	Sz124	...	...	...	...	...
130	SST-Lup3-1	...	...	...	...	...
131	SSTc2dJ161200.1-385557	...	...	...	...	...
132	SSTc2dJ161204.5-380959	...	...	...	...	...
133	SSTc2dJ161211.2-383220	...	...	...	...	...
134	SSTc2dJ161218.5-393418	...	...	...	...	...

Support for this work, part of the Spitzer Space Telescope Legacy Science Program, was provided by NASA through Contract Numbers 1256316, 1224608 and 1230780 issued by the Jet Propulsion Laboratory, California Institute of Technology under NASA contract 1407. Astrochemistry at Leiden is supported by a NWO Spinoza and NOVA grant, and by the European Research Training Network "The Origin of Planetary Systems" (PLANETS, contract number HPRN-CT-2002-00308). B. M. thanks the Fundación Ramón Areces for early financial support. The authors would like to thank the referee for very good suggestions on the structure and contents of the paper, to E. Solano and R. Gutierrez from the Spanish Virtual Observatory at LAEFF for providing easy automatic access to ancillary Vizier data for the sample, and to Jennifer Hatchell for providing very detailed comments.

REFERENCES

Alcalá, J., Spezzi, L., Chapman, N., et al. 2008, ApJ, in press

Alexander, R. D. & Armitage, P. J. 2007, MNRAS, 375, 500

Allen, L. E., Calvet, N., D'Alessio, P., et al. 2004, ApJS, 154, 363

Allen, P. R., Luhman, K. L., Myers, P. C., et al. 2007, ApJ, 655, 1095

Allers, K. N., Kessler-Silacci, J. E., Cieza, L. A., & Jaffe, D. T. 2006, ApJ, 644, 364

Andreazza, C. M. & Vilas-Boas, J. W. S. 1996, A&AS, 116, 21

Andrews, S. M. & Williams, J. P. 2005, ApJ, 631, 1134

Ballesteros-Paredes, J. & Hartmann, L. 2007, Revista Mexicana de Astronomia y Astrofisica, 43, 123

Ballesteros-Paredes, J., Klessen, R. S., Mac Low, M.-M., & Vazquez-Semadeni, E. 2007, in Protostars and Planets V, ed. B. Reipurth, D. Jewitt, & K. Keil, 63–80

Baraffe, I., Chabrier, G., Allard, F., & Hauschildt, P. H. 1998, A&A, 337, 403

Barrado y Navascués, D., Stauffer, J. R., Morales-Calderón, M., et al. 2007, ApJ, 664, 481

Bate, M. R., Bonnell, I. A., & Bromm, V. 2003, MNRAS, 339, 577

Beckwith, S. V. W. & Sargent, A. I. 1991, ApJ, 381, 250

Bouwman, J., Lawson, W. A., Dominik, C., et al. 2006, ApJ, 653, L57

Table 14—Continued

No.	Object Id.	IRAS 12 μm	IRAS 25 μm	IRAS 60 μm	IRAS 100 μm	Cont. 1300 μm
135	SSTc2dJ161219.6-383742	...	...	...	...	...
136	SSTc2dJ161222.7-371328	...	...	...	...	...
137	SSTc2dJ161243.8-381503	...	...	...	...	...
138	SSTc2dJ161251.7-384216	...	...	...	...	...
139	SSTc2dJ161256.0-375643	...	...	...	...	...
140	SSTc2dJ161341.0-383724	...	...	...	...	...
141	SSTc2dJ161344.1-373646	...	...	...	...	...
			Lupus IV			
142	SSTc2dJ155925.2-423507	...	...	...	...	...
143	SSTc2dJ155945.3-415457	...	...	...	...	...
144	SSTc2dJ160000.6-422158	...	...	...	...	...
145	SSTc2dJ160002.4-422216	...	...	...	...	...
146	IRAS15567-4141	2590.00 ± 259.00	1410.00 ± 141.00	479.00 ± 479.00	4480.00 ± 4480.00	...
147	SSTc2dJ160026.1-415356	...	...	...	...	...
148	Sz130	...	...	...	...	...
149	SSTc2dJ160034.4-422540	...	...	...	...	...
150	F403	289.00 ± 60.00	778.00 ± 77.80	1170.00 ± 117.00	4550.00 ± 4550.00	...
151	Sz131	...	...	...	...	...
152	SSTc2dJ160111.6-413730	...	...	...	...	...
153	SSTc2dJ160115.6-415235	...	...	...	...	...
154	SSTc2dJ160129.7-420804	...	...	...	...	...
155	SSTc2dJ160143.3-413606	...	...	...	...	...
156	IRAS15585-4134	966.00 ± 96.60	397.00 ± 397.00	447.00 ± 447.00	4550.00 ± 4550.00	...
157	IRAS15589-4132	373.00 ± 37.30	261.00 ± 26.10	1050.00 ± 105.00	4620.00 ± 462.00	...
158	SSTc2dJ160229.9-415111	...	...	...	...	...
159	Sz133	...	...	...	...	...

Note. — IRAS fluxes are from the IRAS Point Source Catalogue.

Note. — 1.3 mm fluxes are from Nuernberger et al. (1997), except those marked with [a], which are from Reipurth et al. (1993).

Brown, J. M., Blake, G. A., Dullemond, C. P., et al. 2007, ApJ, 664, L107

Calvet, N., D'Alessio, P., Watson, D. M., et al. 2005, ApJ, 630, L185

Cambrésy, L. 1999, A&A, 345, 965

Cambrésy, L., Epchtein, N., Copet, E., et al. 1997, A&A, 324, L5

Carballo, R., Wesselius, P. R., & Whittet, D. C. B. 1992, A&A, 262, 106

Chapman, N. L., Lai, S.-P., Mundy, L. G., et al. 2007, ArXiv e-prints, 706

Cieza, L., Padgett, D. L., Stapelfeldt, K. R., et al. 2007, ArXiv e-prints, 706

Comerón, F. 2008, The Lupus Dark Clouds, ed. B. Reipurth (Handbook of Low Mass Star Formation in Southern Molecular Clouds), submitted

Comerón, F., Fernández, M., Baraffe, I., Neuhäuser, R., & Kaas, A. A. 2003, A&A, 406, 1001

Currie, T., Kenyon, S., Balog, Z., et al. 2007, ArXiv e-prints, 709

Cutri, R. M., Skrutskie, M. F., van Dyk, S., et al. 2003, 2MASS All Sky Catalog of point sources. (The IRSA 2MASS All-Sky Point Source Catalog, NASA/IPAC Infrared Science Archive. http://irsa.ipac.caltech.edu/applications/Gator/)

D'Alessio, P., Calvet, N., Hartmann, L., Lizano, S., & Cantó, J. 1999, ApJ, 527, 893

D'Alessio, P., Merín, B., Calvet, N., Hartmann, L., & Montesinos, B. 2005, Revista Mexicana de Astronomia y Astrofisica, 41, 61

Dullemond, C. P., Hollenbach, D., Kamp, I., & D'Alessio, P. 2007, Protostars and Planets V, 555

Edgar, R. G. 2007, ApJ, 663, 1325

Evans, II, N. J., Allen, L. E., Blake, G. A., et al. 2003, PASP, 115, 965

Evans, II, N. J., Harvey, P. M., Dunham, M. M., et al. 2007, http://ssc.spitzer.caltech.edu/legacy/original.html

Fazio, G. G., Hora, J. L., Allen, L. E., et al. 2004, ApJS, 154, 10

Fernández, M. & Comerón, F. 2005, A&A, 440, 1119

Ghez, A. M., McCarthy, D. W., Patience, J. L., & Beck, T. L. 1997, ApJ, 481, 378

Gondoin, P. 2006, A&A, 454, 595

Greene, T. P., Wilking, B. A., Andre, P., Young, E. T., & Lada, C. J. 1994, ApJ, 434, 614

Gutermuth, R. A., Megeath, S. T., Pipher, J. L., et al. 2005, ApJ, 632, 397

Haisch, Jr., K. E., Lada, E. A., & Lada, C. J. 2001, ApJ, 553, L153

Hara, A., Tachihara, K., Mizuno, A., et al. 1999, PASJ, 51, 895

Hartmann, L., Megeath, S. T., Allen, L., et al. 2005, ApJ, 629, 881

Harvey, P., Merín, B., Huard, T. L., et al. 2007a, ApJ, 663, 1149

Harvey, P. M., Chapman, N., Lai, S.-P., et al. 2006, ApJ, 644, 307

Harvey, P. M., Rebull, L. M., Brooke, T., et al. 2007b, ApJ, 663, 1139

Hauschildt, P. H., Allard, F., Ferguson, J., Baron, E., & Alexander, D. R. 1999, ApJ, 525, 871

Henize, K. G. 1954, ApJ, 119, 459

Heyer, M. H. & Graham, J. A. 1989, PASP, 101, 816

Hughes, J., Hartigan, P., Krautter, J., & Kelemen, J. 1994, AJ, 108, 1071

Jørgensen, J. K., Harvey, P. M., Evans, II, N. J., et al. 2006, ApJ, 645, 1246

Kenyon, S. J. & Hartmann, L. 1987, ApJ, 323, 714

Krautter, J. 1986, A&A, 161, 195

Krautter, J. 1991, The Lupus Dark Clouds, ed. B. Reipurth, Vol. 11 (Handbook of Low Mass Star Formation in Southern Molecular Clouds), 127–

Krautter, J., Wichmann, R., Schmitt, J. H. M. M., et al. 1997, A&AS, 123, 329

Lada, C. J. & Lada, E. A. 2003, ARA&A, 41, 57

Lada, C. J., Muench, A. A., Luhman, K. L., et al. 2006, AJ, 131, 1574

Lada, C. J. & Wilking, B. A. 1984, ApJ, 287, 610

López Martí, B., Eislöffel, J., & Mundt, R. 2005, A&A, 440, 139

Mayne, N. J., Naylor, T., Littlefair, S. P., Saunders, E. S., & Jeffries, R. D. 2007, MNRAS, 375, 1220

Merín, B., Augereau, J. C., van Dishoeck, E. F., et al. 2007, ApJ

Mizuno, A., Hayakawa, T., Tachihara, K., et al. 1999, PASJ, 51, 859

Murphy, D. C., Cohen, R., & May, J. 1986, A&A, 167, 234

Nakajima, Y., Tamura, M., Oasa, Y., & Nakajima, T. 2000, AJ, 119, 873

Noriega-Crespo, A., Morris, P., Marleau, F. R., et al. 2004, ApJS, 154, 352

Nuernberger, D., Chini, R., & Zinnecker, H. 1997, A&A, 324, 1036

Padgett, D. L., Strom, S. E., & Ghez, A. 1997, ApJ, 477, 705

Pascucci, I., Apai, D., Hardegree-Ullman, E. E., et al. 2007, ArXiv e-prints, 710

Porras, A., Jørgensen, J. K., Allen, L. E., et al. 2007, ApJ, 656, 493

Reipurth, B., Chini, R., Krugel, E., Kreysa, E., & Sievers, A. 1993, A&A, 273, 221

Reipurth, B. & Graham, J. A. 1988, A&A, 202, 219

Reipurth, B. & Zinnecker, H. 1993, A&A, 278, 81

Rieke, G. H., Young, E. T., Engelbracht, C. W., et al. 2004, ApJS, 154, 25

Robitaille, T. P., Whitney, B. A., Indebetouw, R., Wood, K., & Denzmore, P. 2006, ApJS, 167, 256

Schwartz, R. D. 1977, ApJS, 35, 161

Sicilia-Aguilar, A., Hartmann, L., Calvet, N., et al. 2006, ApJ, 638, 897

Strauss, M. A., Huchra, J. P., Davis, M., et al. 1992, ApJS, 83, 29

Surace, J. A., Shupe, D. L., Fang, F., et al. 2004, VizieR Online Data Catalog, 2255, 0

Tachihara, K., Dobashi, K., Mizuno, A., Ogawa, H., & Fukui, Y. 1996, PASJ, 48, 489

Tachihara, K., Rengel, M., Nakajima, Y., et al. 2007, ApJ, 659, 1382

Tachihara, K., Toyoda, S., Onishi, T., et al. 2001, PASJ, 53, 1081

Thé, P.-S. 1962, Contributions from the Bosscha Observervatory, 15, 0

Vilas-Boas, J. W. S., Myers, P. C., & Fuller, G. A. 2000, ApJ, 532, 1038

Wainscoat, R. J., Cohen, M., Volk, K., Walker, H. J., & Schwartz, D. E. 1992, ApJS, 83, 111

Weingartner, J. C. & Draine, B. T. 2001, ApJ, 548, 296

Werner, M. W., Roellig, T. L., Low, F. J., et al. 2004, ApJS, 154, 1

Whitney, B. A., Wood, K., Bjorkman, J. E., & Cohen, M. 2003, ApJ, 598, 1079

Wichmann, R., Covino, E., Alcalá, J. M., et al. 1999, MNRAS, 307, 909

Young, K. E., Harvey, P. M., Brooke, T. Y., et al. 2005, ApJ, 628, 283

Zacharias, N., Monet, D. G., Levine, S. E., et al. 2005, VizieR Online Data Catalog, 1297, 0